Application of bivariate spectral quasilinearization method to second grade fluid flow equations

A DISSERTATION SUBMITTED TO THE UNIVERSITY OF KWAZULU-NATAL

FOR THE DEGREE OF MASTER OF SCIENCE

IN THE COLLEGE OF AGRICULTURE, ENGINEERING AND SCIENCE

by

Simphiwe Gloria Dlongolo

School of Mathematics, Statistics and Computer Science

January 2020

Declaration

This work was carried out in the School of Mathematics, Statistics and Computer Science, University of KwaZulu-Natal, Pietermaritzburg under the supervision of Prof. P. Sibanda and Dr. S. P. Goqo from February 2018 to January 2020.
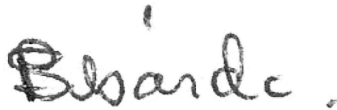
I hereby declare that except where due credit is given, no portion of this work has been presented wholly or in part for the award of any degree or qualification at University of KwaZulu-Natal or any other institution.

Simphiwe G. Dlongolo   Date: 23/09/2020

Prof. P. Sibanda   Date: 23/09/2020

Dr. S. P. Goqo   Date: 23/09/2020

Acknowledgements

Abstract

In this study, the steady flow of a second grade magnetohydrodynamic fluid in a porous channel is investigated. We further investigate the hydromagnetic flow of a second grade fluid over a stretching sheet. The partial differential equations that describe the flows are solved numerically using the bivariate spectral quasilinearization method. The method is extended to a system of non-similar partial differential equations that model the steady two dimensional flow of Falkner-Skan flow of an incompressible second grade nanofluid. The work is also concerned with heat and the mass transfer from the electrically conducting second grade magnetohydrodynamic fluid over a stretching sheet. The sensitivity of the flow characteristics with respect to the second grade fluid parameter, magnetic field parameter, thermal radiation parameter, and the chemical reaction parameter are investigated. The accuracy of the numerical method is determined using the residual error analysis.

Contents

List of Figures

List of Tables

List of Abbreviations

BSQLM   Bivariate-Spectral Quasilinearization Method

DTM   Differential Transform Method

FDM   Finite Difference Method

GAM   Generalized Approximation

HPM   Homotopy Perturbation Method

HSR   Helical Screw Rheometer

MDTM   Multi-step Difference Transform Method

MHD   Magnetohydrodynamic flow

MVIM   Modified Variational Iteration Method

NSDF   Non-Standard Finite Difference Scheme

OHAM   Optimal Homotopy Asymptotic Method

ODE   Ordinary Differential Equations

PDE   Partial Differential Equations

PHF   Prescribed Stretching Surface Flux Flow

PST   Prescribed Stretching Temperature

SLLM   Spectral Local Linearization Method

SQLM   Spectral Quasilinearization Method

Nomanclature

A	the ratio of rates
B_0	is a constant magnetic field
C	the concentration of the fluid within the boundary layer
C_∞	ambient concentration
C_p	specific heat capacity at constant pressure
C_w	is the concentration of the fluid at the plate
D_B	the Brownian diffusion coefficient
D_T	the thermophoresis diffusion coefficient
Ec	is the Eckert number
f	dimensionless stream function
F	local inertial coefficient
$F*$	inertial coefficient of the porous medium
g	the acceleration due to gravity
Gr_c	the solutal Grashof Number
Gr_t	the thermal Grashof Number
Ha	the modified magnetic parameter
h_w	is a heat transfer coefficient
k_1	is the porous parameter
k	the thermal conductivity of the fluid/ thermophoretic coefficient

k^*	permeability of the porous medium
k_r	is the rate of chemical reaction
Kr	is the modified chemical reaction parameter
m	velocity exponent parameter
M	is the melting parameter
Pr	is the Prandtl number
Q	the dimensional heat generation/absorption coefficient
q_r	radiative heat flux
R	the suction parameter
R_d	thermal radiation parameter
Sc	the Schmidt number
Sr	the Soret number
T	the temperature of the fluid within the boundary layer
T_∞	ambient temperature
T_w	is the uniform temperature of the fluid at the plate
u	the velocity component along the x-axis
$U_e(x)$	is the free stream velocity
u_w	is the mass transfer velocity at the surface of the plate
v_0	is the suction/injection velocity
v	the velocity component along the y-axis
V	the velocity

Greek symbols

α_1	second grade parameter
β_T	volumetric coefficient of thermal expansion
γ_1	the heat generation/absorption parameter
λ	is the modified second grade fluid parameter
μ	fluid viscosity
ν	kinematic viscosity
ν_0	is the suction/injection velocity
θ	dimensionless temperature
ρ	is the density of the fluid
σ	the electrical conductivity
ψ	wedge angle parameter/ Inclination angle
ω	is the surface convection parameter

Chapter 1

Introduction

Newtonian and non-Newtonian fluids have been studied extensively, although there are research gaps that still need to be investigated. The fluid types differ in that Newtonian fluids have a constant viscosity for a given set of conditions while non-Newtonian fluids may have a viscosity that depends on the applied external force. In their behaviour and nature, Newtonian fluids are described by simpler mathematical equations as compared to non-Newtonian fluids. Examples of Newtonian fluids include, but are not limited to, liquids and gases such as water, organic solvents and air. Fluids such as brine, polymer solutions, certain oils and greases, and many emulsions are classified as non-Newtonian fluids [1]. Non-Newtonian fluids give a nonlinear relationship between stress and the rate of strain at any point in the flow. Due to the different physical structures found in non-Newtonian fluids, a single constitutive model can not present all the prominent characteristics of such fluids. In general, each non-Newtonian fluid has its own mathematical constitutive equation. Viscoelastic fluids are an important class of non-Newtonian fluids, in which viscosity may depend upon deformation rate and elastic behaviour. The most commonly used and simplest subclass of viscoelastic fluids is referred to as second grade fluids. The viscoelasticity leads to an increase in the order of differential equation(s) characterizing the flow. Second grade fluid problems are challenging to solve because the nonlinearity occurs not only in the inertia part of the equations but also the viscous terms. For this reason, inverse methods have been used in the study of non-Newtonian second grade fluids [2].

In the next sections, Newtonian and non-Newtonian models are discussed in detail. These sections focus on the description of the two broad categories of fluids, coupled with a review of the work that has been done on the flow and applications of these fluid types. We further discuss first, second and third grade fluids outlining their differences and the equations that differentiate the three models. This is followed by Falkner-Skan fluid flow, heat and mass transfer, stretching flow in non-Newtonian fluids, methods for solution of fluid flow equations, residual error and convergence, and finally the motivation for this research and the research objectives.

1.1 Newtonian fluids and non-Newtonian fluids

A Newtonian fluid is a power law fluid with a behaviour index $n = 1$, where the shear stress, τ is directly proportional to the rate of strain, that is,

$$\tau = \mu \frac{\partial u}{\partial y},$$

where μ is the fluid viscosity, u is the fluid velocity and y is the distance in the normal direction. For a contant temperature, these fluids have a constant viscosity, regardless of the shear stress applied. Common examples of Newtonian fluids include water, organic solvents, glycerine, air, honey, and other gases [3]. For Newtonian fluids, figure 1.1 shows an increase in stress with increasing shear rates, where the slope is the viscosity of the fluid.
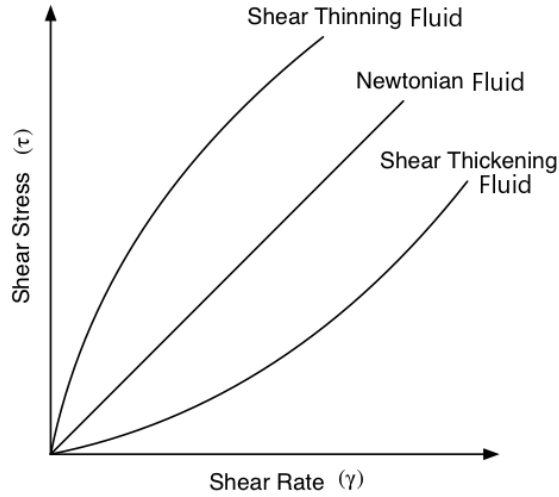
Figure 1.1: Behaviour of Newtonian, shear thinning and shear thickening fluids as a function of shear rate [4].

Sakiadis [5, 6] was the first to study a two dimensional, axisymmetric boundary layer flow over a stretched surface moving with constant velocity. Both exact and approximate solutions were presented for laminar flow with the latter obtained using the integral method. Crane [7] was among the first researchers to consider a steady boundary layer flow of a viscous incompressible fluid over a linearly stretching plate and gave a similarity solution in closed form. Rajagopal et al. [8] studied the flow of an incompressible second grade fluid past a stretching sheet. For varying elastic parameter values, it was found that the boundary layer thickness increases with the increase in the elastic parameter. For industrial applications, this showed the presence of normal stress inside the boundary layer. Chakrabart and Gupta [9] studied the magnetohydrodynamics flow of a Newtonian fluid initially at rest over a stretching sheet. Wu [10] carried out a comprehensive theoretical study of the flow behaviour of both single and multiple phase non-Newtonian fluids in porous media. A Buckley-Leverett type analytical solution for one-dimensional, immiscible non-Newtonian fluids in porous media was obtained. Moreover, an integral method was used to solve the equations of the transient flow of Bingham fluids in porous media. Simpson and Janna [11] studied power law fluids (pseudoplastic and dilatant), and Bingham fluids, and compared their solutions to those of Newtonian fluids for laminar flow in a circular duct. The velocity profiles for Newtonian and non-Newtonian fluid flow in a circular duct were described and sketched. Chamkha et al. [12] investigated the effects

3

of a chemical reaction on unsteady free convective heat and mass transfer on a stretching surface in a porous medium. The equations were solved numerically using a fourth order Runge-Kutta scheme with the shooting method. A parametric study illustrating the effects of various parameters on the flow and heat and mass transfer characteristics was performed. It was found that the skin friction coefficient increased as a result of increasing the unsteadiness parameter, suction/injection parameter, Prandtl number, Schmidt number, or the chemical reaction parameter. The Nusselt number was also predicted to increase due to increases in the Prandtl number, suction/injection parameter, or the unsteadiness parameter, and to decrease as either the chemical reaction parameter or the Schmidt number increased. The results obtained show that the flow field is influenced appreciably by the presence of the unsteadiness parameter, chemical reaction parameter, permeability parameter, and suction/injection parameter. Bhattacharyya et al. [13] used Lie's scaling group of transformations to study the flow of a Newtonian fluid over a stretching sheet with a chemically reactive species and first-order reaction. The reduced self-similar ordinary differential equations were solved by means of the finite difference method and Thomas algorithm. For the velocity field the exact solution was obtained while, for the concentration distribution, a numerical solution was found. However, the results showed that the concentration boundary layer thickness decreases with an increase in the Schmidt number as well as the reaction-rate parameter. Gireesha et al. [14] analyzed the influence of magnetohydrodynamic effects on melting in boundary layer stagnation-point flow of an electrically conducting nanofluid along a stretching surface. The nonlinear partial differential equations were transformed into ordinary differential equations using suitable similarity transformations. Using the Runge–Kutta–Fehlberg method, the transformed equations were solved numerically. The effect of flow parameters on different flow fields was determined and discussed in detail. For some limiting cases, the numerical results were found to be in good agreement with previously published results. It was also found that the induced magnetic field and temperature distributions increased with the strengthening of the hydromagnetic field. Mabood et al. [15] obtained an approximate solution for the MHD boundary layer flow of a viscous incompressible fluid over an exponentially stretching sheet. Through suitable similarity transformations, the flow equations were transformed into a system of nonlinear ordinary differential equations. The homotopy analysis method

4

(HAM) was used to solve the equations that describe the effects of radiation inside the hydrodynamic boundary layer. For some special cases, a comparison of the results with those previously published showed excellent agreement. Recently, Capobianchi et al. [16] investigated numerically, the thermocapillary motion of a Newtonian deformable droplet surrounded by a viscoelastic immiscible liquid for a wide range of conditions. The classical Oldroyd-B model was used for relatively small values of the thermal Deborah number.

Fluids in which the shear stress is not proportional to the shear strain at a given temperature and pressure are non-Newtonian. These are placed into three broad groups based on the behaviour of shear with stress. There are time-dependent fluids where the shear rate is a function of both the magnitude and the duration for the stress. Time-independent fluids are those for which the rate of shear is dependant merely upon the instantaneous shear stress at that point. Viscoelastic fluids show partial elastic recovery upon the removal of the deforming shear stress. Fluids that show both elastic and viscous properties are called elastic solids. In reality, most fluids are non-Newtonian, with viscosity being dependent on the shear rate, and so the fluids may be either shear thinning or thickening.As shown in Figure 1.1, a fluid is shear thinning if the viscosity decreases as the shear rate increases. Shear thinning fluids are also known as pseudo-plastics and include common fluids such as tomato ketchup, paints, and blood. In the case of shear thickening fluids, the viscosity of the fluid increases as the shear rate increases and include, for example, cornstarch [17–19].

1.2   First and second grade fluids

First grade fluids are considered to be Newtonian fluids. The viscosity of a first grade fluid is constant and does not change with time. The constitutive equation (1.1) is considered as an exact model for the classical Navier-Stokes theory. For a first grade fluid it is of the form,

$$\boldsymbol{T} = -p\mathbf{I} + \mu\mathbf{A_1}, \tag{1.1}$$

where $\boldsymbol{T}$ is a Cauchy stress tensor, p denotes the pressure, $\mathbf{I}$ is the identity tensor, μ is the coefficient of viscosity and $\mathbf{A_1}$ is a Rivlin-Ericksen tensor.

Non-Newtonian fluids may also be called differential type fluids. An important subclass of these differential type of fluids is second grade fluids. Second grade fluids are the simplest subclass because exact solutions can be found for their constitutive equations. Examples of second grade fluids include blood, butter, starch suspension, coconut oil, shampoo, and paints. The viscoelasticity of second grade fluids leads to an increase in the order of differential equation(s) characterizing the flow [20]. Although, it is well established that second grade fluids do not show the shear thinning and shear thickening behavior. The general equation of the flow is, nevertheless, highly nonlinear in comparison to the equation for Newtonian fluids. The first model for a second grade fluids was proposed by Rivlin and Erickson [21] in the form

$$\boldsymbol{T} = -p\mathbf{I} + \mu\mathbf{A_1} + \alpha_1\mathbf{A_2} + \alpha_2\mathbf{A_1}^2, \tag{1.2}$$

where $\boldsymbol{T}$, p, $\mathbf{I}$ and μ are as defined earlier, α_1 and α_2 denote the elasticity and cross-viscosity, while $\mathbf{A_1}$ and $\mathbf{A_2}$ are Rivlin-Ericksen tensors defined by

$$\begin{aligned} \mathbf{A_1} &= \mathbf{L} + \mathbf{L}^\mathsf{T}, \\ \mathbf{A_2} &= \frac{d}{dt}\mathbf{A_1} + \mathbf{A_1}\mathbf{L} + \mathbf{L}^\mathsf{T}\mathbf{A_1}. \end{aligned} \tag{1.3}$$

Here $\mathbf{L}$ is the velocity gradient, d/dt denotes the material derivative and the superscript T indicates the transpose operation. In recent years, researchers have studied the flow and heat transfer characteristics of viscoelastic fluids. The idea of MHD channel flows

has generated great interest due to their applicability in cooling systems, MHD generators, pumps, and flow meters. Mohyuddin and Ashraf [22] obtained the exact solutions of nonlinear equations describing the flow for a second grade fluid in a porous medium. It was indicated that the velocity, stream function, and pressure are strongly dependant upon the second grade fluid parameter. It was also shown that an increase in the second grade parameter leads to a decrease in the velocity. Hayat et al. [23] found the analytic solutions for a second grade fluid using the homotopy analysis method. Parida et al. [24] studied the effect of a magnetic field on an electrically conducting second grade fluid in a channel. Numerical solutions were obtained using the Runge-Kutta fourth order method together with a shooting technique. Using the homotopy analysis method to obtain analytical solutions, Nadeem et al. [25] studied the boundary layer flow and heat transfer in a second grade fluid flow through a horizontal cylinder, wherein they analyzed the influence of various parameters on velocity. Akbar et al. [26] presented a study of the theoretical properties of a second grade fluid flow in a porous medium. Shah et al. [27] studied the effects of the Grashof and Prandtl numbers on MHD second grade fluid flow over a stretching sheet. The system of two dimensional partial differential equations was transformed into a system of ordinary differential equations, which was then solved using the homotopy analysis method. The effects of non-dimensional parameters such as the unsteadiness parameter, film thickness, Hartmann number, surface skin friction coefficient, Prandtl number, thermocapillary number, heat flux, and free surface temperature were discussed and sketched. Fetecau et al. [28] provided some exact solutions for the laminar flow of a second grade fluid due to a sphere with oscillatory shear stresses. Using finite Henkel transformations the non-trivial shear stresses corresponding to the meridional flow component of the velocity were determined. An investigation by ur Rahman et al. [29] into the flow and heat transfer from a modified second grade nanofluid over a nonlinearly stretching sheet assumed passive control of nanoparticles at the boundary. The shooting method along with the Runge-Kutta Fehlberg scheme was used to solve the boundary value problem. The study showed that increasing the Brownian motion parameter leads to a decay in the nanoparticle concentration profiles, while increasing the thermophoresis parameter leads to an increase in the concentration of nanoparticles.

The magnetohydrodynamic flow of differential type fluids has also been studied over the years. Different experimental, mathematical and numerical methods have been used to simplify and find the solutions for the boundary layer flow equations. Das et al. [30] studied the impact of thermal radiation in the MHD boundary layer flow of a second grade fluid past a stretching sheet with convective heat flux. The Nachtsheim-Swigert iteration technique together with a Runge-Kutta sixth-order integration scheme was used to solve the equations. The results were presented through graphs and tables showing the effect of the thermal radiation parameter on the fluid velocity, temperature, and concentration. Recently, Aman et al. [31] considered the unsteady heat and mass transfer in a second grade fluid flow over a flat plate with wall suction and injection. Their model assumed mixed convection, convective boundary conditions, and an oscillating wall. Approximate solutions of the model equations were obtained using Laplace transforms. The results were validated by comparison with the Stehfest algorithm. Recently, Prasad and Reddy [32] considered Hall effects on the hydromagnetic convective flow of an electrically conducting second grade fluid in a rotating porous channel using the Brinkman model. The exact solutions were found using the Laplace transform technique. They determined the steady-state velocity and temperature distributions, the shear stresses, and the Nusselt number.

1.3   Third grade fluids

It has been suggested that second grade fluids do not show the shear thinning and shear thickening behaviour. However, the model for third grade fluids is capable of describing such behavior. The equation of motion for a third grade fluid is, however, more complicated than the corresponding equation for second grade fluids [33]. The Cauchy stress tensor T for a third grade fluid is given as

$$\boldsymbol{T} = -p\mathbf{I} + \mu\mathbf{A_1} + \alpha_1\mathbf{A_2} + \alpha_2\mathbf{A_1}^2 + \beta_1\mathbf{A_3} + \beta_2(\mathbf{A_1}\mathbf{A_2} + \mathbf{A_2}\mathbf{A_1}) + \beta_3(\mathbf{tr}\mathbf{A_1}^2)\mathbf{A_1}, \quad (1.4)$$

8

where α_i, β_j for $i = 1,2$ and $j = 1,2,3$ are the material parameters of a third grade fluid and $\mathbf{A_i}$ for $i = 1,2,3$ are the first three Rivlin-Ericksen tensors defined by

$$\mathbf{A_1} = (\nabla V) + (\nabla V)^{\mathrm{T}}, \tag{1.5}$$

$$\mathbf{A_{n+1}} = \frac{d\mathbf{A_n}}{dt} + \mathbf{A_n}(\nabla V) + (\nabla V)^{\mathrm{T}}\mathbf{A_n} \qquad \mathbf{n = 1, 2}, \tag{1.6}$$

where ∇ is the gradient operator and the other terms are as previously defined. Using the thermodynamic compatibility conditions when the fluid is locally at rest, the Clausius-Duhem inequality holds and the assumption that the Helmholtz free energy is a minimum at equilibrium provides the following restrictions [34]:

$$\mu \geq 0, \quad \alpha_1 \geq 0, \quad \beta_1 = \beta_2 = 0, \quad -\sqrt{24\mu\beta_3} \leq \alpha_1 + \alpha_2 \geq \sqrt{24\mu\beta_3}. \tag{1.7}$$

Thus, model (1.4) reduces to

$$\boldsymbol{T} = \mu\mathbf{A_1} + \alpha_1\mathbf{A_2} + \alpha_2\mathbf{A_1}^2 + \beta_3(\mathbf{trA_1}^2)\mathbf{A_1}. \tag{1.8}$$

A large body of literature exists on the boundary layer flow and heat transfer in viscous second grade fluids. The third grade fluid model represents an attempt to provide a comprehensive description of the properties of viscoelastic fluids. Erdoğan [35] considered the flow of a third order fluid in the vicinity of a plane wall, suddenly set in motion. The velocity field was described by a fourth order nonlinear partial differential equation. The solution of the differential equation showed that for a short time, the fluid is non-Newtonian. However, for a long time, the fluid behaves like a Newtonian flow. Hayat et al. [36] studied the flow of a third grade fluid occupying the space above a wall. The Lie group method was used to reduce the third order partial differential equation to a second order ordinary differential equation. The perturbation method was then used to solve the reduced equa-

tion. Hayat and Kara [37] obtained the analytic solution for the time-dependent flow of an incompressible third grade fluid under the influence of a magnetic field of variable strength. The fluid was confined to an annular region between two coaxial cylinders, with the fluid motion being induced by the rotation of the inner cylinder with arbitrary velocity. Group theoretic methods were employed to analyze the nonlinear equations and a solution for the velocity field was obtained analytically. Hayat et al. [38] considered the steady third grade fluid in a porous half-space. The constitutive relationship for the modified Darcy law in a third grade fluid was proposed and the equations solved analytically using the homotopy analysis method. The significant impact of the non-Newtonian parameters on the velocity profiles was analyzed. Hayat et al. [39] investigated the heat transfer effects on the flow of a third grade fluid. Series solutions for the velocity and temperature were constructed. The nonlinear equations were solved using the homotopy analysis method. The influence of different parameters on the temperature profiles was discussed. The solution demonstrated the dependency of the flow behaviour on the viscoelastic parameters. Keimanesh et al. [40] studied a third grade non-Newtonian fluid flow between two parallel plates using the multistep differential transform technique as the method of solution. The multistep differential transform method (MDTM) was applied directly without requiring linearization, discretization, or perturbation. The performance of the MDTM was compared with the fourth order Runge–Kutta and other analytical methods such as the the homotopy perturbation method (HPM), homotopy analysis method (HAM), and differential transform method (DTM). The DTM was found to be a reliable method for solving certain nonlinear problems but it diverged for some highly nonlinear equations. Zaman et al. [41] analyzed Stokes's first problem for an MHD third grade fluid in a non-porous half-space with Hall currents. The nonlinear partial differential equations describing the problem were converted to a system of nonlinear ordinary differential equations using similarity transformations. The homotopy analysis method was used to find an analytical solution. The effects of dimensionless parameters on the velocity were shown as well as the effects of the fluid and physical parameters on the local skin friction coefficient. Recently, Zeb et al. [42] studied the flow of a third grade fluid in a helical screw rheometer, (HSR) with the effects of curvature neglected. The problem was described by second order nonlinear coupled differential equations, which were reduced to a single differential equation by us-

10

ing transformations. The Adomian decomposition method was used to obtain analytical expressions for the flow profiles and the volume flow rate.

Another flow of particular interest in this study is Falkner-Skan fluid flow. Many researchers have contributed to the literature on Falkner-Skan flows, both with and without an applied magnetic field. Falkner-Skan fluid flow has extensive applications within the field of aerodynamics and hydrodynamics. In this dissertation, we consider the Falkner-Skan boundary layer flow of a second grade nanofluid.

1.4   Falkner-Skan fluid flow

The study of the fluid flow moving towards a wedge is an important and essential aspect of fluid dynamics and heat rate transfer. The Falkner-Skan equation describes the class of the so-called similar laminar flows in the boundary layer on a permeable wall, and at varying main-stream velocity [43]. The nonlinear third order ordinary differential is given in the form

$$f''' + ff'' + \beta\big(1 - (f')^2\big) = 0, \tag{1.9}$$

subject to the boundary conditions,

$$f(0) = \gamma, \quad f'(0) = 0, \quad f'(\infty) = 1, \tag{1.10}$$

where f is a stream function, η is a dimensionless distance from the wall and β measures the pressure gradient in the stream direction, f' is the velocity component in the η-direction and f'' is the shear stress at the boundary wall. The parameter γ in the boundary condition is a measure of the mass flow rate through the boundary wall in either direction.

This equation was first derived by Falkner and Skan [44] and may be used to study convective heat transfer. Riley and Weidman [45] found similarity solutions for pressure gradient driven flow over a stretching boundary. Guedda and Hammouch [46] considered the laminar two dimensional steady incompressible, boundary layer flow past a stretching surface. Firstly, a family of velocity distributions outside the boundary layer with similarity solutions was determined. Then new exact solutions, called Pseudo-similarity, where the external velocity varies inversely-linear with the distance along the surface were examined. The properties of the solutions depended on the suction parameter. Furthermore, using the fourth order Runge-Kutta scheme together with the shooting method, numerical solutions were obtained. Ishak et al. [47] studied the problem of steady two dimensional laminar fluid flow past a moving wedge with suction or injection. The partial differential equations were transformed into the Falkner-Skan ordinary differential equation by means of suitable similarity variables. The implicit finite difference scheme known as the Keller-box method was used to solve the transformed equations. Numerical results for the velocity profiles and the skin friction coefficient were determined for several values of such parameters as the Falkner-Skan power law parameter. The numerical results showed reverse flow, as had also been found earlier by Riley and Weidman [45]. Seddeek et al. [48] studied the steady MHD Falkner-Skan flow and heat transfer over a wedge with variable viscosity, and thermal conductivity. Using a scaling group of transformations, the equations were transformed into ordinary differential equations and solved numerically using the Keller-box method. Numerical results for the local skin friction coefficient and the local Nusselt number, as well as the velocity and the temperature profiles, were presented for different physical parameters. Khan [49] studied the Falkner-Skan boundary layer flow of an incompressible viscous fluid and developed an iterative scheme to provide estimates for the exact solution of the problem. Based on the estimates, the generalized approximation method (GAM) was applied to obtain the approximate solution of the problem. The numerical simulation showed that only a few iterations generated by the GAM could lead to the exact solution. Martin and Boyd [50] obtained the Falkner–Skan solution for laminar boundary layer flow over a wedge with a slip boundary condition. A marching scheme was used to solve the boundary layer equations in the rarefied flow regime. Duque-Daza et al. [51] presented a computational study of the solution of the

Falkner-Skan equation using high order compact finite difference schemes. The accuracy of this technique was established by comparison of the data generated for accelerating, constant and decelerating flows with published data. An excellent agreement was observed. Hendi and Hussain [52] considered Falkner-Skan flow over a porous surface. Stream function formulation and suitable transformations reduced the problem to ordinary differential equations. The homotopy analysis method was used to solve the transformed equations. Keshtkar [53] analyzed the effect of variable viscosity and heat generation on classical Falkner–Skan flow. The velocity and temperature distribution were obtained for a wide range of Prandtl numbers. Marinca et al. [54] proposed an optimal homotopy approach to obtain approximate analytical solutions for the nonlinear Falkner-Skan differential equation. The effect of parameter β, a measure of the pressure gradient, was examined. Raju and Sandeep [55] studied thermophoresis and Brownian motion effects on magnetohydrodynamic radiative Casson fluid flow for a wedge. The transformed nonlinear differential equations were solved numerically using the Runge-Kutta and Newton methods. The results showed that the thermal, solute and momentum boundary layers are not uniform at different wedge positions. It was also observed that the heat and mass transfer rates are high when the wedge is moving forward. Madaki et al.[56] proposed a new analytical technique to obtain a solution to the Falkner–Skan equation, whereby a revised optimal homotopy asymptotic method (OHAM) was used to find an explicit analytical solution for two dimensional laminar, incompressible viscous fluid flow for Falkner–Skan wedge flow. The study showed the OHAM to be an effective analytical technique in comparison with other numerical and analytical methods, such as the fourth order Runge–Kutta, and HPM-Padé schemes. Bougoffa and Alqahtani [57] proposed a transformation variable that reduces the Falkner-Skan equation into an equivalent boundary value problem in a finite domain. They considered three special cases: Heimenz flow, Homann flow, and the Blasius problem. Analytic solutions were obtained by a direct method for large values of β.

1.5   Heat and Mass Transfer

Heat transfer is the exchange of thermal energy between physical systems at different temperatures. The rate of heat transfer is dependent on the temperatures of the systems and the properties of the intervening medium through which the thermal energy is being transferred. Heat is normally transferred from an object at a higher temperature to one at a lower temperature. There are three fundamental ways the heat can be transferred. These are firstly, conduction whereby heat is transferred between objects through direct contact. For example, the heat generated inside an enclosure is transferred to the outer surface using conduction. The second method is convection, which occurs when heat is transferred through a medium such as a fluid. As the fluid moves, the convective heat transfer increases. Lastly, radiation energy is transferred through the air as electromagnetic radiation. This method of heat transfer does not rely upon any contact between the heat source and the heated object [58, 59].

Mass transfer describes the net movement of a solute from one location to another. In other words, mass transfer is the transport of a substance in the liquid or gaseous phase. Mass transfer occurs in many processes, such as absorption, evaporation, adsorption, drying, precipitation, membrane filtration, and distillation. In many technical applications, heat transfer processes occur simultaneously with mass transfer processes [60, 61]. Depending on the context, an optical thickness maybe a measure for the absorption or for the effective optical path length of the sample. Optical thickness is applied to an entire path through a medium.

In this study, we study heat and mass transfer due to the motion of second grade fluids, in a porous medium and along a stretching sheet. In the next section, we give a brief literature review of non-Newtonian fluid flows along a stretching sheet.

1.6 Stretching flow in non-Newtonian fluids

The viscous flow and heat transfer in the boundary layer region due to a stretching sheet has wide theoretical and technical applications in manufacturing and industries, such as the extraction of polymer sheets, wire drawing, glass fibre production, and the cooling and drying of paper and textiles. Banks [62] found similarity solutions of the boundary layer equations for a stretching wall. His solutions did not find dual solutions for impermeable stretched surfaces. Banks and Zaturska [63] found eigen solutions for a one-parameter family of boundary layer solutions corresponding to a stretching wall. The eigen solution was found to represent a disturbance that decays in an appropriate region of the flow field. Pontrelli [64] solved the full set of partial differential equations by a collocation method using B-splines. Rao [65] extended the study by specifying the range of the non-Newtonian parameter for which the solution of the problem is unique. The positive non-Newtonian parameter gives a unique solution to the problem. Liao [66] used the homotopy analysis method to solve the equations for the magnetohydrodynamic viscous flows in non-Newtonian fluids. For the second and third order power-law power-law fluids, explicit analytic solutions were expressed by recursive formulae of constant coefficients. In particular, a simple analytic formula for the dimensionless velocity gradient at the wall was found. Liao [67] solved the boundary layer flow over a stretched impermeable wall using the homotopy analysis method. Two branches of solutions were found. It was noted that the difference in skin friction in the two branches is small, even when the corresponding profiles of velocity were distinct.

Miklavčič and Wang [68] investigated the viscous fluid flow induced by its flowing over a shrinking sheet. For the shrinking sheet, the fluid behaviour was found to differ from that in the case of stretching. Fang [69] extended the shrinking sheet problem by assuming a power law velocity. The effect of the power index on the wall drag was investigated. Unique solution behaviours were found for a shrinking sheet and compared to those for a stretching sheet. Cortell [70] examined steady laminar boundary layer flow in terms of heat transfer for an electrically conducting second grade fluid, subject to suction and a transverse uniform magnetic field past a semi-infinite stretching sheet. The resulting partial

differential equations were converted into ordinary differential equations using a suitable similarity transformation. The effects of viscous dissipation and work due in deformation were considered in the energy equation. Abel and Mahesha [71] investigated the magnetohydrodynamic boundary layer flow behaviour and heat transfer in viscoelastic flows over a stretching sheet with radiation. The boundary layer partial differential equations were converted into a set of nonlinear ordinary differential equations by applying similarity transformations. Nadeem et al. [72] derived the analytic solutions of a boundary layer flows bounded by a shrinking sheet. Sajid and Hayat [73] considered the MHD viscous flow problem for a shrinking sheet. Exact series solution of two dimensional and axisymmetric shrinking was obtained using the homotopy analysis method. Fang et al. [74] solved the equations for a viscous flow over a shrinking sheet subject to a second order slip velocity flow model. A closed-form solution was derived. The effects of the two slip parameters and the mass suction parameter on the velocity distribution were presented. The velocity and the surface shear stress on a shrinking sheet are strongly influenced by the mass transfer and the slip flow parameters. Akyildiz et al. [75] considered a class of nonlinear third order differential equations arising in a fluid flow over a nonlinearly stretching sheet. Numerical solutions were obtained and presented through graphs, and the influence of the physical parameter on the flow characteristics discussed. Similarity solutions for the nano-boundary layer flows with a Navier boundary condition were presented by van Gorder et al. [76]. The nonlinear ordinary differential equations were solved analytically using the homotopy analysis method. Ahmad and Asghar [77] investigated the boundary layer flow of a second grade fluid over a permeable stretching surface with arbitrary velocity and appropriate wall transpiration. The fluid was electrically conducting and subjected to a constant applied magnetic field. The exact solutions were derived and presented. Bhattacharyya and Vajravelu [78] presented an analysis of stagnation-point flow and heat transfer over an exponentially shrinking sheet. The similarity equations were obtained and solved numerically using a shooting method. The study revealed that the range of velocity ratio parameter is larger than in the linear sheet shrinking case. Zheng et al. [79] presented a study of the boundary layer flow and heat transfer of a micropolar fluid over a nonlinearly stretching/shrinking sheet. The flow was generated due to the power law surface velocity and temperature distributions. Dual solutions were obtained using the

homotopy analysis method. For the shrinking case, the influence of physical parameters on the two branches was determined. For the stretching case, the influence on the temperature distribution was comparatively more complicated. Patil [80] performed a numerical study for the problem of steady mixed convection flow from a vertical stretching sheet in a parallel free stream with variable wall temperature and concentration. An implicit finite difference scheme in combination with the quasilinearization technique was used to obtain non-similar solutions of the boundary layer equations. The effect of parameters on the velocity and temperature profiles was presented. Misra et al. [81] considered an unsteady boundary layer flow of a viscous incompressible fluid over a stretching plate. The heat flow problem was solved for two different cases; namely the prescribed stretching surface temperature (PST) and prescribed stretching surface heat flux (PHF) flow. Mahanta [82] investigated the flow and heat transfer in two dimensional electrically conducting second grade fluids over a stretching surface subjected to a uniform magnetic field. The non-linear boundary layer equations were solved numerically using the Runge-Kutta shooting method. Numerical solutions were presented for the fluid flow and heat transfer characteristics for different values of fluid and physical parameters.

Until relatively recently, it had been emphasized by many authors that a solution for a shrinking sheet is only possible for permeable sheets and that no solution exists for impermeable sheets. However, in 2013, Asghar et al. [83] presented an exact analytical solution for the boundary layer flow of a viscous fluid over an impermeable sheet of variable thickness. The skin friction coefficient was found to differ from that of a permeable sheet. Also, the solution was unique, in contrast to the dual solution for a flat shrinking sheet. Khan and Shahzad [84] analyzed the development of the steady boundary layer flow over a nonlinearly stretching sheet in a Sisko fluid. The equations were solved analytically using the homotopy analysis method. Chaudhary and Kumar [85] studied the stagnation point flow of a two dimensional electrically conducting fluid past a shrinking sheet with slip boundaries and a magnetic field. The similarity equations were derived and then solved numerically using the shooting method. Munir et al. [86] investigated heat transfer in the steady axisymmetric flow of a second grade fluid over a radially stretching porous sheet. The transformed ordinary differential equations were solved analytically using the

homotopy analysis method and numerically using both the shooting and adaptive Runge Kutta methods. The reliability of numerical solutions was verified using the analytical results. Khan and Rahman [87] analyzed the two dimensional boundary layer flow and heat transfer in a modified second grade fluid over a nonlinearly stretching sheet at constant surface temperature. The equations were solved numerically using the fourth and fifth order Runge-Kutta-Fehlberg method. It was found that the power law index reduces both the momentum and thermal boundary layer thicknesses.

Recently, Bakar et al. [88] made a numerical study of the steady boundary layer flow over a stretching/shrinking cylinder with suction effect. The partial differential equations were solved numerically using a bvp4c code in Matlab software. The numerical results so obtained confirmed that for a certain range of values for the stretching/shrinking and suction parameters, there exist two solution branches for different values of the curvature parameter. Stability analysis showed that the first solution is linearly stable, while the second solution is linearly unstable. Kumar et al. [89] studied the effect of Brownian motion and thermophoresis on MHD Carreau and Casson fluid flows towards a stretching surface with a magnetic field effect. Numerical results showed that the thermal and concentration transport in a Casson fluid is comparatively higher than in the case of a Carreau fluid. It was also noticed that the Carreau fluid is highly affected by a Lorentz force , unlike the case of the Casson fluid.

1.7 Solution of fluid flow equations

In this section, we discuss the numerical and analytic methods that have been used to solve nonlinear partial differential equations, more especially the second grade fluid equations. For the different methods, we discuss their properties, strengths, and weaknesses, and consider some suggestions offered to overcome the disadvantages.

1.7.1 The homotopy analysis method

The homotopy analysis method developed by Liao [90] is a powerful mathematical tool for solving nonlinear problems. The HAM provides a useful analytic tool for investigating problems in science, finance, and engineering that are highly nonlinear and have multiple solutions and singularity. Unlike other analytic techniques, the HAM provides a convenient way of guaranteeing that the solution series converges, so that it will be valid for highly nonlinear problems. It also provides great freedom in choosing the base functions for the solution. In the literature, the following advantages of the homotopy analysis method have been cited: using the method does not depend on the existence of small or large physical parameters, it guarantees convergence, and, as stated already, it offers flexibility in the choice of base functions and initial guess to the solution [91]. Turkyilmazoglu [92] used the homotopy analysis method to obtain convergent series solutions of strongly nonlinear problems. Lu and Liu [93] used the method to solve the variable coefficient KdV-Burgers equation. They used the generalized elliptic method and Fourier's transform method to obtain approximate solutions of double periodic form. The results indicated that the homotopy analysis method is efficient for nonlinear models with dissipative terms and variable coefficients. Akram and Sadaf [94] also applied the homotopy analysis method to solve a ninth order boundary value problem. Their numerical results showed the homotopy analysis method to give a good approximation for the exact solutions. Various improvements to this method have been proposed in the past two decades.

1.7.2 Finite difference methods

The finite difference method (FDM) is a method for finding approximate solutions for differential equations. It has been used to solve a wide range of problems, including linear and nonlinear, time-independent and dependent problems. This method can be applied to problems with different boundary shapes, different kinds of boundary conditions, and a region containing several different materials [95]. When using the FDM, the idea is to replace the derivatives of an unknown function by difference equations. The stability of the scheme depends on the physical problem modelled. Finite differences are particularly

suitable for regular grids, where boundary conditions are easier to implement than over irregular grids [96]. An approach corresponding to a particular mathematical model may result in either explicit and implicit finite difference schemes. The explicit finite difference schemes use a forward difference in time and a central difference in space. For this method, one needs to know the values at the current time interval to determine the values at the next time interval. The implicit schemes solves an equation using both the current state of the system and a later one. It is dependent on the solution of a large number of linear algebraic equations. Using this method may often be tedious and intensive as it requires solving a large system of equations. Nevertheless, implicit finite difference schemes have the advantage of often being unconditionally stable [97].

In many nonlinear problems, the standard difference schemes exhibit numerical instability and give spurious solutions. The standard numerical integrators are referred to as the explicit forward Euler and the Runge–Kutta family of finite difference methods [98]. In general, standard difference schemes preserve the properties of the differential equations only if the discretization parameter h is sufficiently small. To find approximations for the solutions, equations are often linearized and the nonlinear terms discarded. Therefore, application to models over large time intervals using small-time steps requires very large computational effort, so these discrete models are inefficient. Furthermore, for some problems, standard difference schemes cannot preserve the properties of the problem for any step size. To overcome the phenomenon of numerical instabilities, Mickens introduced the concept of non-standard finite difference (NSDF) schemes [99]. The NSDF schemes are constructed following a set of five basic rules. The NSDF schemes preserve the main properties of the differential equation, such as positivity, monotonicity, periodicity, stability and some other invariants including energy and geometrical shapes. However, the approach also has some weaknesses and limitations; for example, it is applicable only when all the equilibrium points are hyperbolic.

Common examples of finite difference schemes include the Keller-box method, which was

developed by Cebeci and Bradshaw [100]. It is the most popular numerical method used to solve unsteady boundary layer flow problems. It is one of the important techniques for solving the parabolic flow equation, especially the boundary layer equations. The disadvantage of the method is that the computational effort per time step is expensive [101].

1.7.3 Runge-Kutta-Fehlberg method

The Runge–Kutta method is an effective and widely used method for solving initial value problems. Since the instability that may arise in the Runge–Kutta methods can usually be reduced by minimuzing the step size reduction, the method has partial instability. To avoid repeated reduction of the value of h-size and rerunning the method, an estimate of the value of h-size that would provide stability for the fourth order Runge–Kutta methods can usually be determined [102]. Runge–Kutta methods are classified as being second order, third order, fourth and fifth order, or the Runge–Kutta–Fehlberg method. The Runge–Kutta–Fehlberg method is the most commonly used method for solving second grade fluid problems. The Runge–Kutta–Fehlberg method guarantees accuracy in the solution of an initial value problem (IVP) by solving the problem twice using step sizes h and $h/2$ and comparing answers at the mesh points corresponding to the larger step size [103].

1.7.4 Spectral methods

Spectral methods were developed by Orszag starting in 1969 for finite and unbounded problems [104–106]. Spectral methods can achieve high accuracy with comparatively few grid points, because they use all available function values to construct the required approximations. They are thus called global methods. These methods become less accurate for problems with complex geometries and discontinuous coefficients. Furthrmore, they can provide higher accuracy, at the expense of domain flexibility. The most commonly used basis functions are the Legendre, Lagrange, Laguerre, and Chebyshev polynomials [107].

Spectral methods are accurate, easy to implement and are computationally efficient. Partial differential equations have been solved using spectral collocation in space and finite differences in time. In recent years methods that involve quasilinearization together with spectral methods have become common. These include the spectral quasilinearization method (SQLM), spectral relaxation method (SRM) and spectral local linearization method (SLLM) [108–110]. Applying the spectral method in space improves the accuracy, convergence and computational time of the finite differences methods. Motsa et al. [110] used relaxation and quasilinearization schemes to solve unsteady boundary layer problems. The SRM and SQLM are Chebyshev pseudospectral based methods that have been successfully used to solve nonlinear boundary layer flow problems described by systems of ordinary differential equations. These methods were extended, to systems of nonlinear partial diferential equations (PDEs) describing unsteady boundary layer flows. Numerous studies were conducted to determine the accuracy of the methods and compare theIR computational performance against the popular Keller-box finite difference scheme. Although these spectral methods in space improved the accuracy, convergence and computational time of the finite differences methods, these aspects were, nevertheless, still compromised. Accordingly, to overcome these disadvantages, Motsa et al. [111] introduced a new bivariate spectral quasilinearization method (BSQLM) that uses Chebyshev spectral collocation, bivariate Lagrange interpolation polynomials together with quasilinearization techniques. The nonlinear evolution equations are first linearized using the quasilinearisation method. The discretization is done independently in space and time variables of the linearized differential equation.

The bivariate method is suitable for, among other applications, solving equations arising in fluid mechanics. In order to develop the iteration scheme for a third order coupled system of three nonlinear partial differential equations, we write the equations as

$$\Omega_k[F, T, H] = 0, \quad k = 1, 2, 3, \tag{1.11}$$

where $\Omega_1, \Omega_2, \Omega_3$ are nonlinear operators and F, T, H are defined as

$$F = \left\{ f, \frac{\partial f}{\partial \eta}, \frac{\partial^2 f}{\partial \eta^2}, \frac{\partial^3 f}{\partial \eta^3}, \frac{\partial^2 f}{\partial \xi \partial \eta} \right\}, \qquad T = \left\{ \theta, \frac{\partial \theta}{\partial \eta}, \frac{\partial^2 \theta}{\partial \eta^2}, \frac{\partial^2 \theta}{\partial \xi \partial \eta}, \frac{\partial \theta}{\partial \xi} \right\},$$
$$H = \left\{ \phi, \frac{\partial \phi}{\partial \eta}, \frac{\partial^2 \phi}{\partial \eta^2}, \frac{\partial^2 \phi}{\partial \xi \partial \eta}, \frac{\partial \phi}{\partial \xi} \right\}, \tag{1.12}$$

where f is the stream function, θ is a temperature, and ϕ is the solute concentration. The quasilinearization method uses the Taylor series expansion of Ω_k about some previous approximation of the solution denoted by F_r, T_r, H_r. The assumption is that the difference between current and previous solutions is small. Thus, applying quasilinearization to (1.11) gives

$$\Omega_k[F, T, H] \approx \Omega_k[F_r, T_r, H_r] + (F - F_r, T - T_r, H - H_r). \triangledown \Omega_k[F_r, T_r, H_r],$$

where ∇ is a vector of partial derivatives defined as

$$\nabla = \{\nabla_f, \nabla_\theta, \nabla_\phi\},$$

and,

$$\nabla_f = \left\{ \frac{\partial}{\partial f}, \frac{\partial}{\partial f'}, \frac{\partial}{\partial f''}, \frac{\partial}{\partial f''}, \frac{\partial}{\partial f'''}, \frac{\partial}{\partial f'_\xi}, \right\}, \qquad \nabla_\theta = \left\{ \frac{\partial}{\partial \theta}, \frac{\partial}{\partial \theta'}, \frac{\partial}{\partial \theta''}, , \frac{\partial}{\partial \theta_\xi}, \right\},$$
$$\nabla_\phi = \left\{ \frac{\partial}{\partial \phi}, \frac{\partial}{\partial \phi'}, \frac{\partial}{\partial \phi''}, , \frac{\partial}{\partial \phi_\xi}, \right\}. \tag{1.13}$$

The prime in (1.13) denotes partial derivatives with respect to η. The solution procedure assumes that the solution for $f(\xi, \eta)$, $\theta(\xi, \eta)$ and $\phi(\xi, \eta)$ can be approximated using a bivariate Lagrange interpolation polynomial of the form

$$f(\xi, \eta) = \sum_{i=0}^{N_x} \sum_{j=0}^{N_t} f(\tau_i, \zeta_j) L_i(\tau) L_j(\zeta),$$

$$\theta(\xi, \eta) = \sum_{i=0}^{N_x} \sum_{j=0}^{N_t} \theta(\tau_i, \zeta_j) L_i(\tau) L_j(\zeta), \tag{1.14}$$

$$\phi(\xi, \eta) = \sum_{i=0}^{N_x} \sum_{j=0}^{N_t} \phi(\tau_i, \zeta_j) L_i(\tau) L_j(\zeta),$$

where N_x and N_t are the number of grid points in the x and t directions respectively, L_i and L_j are the standard Lagrange cardinal functions and τ and ζ are in $[-1, 1]$. Moreover, a linear transformation is used to map η and ξ to τ and ζ. Approximate equations (1.14) interpolate $f(x,t)$, $\theta(x,t)$ and $\phi(x,t)$ at selected collocation points in both the x and t directions defined by

$$\tau_i = \cos\left(\frac{\pi i}{N_x}\right), \quad \zeta_j = \cos\left(\frac{\pi}{N_t}\right), \quad i = 0, 1, 2...N_x, \qquad j = 0, 1, 2...N_t. \tag{1.15}$$

Collocating at the Gauss-Lobatto points ensures that there is a simple conversion of the continuous derivatives, in both space and time, to discrete derivatives at the grid points. The derivatives are approximated at the collocation points using the Chebyshev differentiation matrix with

$$\frac{\partial G}{\partial \eta} = \sum_{p=0}^{N_\eta} D_{ip} G(\tau_p, \zeta_j) = \mathbf{D}G(\tau_i, \zeta_j); \qquad \frac{\partial G}{\partial \xi} = \sum_{k=0}^{N_\xi} d_{jk} G(\tau_i, \zeta_k) = \sum_{k=0}^{N_\xi} \mathbf{d}_{jk} G(\tau_i, \zeta_k),$$

$$\tag{1.16}$$

where $\mathbf{D}$ and $\mathbf{d}$ are the scaled differentiation matrices. Higher-order derivatives with respect to η are defined as

$$G^{(o)}(\eta, \xi) = \mathbf{D}^{(o)}G(\tau_i, \zeta_j), \qquad i = 0, 1, 2...N_\eta, \qquad j = 0, 1, 2...N_\xi. \qquad (1.17)$$

Using the matrix-vector differentiation matrices gives

$$A_{1,1}^i F_i - \zeta_i(1 - \zeta_i) \sum_{j=0}^{N_\eta} \mathbf{d}_{ij}\mathbf{D}F_j + A_{1,2}^i T_i + A_{1,3}^i H_i = R_{1,i}, \qquad (1.18)$$

$$A_{2,1}^i F_i + A_{2,2}^i T_i - \zeta_i(1 - \zeta_i) \sum_{j=0}^{N_\eta} \mathbf{d}_{ij}\mathbf{D}T_j + A_{2,3}^i H_i = R_{2,i}, \qquad (1.19)$$

$$A_{3,1}^i F_i + A_{3,2}^i T_i + A_{3,3}^i H_i - \zeta_i(1 - \zeta_i) \sum_{j=0}^{N_\eta} \mathbf{d}_{ij}\mathbf{D}H_j = R_{3,i}. \qquad (1.20)$$

In the above equations, O is an $(N_x + 1) \times (N_x + 1)$ matrix of zeros and the coefficients $a_{r,i}$, $b_{r,i}$, $c_{r,i}$ are obtained from evaluating $a_{r,i}(\eta, \xi)$, $b_{r,i}(\eta, \xi)$ and $c_{r,i}(\eta, \xi)$ at the collocation points for $r = 1, 2, \dots$. The accuracy of the BSQLM improves with an increase in the number of collocation points N_x [112].

1.8   Residual error and convergence

Error norms and residual errors are used to test the convergence and accuracy of the numerical solutions obtained. The error norm is the difference between successive approximations, while the residual error defines the extent to which the solutions are approximated. The residual errors of the solutions $f(\eta, \xi)$, $\theta(\eta, \xi)$, $\phi(\eta, \xi)$ for each ξ are defined approximately as

$$Res(s) = ||\Omega_k[F_{r+1,j}, T_{r+1,j}, H_{r+1,j}]||_\infty \qquad j = 0, 1, 2, ...N_\xi, \qquad (1.21)$$

where $s = [f, \theta, \phi]$. The error norms are defined as

$$E_s = ||\mathbf{S}_{r+1,j} - \mathbf{S}_r, j|| \qquad j = 0, 1, 2, ... N_\xi. \tag{1.22}$$

1.9   Motivation and objectives

The aim of this study is to develop and solve numerically a mathematical model for magnetohydrodynamic (MHD) two dimensional boundary layer flow of a second grade nanofluid in a porous medium. We solve the equations for a second grade fluid flow along a wedge, and for flow past a semi-infinite stretching sheet with a convective surface. The model equations are nondimensionalized and solved numerically using the bivariate spectral-quasilinearization method. We determine the effect of the second grade parameter, magnetic parameter, thermal radiation parameter, porous parameter and chemical reaction parameter on the flow characteristics and behaviour. The residual errors are calculated to determine the accuracy of the method.

In Chapter 2, the MHD flow of a second grade fluid in a porous channel is investigated. The bivariate spectral quasilinearization method for nonlinear evolution equations is used to obtain the numerical solutions. The effect of fluid parameters on the fluid velocity is analyzed. The accuracy and convergence of the method is tested through residual error analysis.

In Chapter 3, the bivariate spectral quasilinearization method is applied to a system of two partial differential equations. The objective is to study the flow of an electrically conducting incompressible second grade fluid past a flat sheet. The BSQLM is used to obtain the temperature and temperature profiles. The behaviour of fluid properties with different physical parameters is discussed. Finally, the residual error analysis is used to determine the convergence and the accuracy of the method.

In Chapter 4, the bivariate spectral quasilinearization method is applied to a system

of transformed partial differential equations describing a second grade nanofluid flow over a wedge in a porous medium with the presence of porosity and inertia coefficient. The velocity and the temperature profiles are determined for several values of parameters such as melting, wedge angle, heat generation, and absorption parameters. The convergence of the method is analyzed using residual error analysis. Moreover, the current results are compared with solutions published in the literature to show the accuracy of the method.

In Chapter 5, we study the effect of a chemical reaction and viscous dissipation on MHD second grade fluid flow past a convectively heated stretching sheet. The partial differential equations are non-dimensionalized using a suitable similarity transformation. The BSQLM is then used to solve the problem numerically. The numerical results are discussed using graphs and tables. The impact of the magnetic field and thermal radiation on heat and mass transfer is analyzed. The results are compared with previous solutions from the literature to gain a sense of the accuracy of the method.

In Chapter 6, we conclude the dissertation by summarizing the findings.

Chapter 2

MHD flow of a second grade fluid in a porous medium

In this chapter, the problem of an incompressible MHD flow of a second grade fluid in a porous channel is investigated using the bivariate spectral quasilinearization method. The equations that model the boundary layer flow are nonlinear partial differential equations in space and time. The effect of the dimensionless parameters on the fluid velocity is considered. We start by formulating the model equations.

Consider an incompressible second grade fluid in a porous channel of width H, as shown in Figure 2.1. The lower and upper walls of the channel are at $y = -H/2$ and $y = H/2$, respectively. We select the x-axis and y-axis to be, respectively, parallel and perpendicular to the channel walls. A constant magnetic field B_0 is applied perpendicular to the channel walls, the induced magnetic field, and the electric field are assumed to be negligible. It is further assumed that the pressure gradient is zero and the flow is symmetric about both axes.
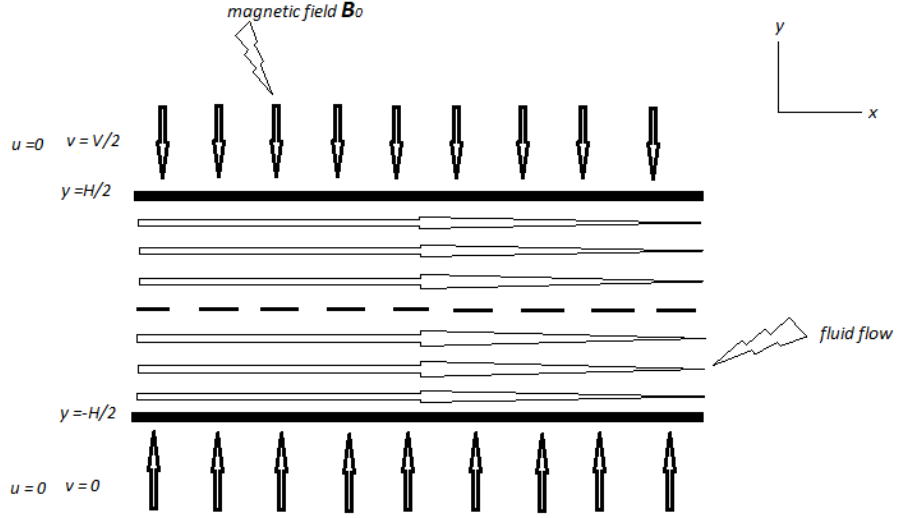
Figure 2.1: The problem set up and orientation of the coordinate system

The conservation equations that describe the MHD boundary layer flow are [70]

$$u\frac{\partial u}{\partial x} + v\frac{\partial u}{\partial y} = 0, \tag{2.1}$$

$$u\frac{\partial u}{\partial x} + v\frac{\partial u}{\partial y} = \nu\frac{\partial^2 u}{\partial y^2} + \frac{\alpha_1}{\rho}\left[\frac{\partial u}{\partial x}\frac{\partial^2 u}{\partial y^2} + u\frac{\partial^3 u}{\partial x\partial y^2} + \frac{\partial u}{\partial y}\frac{\partial^2 v}{\partial y^2} + v\frac{\partial^3 u}{\partial y^3}\right] - \frac{\sigma B_0^2}{\rho}u. \tag{2.2}$$

The boundary conditions,

$$\frac{\partial u}{\partial y} = v = 0 \qquad \text{at} \qquad y = 0,$$

$$u = 0, \qquad v = \frac{V}{2} \qquad \text{at} \qquad y = \frac{H}{2}. \tag{2.3}$$

Here ρ is the density, ν the kinematic viscosity, σ the electrical conductivity and α_1 the material parameter of the second grade fluid, u and v the velocity components in the $x-$ and $y-$directions. The fluid injection or extraction takes place through the porous walls with velocity $V/2$. Note that $V > 0$ corresponds to the suction case and $V < 0$ for injection. Applying the following transformations [80].

$$u = U_0 x^m f'(\xi, \eta), \qquad v = -\frac{1}{2}(\nu U_0) x^{\frac{m-1}{2}} \{(m+1)f + (1-m)(\xi \frac{\partial f}{\partial \xi} - \eta f'),$$

$$T - T_\infty = (T_w - T_\infty)\theta(\xi, \eta), \qquad \xi = \left(\frac{\nu}{U_0}\right)^{\frac{1}{2}} x^{\frac{1-m}{2}}, \qquad \eta = \left(\frac{U_0}{\nu}\right)^{\frac{1}{2}} x^{\frac{m-1}{2}} y,$$

to equations (2.1) - (2.2) , we find that equation (2.1) is identically satisfied, and equation (2.2) reduces to

$$U_0^2 x^{2m-1} \left\{ \frac{1-m}{2} \xi f' \frac{\partial f'}{\partial \xi} + m f'^2 - \frac{m+1}{2} f f'' - \frac{1-m}{2} \xi f'' \frac{\partial f}{\partial \xi} \right\} = U_0^2 x^{2m-1} f'''$$
$$+ \frac{U_0^3 x^{3m-2}}{\rho \nu} \left\{ \frac{1-m}{2} \xi \left(f''' \frac{\partial f'}{\partial \xi} + f^{iv} \frac{\partial f}{\partial \xi} \right) + (3m-1) f' f''' + \frac{1-m}{2} \xi f' \frac{\partial f'''}{\partial \xi} \right.$$
$$\left. + \frac{m+1}{2} f' f^{iv} + \frac{3m-1}{2} f''^2 \right\} - \frac{\sigma B_0^2 U_0 x^m}{\rho} f' \tag{2.4}$$

and then equation (2.4) take the following form,

$$f''' + \frac{m+1}{2} f f'' - m f'^2 - Ha^2 f' + \lambda \left[(3m-1) f' f''' - \frac{m+1}{2} f f^{iv} - \frac{3m-1}{2} f''^2 \right.$$
$$+ \frac{m-1}{2} \xi \left(f^{iv} \frac{\partial f}{\partial \xi} - f''' \frac{\partial f'}{\partial \xi} + f'' \frac{\partial f''}{\partial \xi} - f' \frac{\partial f'''}{\partial \xi} \right) \right]$$
$$- \frac{m-1}{2} \xi \left(f'' \frac{\partial f}{\partial \xi} - f' \frac{\partial f'}{\partial \xi} \right) = 0. \tag{2.5}$$

The boundary conditions (2.3) then become

$$\begin{aligned} f = 0, \qquad f'' = 0 \qquad &\text{at} \qquad \eta = 0, \\ f = \frac{1}{2}, \qquad f' = 0 \qquad &\text{at} \qquad \eta = \frac{1}{2}, \end{aligned} \tag{2.6}$$

where, $\lambda = \alpha_1 U_0 / \rho \nu$ and $Ha = \sigma B_0^2 / \rho U_0$.

We apply the spectral quasilinearization method by assuming that the difference between two successive iterations $||f_{r+1} - f_r||$, and all associated derivatives, are small. Applying the quasilinearization method to equation (2.5) gives

$$a_{0r} f_{r+1}^{iv} + a_{1r} f_{r+1}''' + a_{2r} f_{r+1}'' + a_{3r} f_{r+1}' + a_{4r} f_r + \alpha_{0r} \frac{\partial f_r}{\partial \xi} + \alpha_{1r} \frac{\partial f_r'}{\partial \xi} + \alpha_{2r} \frac{\partial f_r''}{\partial \xi}$$

$$+ \alpha_{3r} \frac{\partial f_r'''}{\partial \xi} = 0, \tag{2.7}$$

and the boundary conditions (2.6) become

$$f_{r+1} = 0, \qquad f_{r+1}'' = 0 \qquad \text{at} \qquad \eta = 0,$$

$$f_{r+1} = \tfrac{1}{2}, \qquad f_{r+1}' = 0 \qquad \text{at} \qquad \eta = \tfrac{1}{2}. \tag{2.8}$$

Applying spectral collocation to (2.7), these equations can be simplified further by introducing coefficients as follows,

$$[a_{0r} D^{iv} + a_{1r} D^3 + a_{2r} D^2 + a_{3r} D + a_{4r}] f_{r+1} + 2 \sum_{j=0}^{N_\xi} [\alpha_{0r} D^3 + \alpha_{1r} D^2 + \alpha_{2r} D$$

$$+ \alpha_{3r} I] f_{r+1} = R_{f,r}, \tag{2.9}$$

where the variable coefficients are given by

$$a_{0r} = \lambda \left(\frac{m-1}{2} \xi \frac{\partial f_r}{\partial \xi} - \frac{m+1}{2} f_r \right),$$

$$a_{1r} = 1 + \lambda \left((3m-1) f_r' - \frac{m-1}{2} \xi \frac{\partial f_r'}{\partial \xi} \right),$$

$$a_{2r} = \frac{m+1}{2}fr - \lambda(3m-1)f_r'' + \frac{m-1}{2}\xi\left(\lambda\frac{\partial f_r''}{\partial \xi} - \frac{\partial f_r}{\partial \xi}\right),$$

$$a_{3r} = -2mf_r' - Ha^2 + \lambda(3m-1)f_r''' + \frac{m-1}{2}\xi\left(\frac{\partial f_r'}{\partial \xi} - \lambda\frac{\partial f_r'''}{\partial \xi}\right),$$

$$a_{4r} = \frac{m+1}{2}(f_r'' - \lambda f_r^{iv}),$$

$$\alpha_{0r} = -\lambda\frac{m-1}{2}\xi f_r',$$

$$\alpha_{1r} = \lambda\frac{m-1}{2}\xi f_r''$$

$$\alpha_{2r} = \frac{m-1}{2}\xi(f_r' - \lambda f_r'''),$$

$$\alpha_{3r} = \frac{m-1}{2}\xi(\lambda f_r^{iv} - f_r'').$$

In matrix form, the above equation can be written as

$$Af_{r+1} = R_{f,r}, \tag{2.10}$$

where the system of linear equations (2.10) is expressed as follows,

$$
\begin{bmatrix}
1 & 0 & 0 & \ldots & 0 \\
D & D & D & \ldots & D \\
\vdots & \vdots & \vdots & \vdots & \\
\vdots & \vdots & \vdots & \vdots & \\
D^2 & D^2 & D^2 & \ldots & D^2 \\
0 & 0 & 0 & \ldots & 1
\end{bmatrix}
\begin{bmatrix}
\vdots \\
f_{r+1} \\
\vdots \\
\vdots \\
f_{r+1} \\
\vdots
\end{bmatrix}
=
\begin{bmatrix}
\frac{1}{2} \\
0 \\
\vdots \\
\vdots \\
0 \\
1
\end{bmatrix}.
$$

The system can be solved after implementing boundary conditions, for the unknown vec-

tors $\mathbf{F_{r+1}}$ at each iteration.

2.1 Results and Discussion

The aim of this section is to analyze the effect of the second grade, magnetic field param-
eters and Reynolds number on the fluid velocity and the transverse velocity in the suction
case. We present the results obtained by the bivariate spectral quasilinearization method.
We compare the results of the spectral quasilinearization method with those obtained by
using the homotopy analysis method [23]. The results are shown in Figures 2.2 - 2.4.

(a) (b)

Figure 2.2: The variation of (a) normal velocity, f and (b) streamwise fluid velocity, f'
profiles for different values of second grade fluid parameter, when m=1 and $Ha = $ -0.2.

Figure 2.2 shows the effect of the second grade fluid parameter, λ, on the normal velocity,
f, and streamwise fluid velocity f'. Figure 2.2(a) shows that the normal velocity increases
with increasing values of the second grade fluid parameter. Figure 2.2 (b) indicates that
there is an initial increase in velocity profiles f' but it then decreases after $\eta = 0.33$.
This increment in the velocity field at the beginning of the flow can be explained by the
increased second grade fluid parameter causing a decrease in the viscosity of the fluid,

which, in turn, is responsible for the increase of velocity field in the boundary layer flow region.
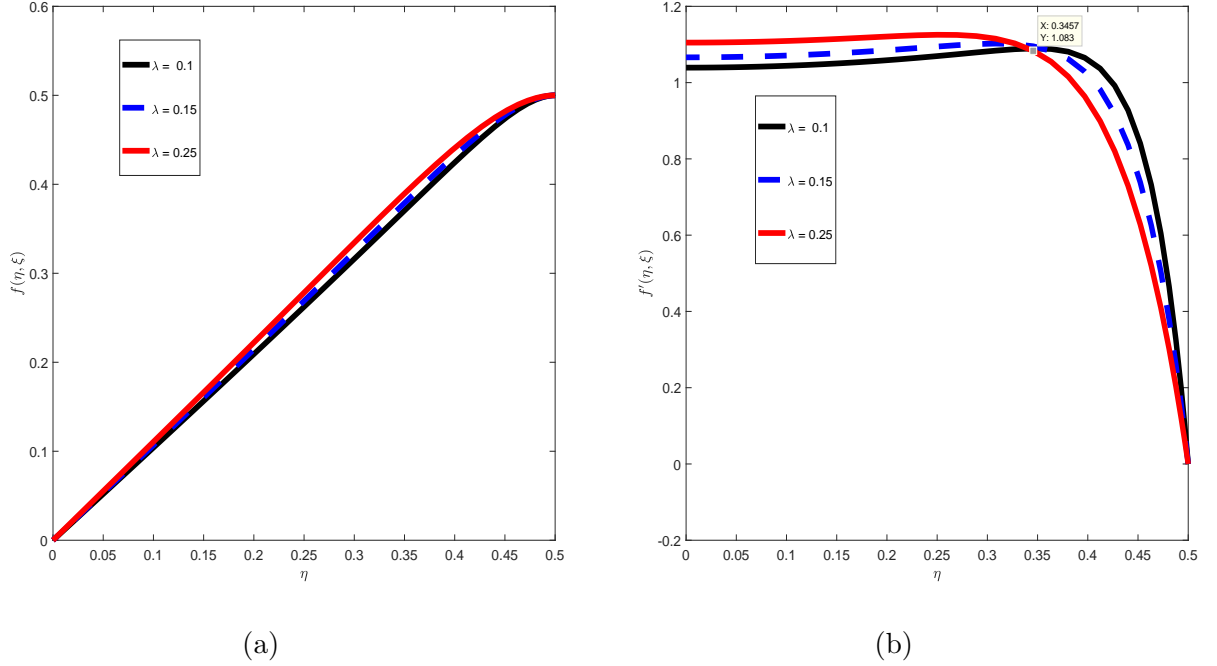

(a)

(b)
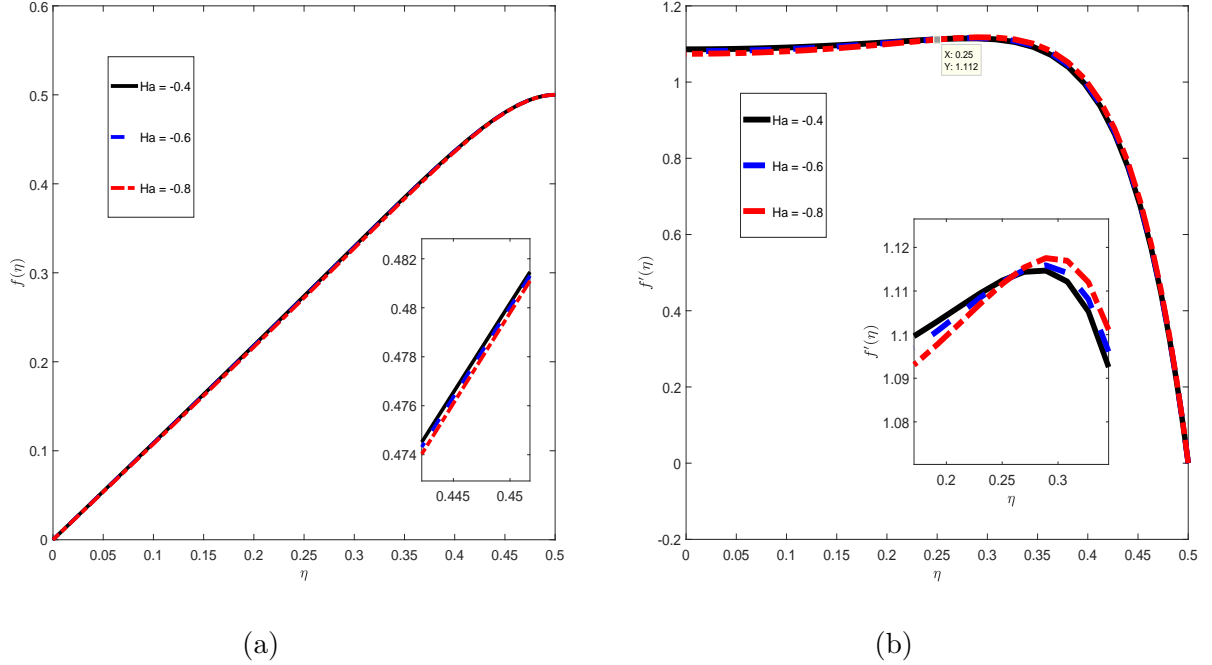
Figure 2.3: The variation of (a) normal velocity, f and (b) streamwise fluid velocity, f' profiles for different values of magnetic field parameter, when $m=1$ and $\lambda = 0.2$.

Figure 2.3 (a) shows that the normal velocity decreases with reducing values of the magnetic field parameter. However, Figure 2.3 (b) shows that the streamwise fluid velocity first decreases when the magnetic field reduces and then increases after $\eta = 0.25$. Physically, this is explained by an increased magnetic field causing the Lorentz force to increase. So with more resistance to the motion of fluid, thus the streamwise velocity of the fluid is reduced. For these profiles, the streamwise fluid velocity begins by decreasing at the channel wall but then rises as the distance from the channel increases and eventually it approaches the bulk velocity of the streams.

Table 2.1 shows the convergence iterations of the bivariate spectral quasilinearization method for the shear stresses in the radial direction at different values a second grade and magnetic field parameters. Increasing the parameter values of both the second grade fluid and the magnetic field results in increased values of the skin friction coefficient. From the results, it can be seen that as the values of both the second grade and the magnetic field

parameters increase the BSQLM required 3 and fewer iterations to converge.

Table 2.1: The BSQLM convergence iterations for values of the skin friction coefficient, $-f''(0)$ at the different values of second grade fluid and magnetic fluid parameters

No. of iterations	λ	$-f''(0)$	No. of iterations	Ha	$-f''(0)$
3	0.1	1.039243	3	-0.4	.085966
2	0.15	1.066280	2	-0.6	1.081103
2	0.25	1.104910	2	-0.8	1.074311

2.2   Residual Error Analysis

In this section, we discuss the convergence and accuracy of the bivariate spectral quasi-linearization method. Suppose that f_{r+1} is the approximation of the differential nonlinear equation

$$H\big(f(\eta,\xi), f'(\eta,\xi), f''(\eta,\xi), ..., f^{(n)}(\eta,\xi)\big) = 0,$$

at iteration level $r+1$ the residual error is defined as

$$R_r(\eta,\xi) = H\bigg(f(\eta,\xi)_{r+1}, f'(\eta,\xi)_{r+1}, f''(\eta,\xi)_{r+1}, ..., f^{(n)}(\eta,\xi)_{r+1}\bigg).$$

An iteration scheme is consistent if the residual error approaches zero as the number of iterations becomes large. The order of iteration scheme is then determined by the order of the truncation error, which is written as

$$O\bigg(\big[\Delta f(\eta,\xi)_r\big]_0^m \big[\Delta f'(\eta,\xi)_r\big]_1^m \big[\Delta f''(\eta,\xi)_r\big]_2^m ... \big[\Delta f^{(}n)(\eta,\xi)_r\big]_n^m\bigg).$$

The accuracy and the convergence rate of the method is determined using residual error analysis. The convergence of the BSQLM is determined for different values of the second grade and magnetic field parameters. Figure 2.4 shows that the BSQLM converges after 2 iterations with changes in the second grade parameter.
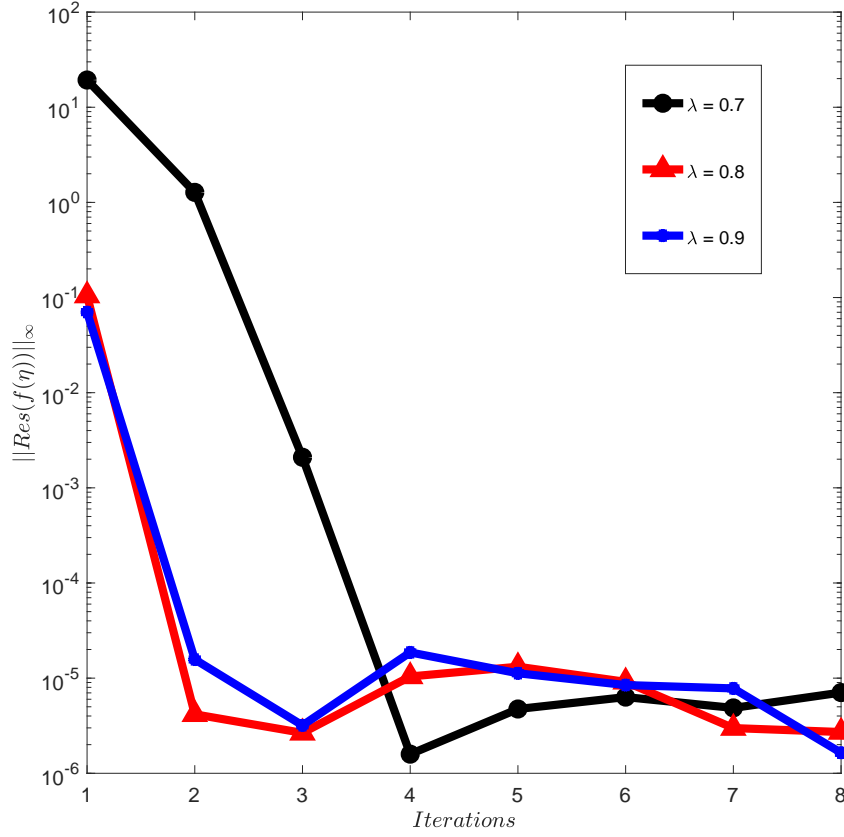
Figure 2.4: The residual error results for different values of a second grade fluid parameter.

Figures 2.5 (a) and (b) show the influence of the number of iterations on the error norm, E_f, for different values of the second grade and magnetic field parameters. From the results, it is seen that the error norm reduces with increase of both the parameter values. The bivariate spectral quasilinearization method converges with error norm of 10^{-9}. It also gives parabolic graphs, which indicate the convergence rate of the BSQLM is second order. Based on the results obtained, the BSQLM is found to be a good method for solving the second grade fluid equations.
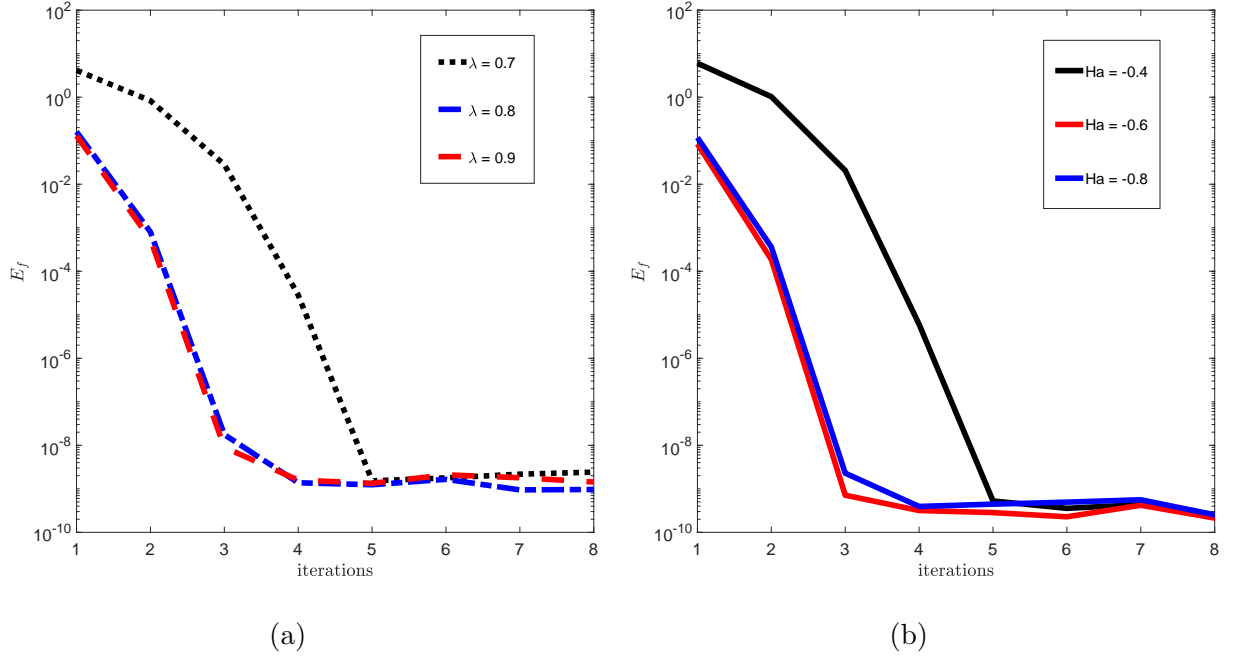
Figure 2.5: The error norm results against the number of iterations for different values of (a) second grade fluid and (b) magnetic fluid parameters.

2.3 Summary

In this chapter, the magnetohydrodynamic flow of a second grade fluid in a porous medium was analyzed. The non-dimensionalized equations were solved using the bivariate spectral quasilinearization method. The results were presented through graphs to illustrate the effect of the second grade parameter and the magnetic field parameter on the fluid properties. It was found that the streamwise fluid velocity increases with large values of the second grade fluid parameter at the beginning of the flow which then decreases after a certain time. The opposite behaviour is observed for the magnetic field parameter. The normal velocity showed to increase with the second grade fluid parameter whereas, decreases with values of the magnetic field parameter. The accuracy and convergence of this method were determined using residual error analysis. The results show that BSQLM is an appropriate method for solving the second grade fluid third order partial differential equations.

Chapter 3

Hydromagnetic flow of a second grade fluid over a stretching sheet

In the previous chapter, the focus was on the fluid velocity. Residual error analysis was used to test the convergence and accuracy of the BSQLM. This chapter deals with the flow of an electrically conducting second grade fluid over a stretching sheet. We explore the effects of thermal fluid properties. This increases the complexity of the model which might have an impact on the accuracy of the method. An increase in temperature on the surface has an effect on the stretching of the surface, which ultimately has an effect on the fluid flow rate. Numerical solutions for the velocity and temperature equations are then obtained using the bivariate spectral quasilinearization method. The behaviour of the fluid properties with different physical and fluid flow parameters is discussed. The residual error analysis will be used to determine the convergence and accuracy of the method.

To set up the problem, we consider the flow of an electrically conducting incompressible second grade fluid past a flat sheet. As shown in Figure 3.1, we take the x-axis to be along the surface, with the y-axis being normal to it. Two equal and opposite forces are applied along the x-axis so that the surface is stretched, while keeping the origin fixed. A uniform magnetic field B_0 is imposed along the y-axis. We define u and v to be the fluid tangential velocity and normal velocity, respectively.
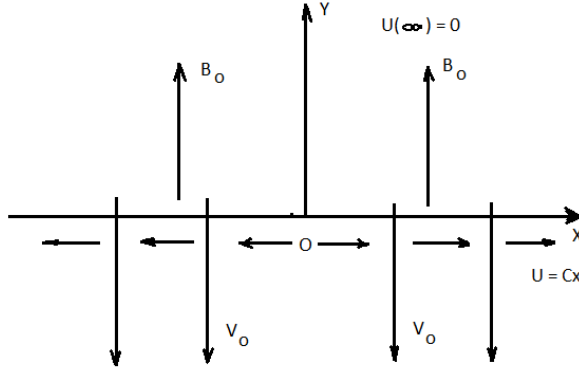
Figure 3.1: The problem set up and orientation of the coordinate system [9]

The steady two dimensional boundary layer equations for this fluid are [70, 113, 114],

$$u\frac{\partial u}{\partial x} + v\frac{\partial u}{\partial y} = 0,$$ (3.1)

$$u\frac{\partial u}{\partial x} + v\frac{\partial u}{\partial y} = \nu\frac{\partial^2 u}{\partial y^2} + \frac{\alpha_1}{\rho}\left[\frac{\partial u}{\partial x}\frac{\partial^2 u}{\partial y^2} + u\frac{\partial^3 u}{\partial x\partial y^2} + \frac{\partial u}{\partial y}\frac{\partial^2 v}{\partial y^2} + v\frac{\partial^3 u}{\partial y^3}\right] - \frac{\sigma B_0^2}{\rho}u,$$ (3.2)

$$u\frac{\partial T}{\partial x} + v\frac{\partial T}{\partial y} = k\frac{\partial^2 T}{\partial y^2} + \frac{\nu}{C_p}\left(\frac{\partial u}{\partial y}\right)^2 + \alpha_1\frac{\partial u}{\partial y}\left[\frac{\partial}{\partial y}\left(u\frac{\partial u}{\partial x} + v\frac{\partial u}{\partial y}\right)\right].$$ (3.3)

The corresponding boundary conditions for the velocity and temperature fields are,

$$u = cx, \qquad v = -v_0, \qquad T = T_w, \qquad \text{at} \qquad y = 0,$$

$$u \to 0, \qquad \tfrac{\partial u}{\partial y} \to 0, \qquad T \to T_\infty, \qquad \text{as} \qquad y \to \infty,$$ (3.4)

where ν is the kinematic viscosity, ρ is the density, α_1 the material parameter of second grade fluid, σ the electrical conductivity, k the fluid thermal conductivity, C_p is the specific

39

heat capacity, c is the stretching rate, T_w is the uniform temperature in the wall and T_∞ is the ambient temperature. Applying the transformations,

$$u = U_0 x^m f'(\xi, \eta), \qquad v = -\frac{1}{2}(\nu U_0)x^{\frac{m-1}{2}}\{(m+1)f + (1-m)(\xi\frac{\partial f}{\partial \xi} - \eta f')\},$$

$$T - T_\infty = (T_w - T_\infty)\theta(\xi, \eta), \qquad \xi = \left(\frac{\nu}{U_0}\right)^{\frac{1}{2}}x^{\frac{1-m}{2}}, \qquad \eta = \left(\frac{U_0}{\nu}\right)^{\frac{1}{2}}x^{\frac{m-1}{2}}y,$$

to equations (3.1) - (3.3), equations (3.2) and (3.3) reduce to

$$U_0^2 x^{2m-1}\left\{\frac{1-m}{2}\xi f'\frac{\partial f'}{\partial \xi} + mf'^2 - \frac{m+1}{2}ff'' - \frac{1-m}{2}\xi f''\frac{\partial f}{\partial \xi}\right\} = U_0^2 x^{2m-1}f'''$$
$$+ \frac{U_0^3 x^{3m-2}}{\rho\nu}\left\{\frac{1-m}{2}\xi\left(f'''\frac{\partial f'}{\partial \xi} + f^{iv}\frac{\partial f}{\partial \xi}\right) + (3m-1)f'f''' + \frac{1-m}{2}\xi f'\frac{\partial f'''}{\partial \xi}\right.$$
$$\left.+ \frac{m+1}{2}f'f^{iv} + \frac{3m-1}{2}f''^2\right\} - \frac{\sigma B_0^2 U_0 x^m}{\rho}f' \tag{3.5}$$

$$U_0 x^{m-1}(T_w - T_\infty)\left\{\frac{1-m}{2}\xi\frac{\partial \theta}{\partial \xi} - \frac{1+m}{2}f\theta' - \frac{1-m}{2}\xi\frac{\partial f}{\partial \xi}\right. = \frac{k}{\nu\rho c_p}\theta'' + \frac{\mu U_0^3 x^{3m-1}}{\nu\rho c_p}f''^2$$
$$- \frac{16T_\infty^3 \sigma^*}{3k^*}\frac{U_0 x^{m-1}}{\nu}\theta'' + \frac{\sigma B_0^2 U_0^2 x^{2m}}{\rho c_p}f'^2 + \frac{\alpha_1 U_0^{4m-2}}{\rho\nu c_p}\left\{\frac{3m-1}{2}f'f''^2 - \frac{m+1}{2}ff''f'''\right.$$
$$\left.\left.+ \frac{1-m}{2}\xi\left(f'f''\frac{\partial f''}{\partial \xi} - f''f'''\frac{\partial f}{\partial \xi}\right)\right)\right\} \tag{3.6}$$

which then become equation (3.7) and (3.8) below,

$$f''' + \frac{m+1}{2}ff'' - mf'^2 - Ha^2 f' + \lambda\left[(3m-1)f'f''' - \frac{m+1}{2}ff^{iv} - \frac{3m-1}{2}f''^2\right.$$
$$\left.+ \frac{m-1}{2}\xi\left(f^{iv}\frac{\partial f}{\partial \xi} - f'''\frac{\partial f'}{\partial \xi} + f''\frac{\partial f''}{\partial \xi} - f'\frac{\partial f'''}{\partial \xi}\right)\right]$$
$$- \frac{m-1}{2}\xi\left(f''\frac{\partial f}{\partial \xi} - f'\frac{\partial f'}{\partial \xi}\right) = 0, \tag{3.7}$$

$$\frac{1}{Pr}\theta'' + \frac{m+1}{2}f\theta' + Ec\left[f''^2 + \lambda f''\left(\frac{3m-1}{2}f'f'' - \frac{m+1}{2}ff''' + \frac{m-1}{2}\xi\left(f'''\frac{\partial f}{\partial \xi}\right.\right.\right.$$
$$\left.\left.\left. - f'\frac{\partial f''}{\partial \xi}\right)\right)\right] - \frac{m-1}{2}\xi\left(\theta'\frac{\partial f}{\partial \xi} - f'\frac{\partial \theta}{\partial \xi}\right) = 0. \tag{3.8}$$

The boundary conditions (3.4) become

$$f' = 1, \qquad f = R, \qquad \theta = 1, \qquad \text{at} \qquad \eta = 0,$$
$$f' \to 0, \qquad f'' \to 0, \quad \theta \to 0, \qquad \text{at} \qquad \eta \to \infty, \tag{3.9}$$

such that

$$\lambda = \frac{\alpha_1 U_0 x^{m-1}}{\rho\nu}, \quad Ha = \frac{\sigma B_0^2}{\rho U_0 x^{m-1}}, \quad Ec = \frac{U_0^2 x^{2m}}{c_p(T_w - T_\infty)}, \quad Pr = \frac{\nu\rho C_p}{k}, \quad R = \frac{-2v_0}{(m+1)x^{\frac{m-1}{2}}}.$$

We apply the spectral quasilinearization method, while assuming that the difference $||f_{r+1} - f_r||$, and derivatives, are all small. It is convenient to transform the physical domain $[a, b] \times [c, d]$ to the computational domain $[-1, 1] \times [-1, 1]$ using the linear transformations $x(\xi) = (a+b)/2 + ((b-a)/2)\xi$ and $y(\eta) = (a+b)/2 + ((b-a)/2)\eta$. Applying the quasilinearization method to equations (3.7) and (3.8) gives

$$p_{0r}f_{r+1}^{iv} + p_{1r}f_{r+1}''' + p_{2r}f_{r+1}'' + p_{3r}f_{r+1}' + p_{4r}f_{r+1} + \iota_{0r}\frac{\partial f_r}{\partial \xi} + \iota_{1r}\frac{\partial f_r'}{\partial \xi} + \iota_{2r}\frac{\partial f_r''}{\partial \xi}$$
$$+ \iota_{3r}\frac{\partial f_r'''}{\partial \xi} = 0, \tag{3.10}$$

$$q_{0r}\theta_{r+1}'' + q_{1r}\theta_{r+1}' + q_{2r}\theta_{r+1} + q_{3r}f_{r+1}''' + q_{4r}f_{r+1}'' + q_{5r}f_{r+1}' + q_{6r}f_{r+1} + \chi_{0r}\frac{\partial \theta_{r+1}}{\partial \xi}$$
$$+ \chi_{1r}\frac{\partial f_{r+1}''}{\partial \xi} + \chi_{2r}\frac{\partial f_{r+1}}{\partial \xi} = 0, \tag{3.11}$$

and the boundary conditions (3.9) become

$$f'_{r+1} = 1, \qquad f_{r+1} = R, \qquad \theta_{r+1} = 1 \qquad \text{at} \qquad \eta = 0,$$

$$f'_{r+1} \to 0, \qquad f''_{r+1} \to 0, \qquad \theta_{r+1} \to 0 \qquad \text{at} \qquad \eta \to \infty, \qquad (3.12)$$

where the variable coefficients are given by

$$p_{0r} = \lambda \left(\frac{m-1}{2} \xi \frac{\partial f_r}{\partial \xi} - \frac{m+1}{2} f_r \right),$$

$$p_{1r} = 1 + \lambda \left((3m-1) f'_r - \frac{m-1}{2} \xi \frac{\partial f'_r}{\partial \xi} \right),$$

$$p_{2r} = \frac{m+1}{2} f_r + \lambda \left((3m-1) f'' + \frac{m-1}{2} \xi \frac{\partial f''_r}{\partial \xi} \right) - \frac{m-1}{2} \xi \frac{\partial f_r}{\partial \xi},$$

$$p_{3r} = -2m f'_r - Ha^2 + \lambda \left((3m-1) f'''_r - \frac{m-1}{2} \xi \frac{\partial f'''_r}{\partial \xi} \right) - \frac{m-1}{2} \xi \frac{\partial f'_r}{\partial \xi},$$

$$p_{4r} = \frac{m+1}{2} (f''_r - \lambda f^{iv}_r),$$

$$p_{4r} = \frac{m+1}{2} (f''_r - \lambda f^{iv}_r),$$

$$\iota_{0r} = -\frac{m-1}{2} \xi f'_r,$$

$$\iota_{1r} = -\frac{m-1}{2} \xi f''_r,$$

$$\iota_{2r} = \frac{m-1}{2} \xi (f'_r - \lambda f'''_r),$$

$$\iota_{3r} = \frac{m-1}{2} \xi (\lambda f^{iv}_r - f''_r),$$

$$q_{0r} = (1/Pr),$$

$$q_{1r} = -\frac{m-1}{2} \xi \frac{\partial f_r}{\partial \xi} + \frac{m+1}{2} f_r,$$

$$q_{2r} = 0,$$

$$q_{3r} = Ec\lambda \left(\frac{m-1}{2} \xi f''_r \frac{\partial f_r}{\partial \xi} - \frac{m+1}{2} f_r f''_r \right),$$

$$q_{4r} = 2Ecf'' + Ec\lambda\left[(3m-1)f_r'f_r'' - \frac{m+1}{2}f_r'f_r''' + \frac{m-1}{2}\xi\left(f_r'''\frac{\partial f_r}{\partial \xi} - f_r'\frac{\partial f_r''}{\partial \xi}\right)\right],$$

$$q_{5r} = Ec\left(2Ha^2 f_r'f'' + \lambda\frac{3m-1}{2}f_r''^2\right) + \frac{m-1}{2}\xi\left(\frac{\partial \theta_r}{\partial \xi} - Ec\lambda\frac{\partial f_r''}{\partial \xi}\right),$$

$$q_{6r} = \frac{m+1}{2}(\theta_r - Ec\lambda f_r''f_r''')$$

$$\chi_{0r} = \frac{m-1}{2}\xi f_r',$$

$$\chi_{1r} = -Ec\lambda\frac{m-1}{2}\xi f_r'f_r'',$$

$$\chi_{2r} = \frac{m-1}{2}\xi(Ec\lambda f_r''f_r''' - \theta_r').$$

A Lagrange polynomial is used to interpolate the functions $f(\eta,\xi)$ and $\theta(\eta,\xi)$ at selected collocation points to obtain the approximate solutions for equation (3.10) and (3.11). Applying spectral collocation of Chebyshev differentiation to these equations gives

$$\left[p_{0r}D^{iv} + p_{1r}D^3 + p_{2r}D^2 + p_{3r}D + p_{4r} + 2\sum_{j=0}^{N_\xi}d_{ij}[\iota_{0r}D^3 + \iota_{1r}D^2 + \iota_{2r}D^1\right.$$

$$\left.+ \iota_{3r}I]\right]f_{r+1} = R_{f,r}, \tag{3.13}$$

$$\left[q_{3r}D^3 + q_{4r}D^2 + q_{5r}D + q_{6r}I + 2\sum_{j=0}^{N_\xi}d_{ij}[\chi_{1r}D^2 + \chi_{2r}I]\right]f_{r+1} + \left[q_{0r}D^2 + q_{1r}D + q_{2r}I\right.$$

$$\left.+ 2\sum_{j=0}^{N_\xi}d_{ij}[\chi_{0r}I]\right]\theta_{r+1} = R_{\theta,r}. \tag{3.14}$$

Equations (3.13) and (3.14) can be expressed in matrix–vector form as

$$
\begin{bmatrix}
\begin{bmatrix} \Pi_{11}^{0,0} & \Pi_{12}^{0,0} \\ \Pi_{21}^{0,0} & \Pi_{22}^{0,0} \end{bmatrix} & \begin{bmatrix} \Pi_{11}^{0,1} & \Pi_{12}^{0,1} \\ \Pi_{21}^{0,1} & \Pi_{22}^{0,1} \end{bmatrix} & \cdots & \begin{bmatrix} \Pi_{11}^{0,N_\xi} & \Pi_{12}^{0,N_\xi} \\ \Pi_{21}^{0,N_\xi} & \Pi_{22}^{0,N_\xi} \end{bmatrix} \\[2em]
\begin{bmatrix} \Pi_{11}^{1,0} & \Pi_{12}^{1,0} \\ \Pi_{12}^{1,0} & \Pi_{22}^{1,0} \end{bmatrix} & \begin{bmatrix} \Pi_{11}^{1,1} & \Pi_{12}^{1,1} \\ \Pi_{21}^{1,1} & \Pi_{22}^{1,1} \end{bmatrix} & \cdots & \begin{bmatrix} \Pi_{11}^{1,N_\xi} & \Pi_{12}^{1,N_\xi} \\ \Pi_{21}^{1,N_\xi} & \Pi_{22}^{1,N_\xi} \end{bmatrix} \\[2em]
\vdots & \vdots & \ddots\ \ddots & \vdots \\[1em]
\begin{bmatrix} \Pi_{11}^{N_\xi,0} & \Pi_{12}^{N_\xi,0} \\ \Pi_{21}^{N_\xi,0} & \Pi_{22}^{N_\xi,0} \end{bmatrix} & \begin{bmatrix} \Pi_{11}^{N_\xi,1} & \Pi_{12}^{N_\xi,1} \\ \Pi_{21}^{N_\xi,1} & \Pi_{22}^{N_\xi,1} \end{bmatrix} & \cdots & \begin{bmatrix} \Pi_{11}^{N_\xi,N_\xi} & \Pi_{12}^{N_\xi,N_\xi} \\ \Pi_{21}^{N_\xi,N_\xi} & \Pi_{22}^{N_\xi,N_\xi} \end{bmatrix}
\end{bmatrix}
\begin{bmatrix}
\begin{bmatrix} f_{r+1,0} \\ \theta_{r+1,0} \end{bmatrix} \\[1em]
\begin{bmatrix} f_{r+1,1} \\ \theta_{r+1,1} \end{bmatrix} \\[1em]
\vdots \\[0.5em]
\vdots \\[1em]
\begin{bmatrix} f_{r+1,N_\xi} \\ \theta_{r+1,N_\xi} \end{bmatrix}
\end{bmatrix}
=
\begin{bmatrix}
\begin{bmatrix} R_{f,r,0} \\ R_{\theta,r,0} \end{bmatrix} \\[1em]
\begin{bmatrix} R_{f,r,1} \\ R_{\theta,r,1} \end{bmatrix} \\[1em]
\vdots \\[0.5em]
\vdots \\[1em]
\begin{bmatrix} R_{f,r,N_\xi} \\ R_{\theta,r,N_\xi} \end{bmatrix}
\end{bmatrix},
\tag{3.15}
$$

where

$$\Pi_{11}^{i,i} = p_{0r}D^{iv} + p_{1r}D^3 + p_{2r}D^2 + p_{3r}D + p_{4r} + 2d_{ii}[\iota_{0r}D^3 + \iota_{1r}D^2 + \iota_{2r}D^1], \tag{3.16.0}$$

$$\Pi_{11}^{i,j} = 2d_{ij}[\iota_{0r}D^3 + \iota_{1r}D^2 + \iota_{2r}D^1], \tag{3.16.1}$$

$$\Pi_{12}^{i,i} = O = \text{zero matrix of size } (N_\eta + 1) \times (N_\eta + 1), \tag{3.16.2}$$

$$\Pi_{12}^{i,j} = O = \text{zero matrix of size } (N_\eta + 1) \times (N_\eta + 1), \tag{3.16.3}$$

$$\Pi_{21}^{i,i} = q_{3r}D^3 + q_{4r}D^2 + q_{5r}D + q_{6r}I + 2d_{ii}[\chi_{1r}D^2 + \chi_{2r}I], \tag{3.16.4}$$

$$\Pi_{21}^{i,j} = 2d_{ij}[\chi_{1r}D^2 + \chi_{2r}I], \tag{3.16.5}$$

$$\Pi_{22}^{i,i} = q_{0r}D^2 + q_{1r}D + q_{2r}I + 2d_{ii}\chi_{0r}I, \tag{3.16.6}$$

$$\Pi_{22}^{i,j} = 2d_{ij}\chi_{0r}I. \tag{3.16.7}$$

After imposing boundary and initial conditions, the system of linear equations is solved by finding the inverse of the coefficient matrix to obtain the solutions f_{r+1} and θ_{r+1} at each ξ–level.

3.1 Results and Discussion

In Figures 3.2 we have plotted the velocity and temperature distributions for several values of the suction parameter, R. It is observed that, for a fixed value of the magnetic field parameter, the velocity is enhanced by larger values of the suction parameter while the temperature decreases for corresponding changes. In physical terms, the case of higher suction parameter values means that the fluid is closer to the surface at the ambient conditions and the thermal boundary layer thickness reduces.

(a) (b)

Figure 3.2: The variation of (a) the fluid velocity and (b) temperature profiles for different values of the suction parameter, R.

The opposite behaviour is shown in Figure 3.3, an increase in the magnetic field parameter means the fluid velocity decreases while the temperature increases. This can be explained as the increase of the magnetic field parameter resulting in an increase of the Lorentz force, which inhibits the flow.

It is seen from Table 3.1 that for a given position the skin friction coefficient, decreases as the suction parameter and second grade parameter increase. The dimensionless heat transfer coefficient increases with an increase in suction parameter and second grade parameter. This means the fluid resistance caused by the shear stresses decreases and the

Figure 3.3: The variation of (a) the fluid velocity and (b) temperature profiles for different values of the magnetic field parameter.

Table 3.1: The effect of suction and second grade parameters.

R	$-f''(0)$	$-\theta'(0)$	λ	$-f''(0)$	$-\theta'(0)$
0	1.58111857	0.96293281	0	1.99999859	1.27771290
0.1	1.54668368	1.18583274	1	1.00019123	1.36560387
0.5	1.44946584	2.14640740	1.5	0.89506838	1.37894944
0.9	1.38705344	3.18170263	2	0.78233101	1.38775637

heat transfer rate between the fluid flow and the surface increases.

In Figure 3.4 it is shown that the velocity profile increases with an increase in the second grade parameter. Conversely, the temperature at a given point decreases with an increase in a second grade parameter. This means physically that an increase of the second grade fluid parameter reduces the fluid reaction and the viscous terms resisting the fluid motion, hence significantly decreasing the fluid temperature.
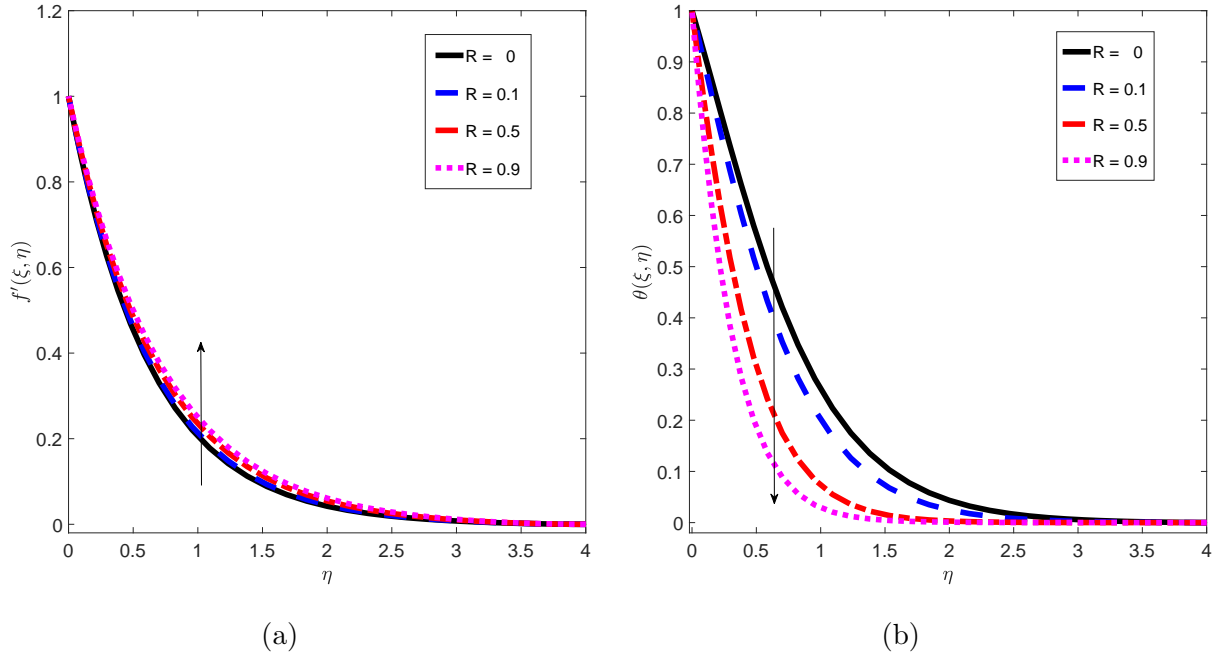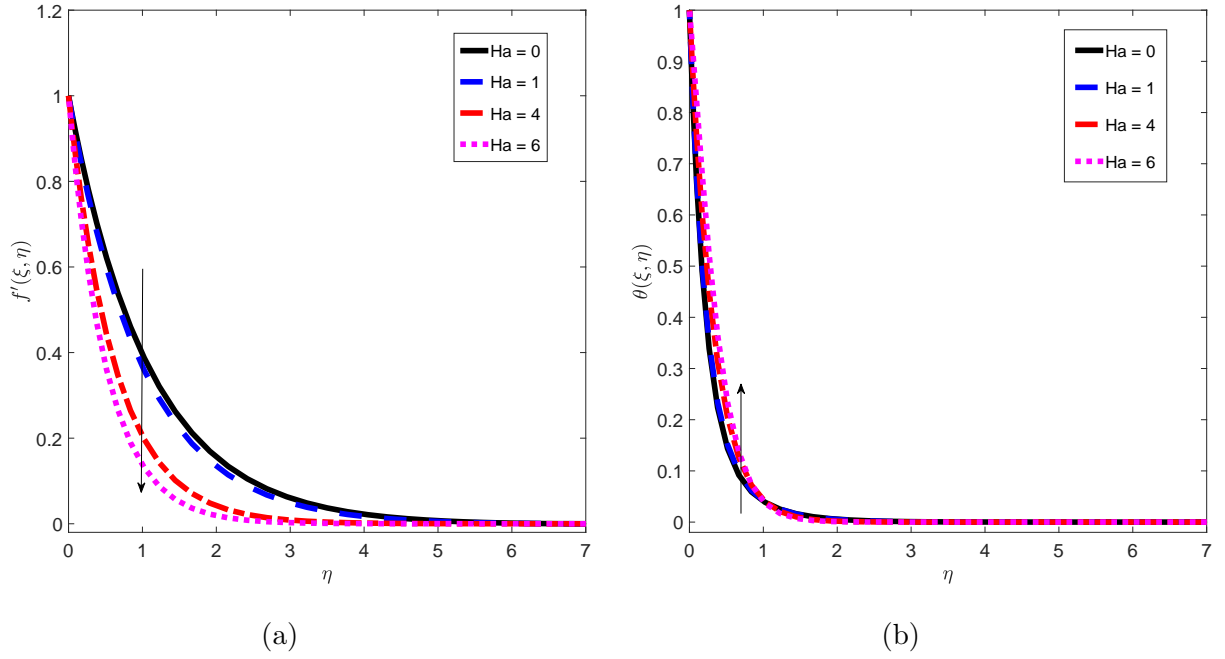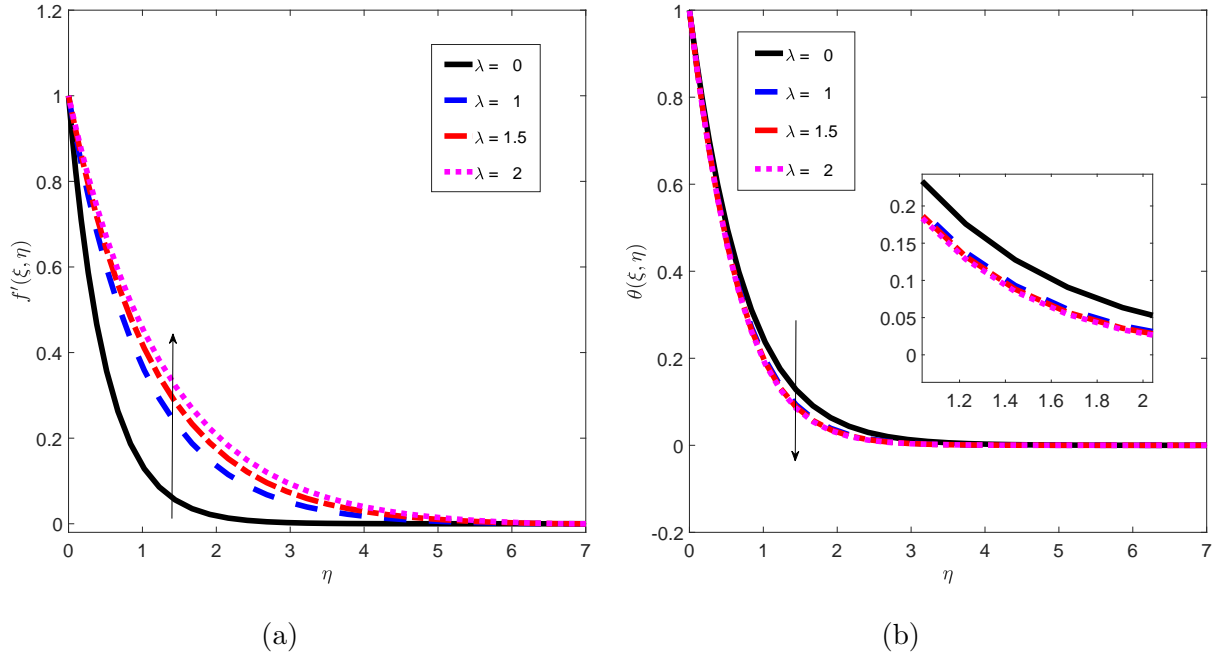
Figure 3.4: The variation of (a) the fluid velocity and (b) temperature profiles for different values of the second grade fluid parameter.

An increase in Prandtl number has no effect on the velocity profiles in the boundary layer, as shown in Figure 3.5 (a). Figure 3.5 (b), however, indicates that the temperature decreases as the Prandtl number, Pr increases. This increase leads to a decrease in the thermal boundary layer thickness when the fluid flow rates are high. Table 3.2 shows that the skin friction increases with the increase in the magnetic field parameter, whereas the Prandtl number has no effect in the skin friction coefficient. The rate of heat transfer increases with the increase of both the magnetic field parameter and Prandtl number.

Table 3.2: The effect of the magnetic field parameter and Prandtl number on the skin friction coefficient and heat rate transfer.

| Ha	$-f''(0)$	$-\theta'(0)$	Pr	$-f''(0)$	$-\theta'(0)$
0	0.92382122	4.29318093	0.3	0.79806748	1.59929669
1	1.00080510	4.16007151	1	-	3.60374539
4	1.58477374	2.85766968	1	-	5.09337498
6	1.98399720	1.67201038	1.5	-	7.56757619
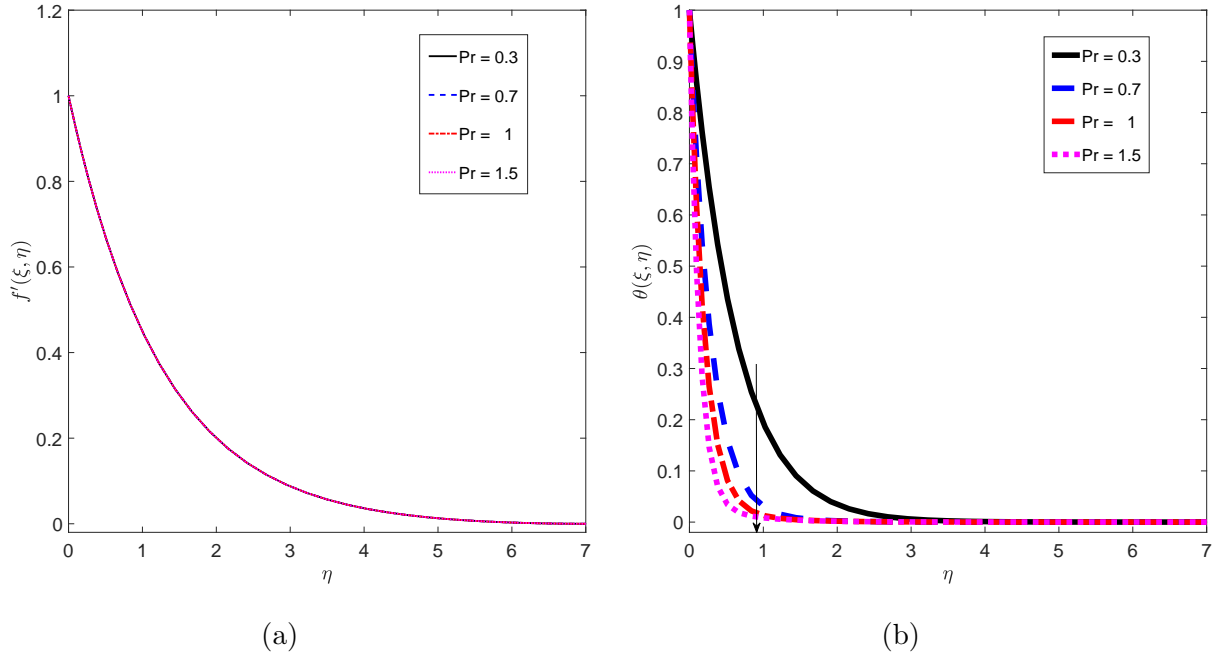
Figure 3.5: The variation of (a) the fluid velocity and (b) temperature profiles for different values of the Prandtl number.

3.2 Residual error analysis

Residual error analysis is used to show the convergence and accuracy of the method. The residual error norms obtained using the BSQLM are shown in Figure 3.6 (a) and (b). The most accurate results were found for suction parameter values. It is observed that the solutions require only a 3 and 4 iterations to converge. For this parameter, the residual error norm decreases with the increase in the number of iterations, giving the maximum values of 10^{-10} and 10^{-13}, respectively, for the velocity and temperature distributions. This means that the approximate solutions obtained using the BSQLM method become more accurate as the number iterations increase.
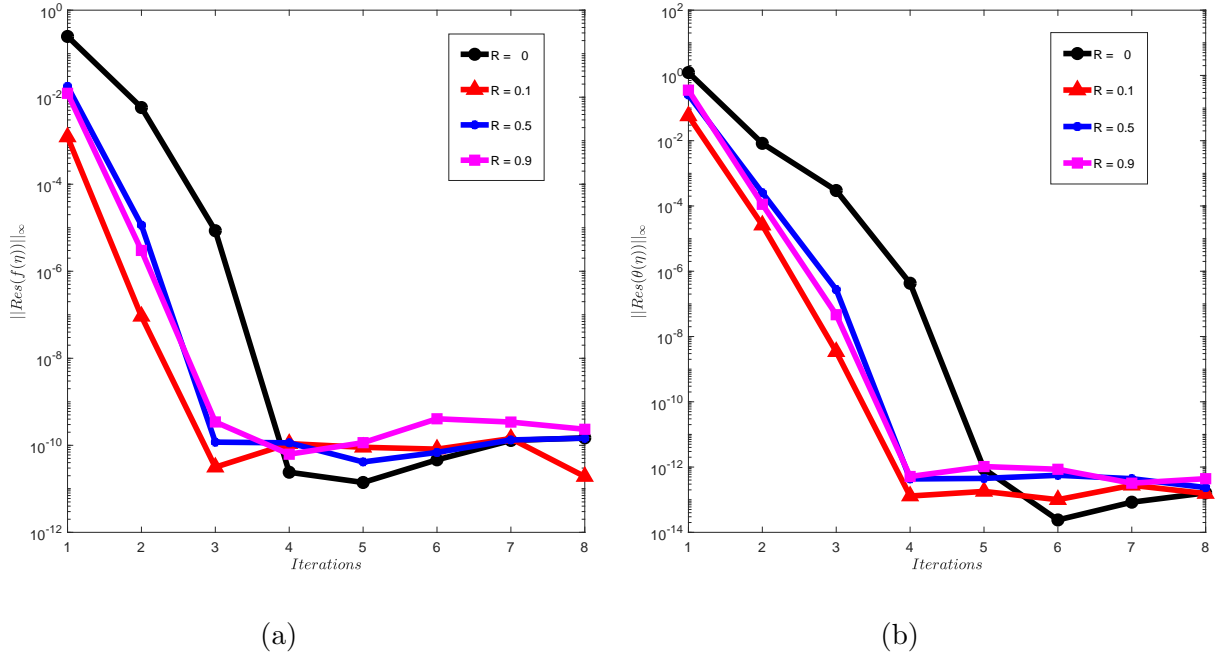
Figure 3.6: The residual error results for different values of suction parameter.

In Figure 3.7 the error norm reduces with the number of iterations. From the graphs, it is observed that the BSQLM converges with a maximum error of the order 10^{-10} for the velocity profiles and 10^{-11} for the temperature profiles. It is also noted that BSQLM gives a parabolic shape for the graphs, which indicates that the method is of second order. Accordingly, as can be seen, the iteration scheme takes only 4 or 5 iterations to converge fully. Beyond this number of iterations, the error norm does not improve with an increase in the number of iterations. This indicates that the BSQLM is a convergent method, and so that is appropriate for solving nonlinear partial differential equations.
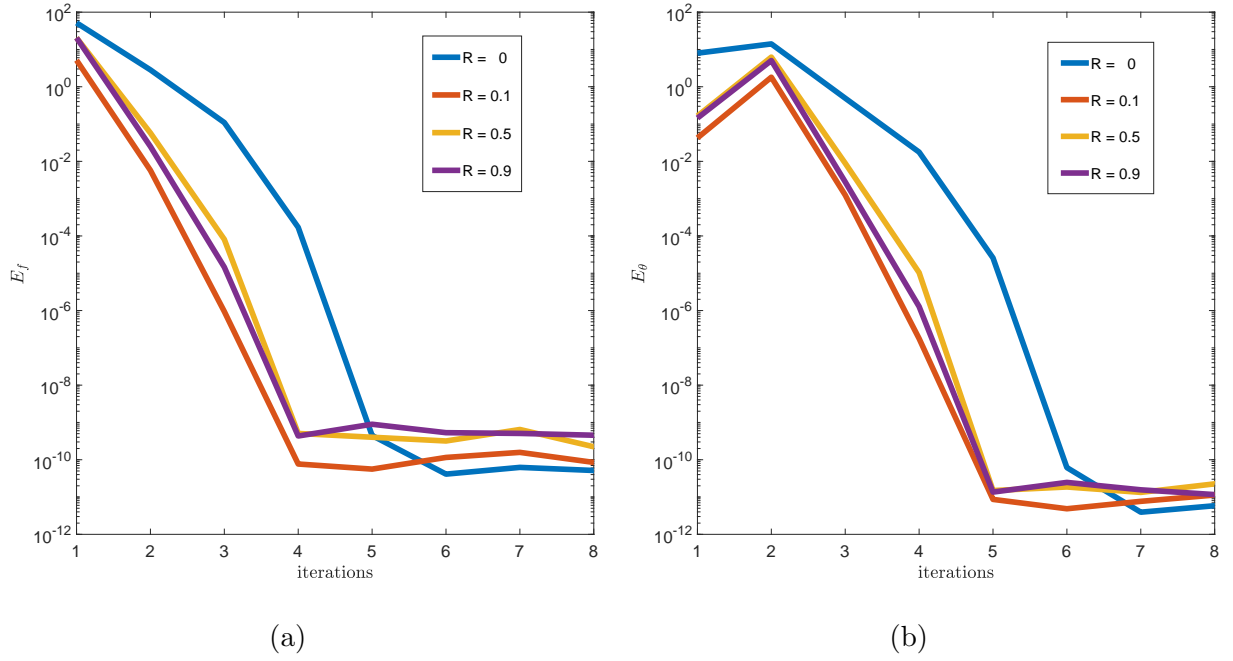
Figure 3.7: Shows the error norm results against iteration for BSQLM with different values of suction parameter.

3.3   Summary

In this chapter, the flow of an electrically conducting incompressible second grade fluid past a stretching surface was analyzed. The non-dimensionalized partial differential equations were solved using the bivariate spectral quasilinearization method. The effects of changing the flow parameters on the fluid properties were investigated. Results show that the fluid flow reduces with the increase in the magnetic field parameter. Increasing the values of the Prandtl number shows no effect on the fluid velocity while reduces the temperature. Among other results, we showed that the shear stress decreases with an increase in the suction and the second grade fluid parameters, whereas the heat transfer rate increases. The accuracy and the convergence rate of the method of solution were determined using residual error analysis. This proves the BSQLM to be an appropriate method for solving nonlinear partial differential equations.

Chapter 4

Second grade nanofluid flow in a porous medium

We now extend the work of Chapter 3 by introducing new terms in the velocity equation, which denote the presence of porosity and inertia in the fluid flow. Porosity describes the presence of pores in the conducting material. The presence of pores makes it possible for some of the fluid to flow out. On the other hand, the inertia coefficient is the fluid's tendency to maintain its state of rest or of motion. These parameters are fused into the model to reflect reality better. In this chapter, we study second grade nanofluid flow over a porous wedge. The partial differential equations are solved using the bivariate spectral quasilinearization method. The velocity and temperature profiles are determined for several values of parameters such as the wedge angle, heat generation, and absorption parameters. The convergence of the method is analyzed. As before we first set up the problem, as illustrated in Figure 4.1.
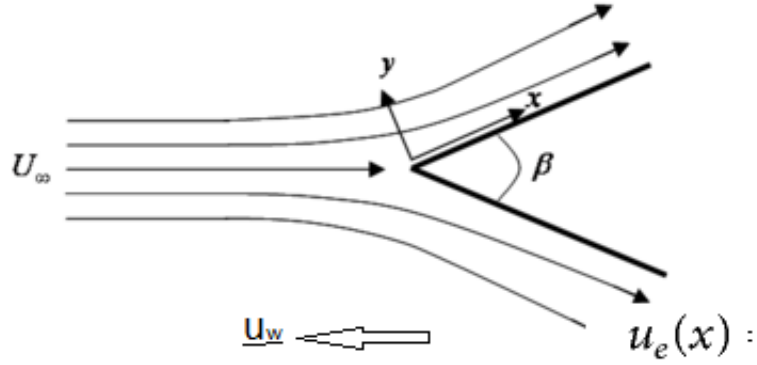
Figure 4.1: The problem set up and orientation of the coordinate system [115]

Consider the steady two dimensional incompressible second grade nanofluid flow induced by a stretching wedge moving with the velocity $u_w(x) = bx^n$. The free stream velocity is $U_e(x) = ax^n$, where a, b and n are positive constants with $0 \leq n \leq 1$, and T_∞ is the ambient temperature. The particle volume fraction flux at the wall is assumed to be zero. A uniform magnetic field of strength B_0 is applied perpendicular to the flow. The electric and induced magnetic fields are neglected. With the stated assumptions, the boundary layer equations describing the flow can be expressed as follows:

$$u\frac{\partial u}{\partial x} + v\frac{\partial u}{\partial y} = \nu\frac{\partial^2 u}{\partial y^2} + \frac{\alpha_1}{\rho}\left[\frac{\partial u}{\partial x}\frac{\partial^2 u}{\partial y^2} + u\frac{\partial^3 u}{\partial x\partial y^2} - m\frac{\partial u}{\partial y}\frac{\partial^2 v}{\partial y^2} + v\frac{\partial^3 u}{\partial y^3}\right] + U_e\frac{dU}{dx}$$
$$- \frac{\sigma B_0^2}{\rho}\sin^2\psi\,(u - U_e) - \frac{\nu}{k^*}u - Fu^2, \tag{4.1}$$

$$\rho C_p\left(u\frac{\partial T}{\partial x} + v\frac{\partial T}{\partial y}\right) = k\frac{\partial^2 T}{\partial y^2} - \frac{\partial q_r}{\partial y} + \mu\left(\frac{\partial u}{\partial y}\right)^2 + \frac{Q_0}{\rho c_p}(T - T_\infty)$$
$$+ \alpha_1\frac{\partial u}{\partial y}\left[\frac{\partial}{\partial y}\left(u\frac{\partial u}{\partial x} + v\frac{\partial u}{\partial y}\right)\right]. \tag{4.2}$$

The corresponding boundary conditions are

$$u = u_w(x) = bx^m, \qquad T = T_w, \qquad \text{at} \qquad y = 0,$$

$$u \to U_e(x) = ax^m, \qquad T \to T_\infty, \qquad \text{as} \qquad y \to \infty, \qquad (4.3)$$

and

$$k\left(\frac{\partial T}{\partial y}\right)_{y=0} = \rho[\lambda + (T_w - T_0)]v(x, 0), \qquad (4.4)$$

where u and v represent the velocity along $x-$ and $y-$ directions, ν the kinematic viscosity, α_1 the second grade fluid parameter, ρ the fluid density, σ the electrical conductivity, T the temperature C_p the specific heat capacity of the nanoparticles in the fluid and Q_0 the dimensional heat generation/absorption coefficient. The boundary condition (4.4) shows that the heat conducted to the surface is equal to the melting heat plus heat required to raise the solid temperature up to T_0, the melting temperature. Using a similarity transformation,

$$u = U_0 x^m f'(\xi, \eta), \qquad v = -\frac{1}{2}(\nu U_0)^{\frac{1}{2}} x^{\frac{m-1}{2}}\{(m+1)f + (1-m)(\xi\frac{\partial f}{\partial \xi} - \eta f'),$$

$$T - T_\infty = (T_w - T_\infty)\theta(\xi, \eta), \qquad \xi = \left(\frac{\nu}{U_0}\right)^{\frac{1}{2}} x^{\frac{1-m}{2}}, \qquad \eta = \left(\frac{U_0}{\nu}\right)^{\frac{1}{2}} x^{\frac{m-1}{2}} y.$$

,

equations (4.1) and (4.2) become

$$U_0^2 x^{2m-1} \left\{ \frac{1-m}{2} \xi f' \frac{\partial f'}{\partial \xi} + mf'^2 - \frac{m+1}{2} ff'' - \frac{1-m}{2} \xi f'' \frac{\partial f}{\partial \xi} \right\} = U_0^2 x^{2m-1} f'''$$

$$+ \frac{\alpha_1 U_0^3 x^{3m-2}}{\rho \nu} \left\{ \frac{1-m}{2} \xi \left(f''' \frac{\partial f'}{\partial \xi} + f'' \frac{\partial f''}{\partial \xi} + f^{iv} \frac{\partial f}{\partial \xi} \right) + (3m-1) f' f''' + \frac{3m-1}{2} f''^2 \right.$$

$$+ (m-1) \eta f'' f''' - \frac{m+1}{2} f f^{iv} \right\} - \frac{\sigma B_0^2}{\rho U_0 x^{m-1}} \sin^2 \psi (f'-1) - \frac{\nu U_0 x^m}{k} f'$$

$$- F U_0^2 x^{2m} f'^2 \qquad (4.5)$$

$$\rho C_p \left\{ \frac{1-m}{2} \xi \frac{\partial \theta}{\partial \xi} - \frac{1-m}{2} \xi \frac{\partial f}{\partial \xi} \theta' - \frac{m+1}{2} f \theta' \right\} = \frac{k}{\nu} \theta'' + \frac{4\sigma^*}{3k\nu} 4T_\infty^3 \theta'' + \frac{\mu U_0 x^{2m}}{\nu (T_w - T_\infty)} f''^2$$

$$+ \frac{\alpha_1 U_0^3 x^{3m-1}}{\nu (T_w - T_\infty)} \left\{ \frac{3m-1}{2} f' f''^2 - \frac{m+1}{2} f f'' f''' + \frac{1-m}{2} \xi \left(f' f'' \frac{\partial f''}{\partial \xi} - f'' f''' \frac{\partial f}{\partial \xi} \right) \right\}$$

$$+ Q(T_w - T_\infty) \theta \qquad (4.6)$$

which then reduces to equation (4.7) and (4.8) as shown below,

$$f''' + \frac{m+1}{2} ff'' - m(1-f'^2) - Ha^2 \sin^2 \psi (f'-1) - k_1 f' - F^* f'^2 + \lambda \left[(3m-1) f' f''' + \right.$$

$$\frac{3m-1}{2} f''^2 + (m-1) \eta f'' f''' - \frac{m+1}{2} f f^{iv} + \frac{1-m}{2} \xi \left(f''' \frac{\partial f'}{\partial \xi} + f'' \frac{\partial f''}{\partial \xi} - f^{iv} \frac{\partial f}{\partial \xi} \right) \right]$$

$$- \frac{1-m}{2} \xi \left(f'' \frac{\partial f}{\partial \xi} - f' \frac{\partial f'}{\partial \xi} \right) = 0, \qquad (4.7)$$

$$(1 + Rd) \theta'' + \gamma_1 \theta - \frac{1-m}{2} \xi \left(f' \frac{\partial \theta}{\partial \xi} - \frac{\partial f}{\partial \xi} \theta' \right) + Ec \lambda f'' \left[\frac{3m-1}{2} f' f'' - \frac{m+1}{2} f f''' \right.$$

$$+ \frac{m-1}{2} \xi \left(f''' \frac{\partial f}{\partial \xi} - f' \frac{\partial f''}{\partial \xi} \right) \right] - \frac{m-1}{2} \xi \left(\theta' \frac{\partial f}{\partial \xi} - f' \frac{\partial \theta}{\partial \xi} \right) = 0. \qquad (4.8)$$

The boundary conditions (4.3) and (4.4) then turn into

$$f' = A, \qquad Pr f(\eta) + M\theta'(\eta) = 0, \qquad \theta = 1, \qquad \text{at} \qquad \eta = 0,$$

$$f' = 1, \qquad \theta = 0, \qquad \text{as} \qquad \eta \to \infty, \qquad (4.9)$$

where,

$$\lambda = \frac{\alpha_1 U_0 x^{m-1}}{\rho \nu}, \quad Ha = \frac{\sigma B_0^2}{\rho U_0 x^{m-1}}, \quad k_1 = \frac{\nu}{U_0^2 k x^{m-1}}, \quad F^* = Fx, \quad R_d = \frac{16\sigma^* T_\infty^3}{3kk*},$$

$$\gamma_1 = \frac{Q}{u_0 x^{m-1}}, \quad Ec = \frac{U_0^2 x^{2m}}{c_p(T_w - T_\infty)}, \quad Pr = \frac{\nu \rho C_p}{k}, \quad M = \frac{C_p(T_w - T_\infty)}{\lambda + C_s(T_w - T_0)} \quad A = \frac{b}{U_0}.$$

Applying the spectral quasilinearization method to the above models implies the assumption that the difference $||f_{r+1} - f_r||$, and all its derivatives, are small. The quasilinearized scheme corresponding to (4.7) and (4.8) becomes

$$b_{0r} f_{r+1}^{iv} + b_{1r} f_{r+1}''' + b_{2r} f_{r+1}'' + b_{3r} f_{r+1}' + b_{4r} f_{r+1} + \gamma_{0r} \frac{\partial f_r}{\partial \xi} + \gamma_{1r} \frac{\partial f_r'}{\partial \xi} + \gamma_{2r} \frac{\partial f_r''}{\partial \xi}$$

$$+ \gamma_{3r} \frac{\partial f_r'''}{\partial \xi} = 0, \tag{4.10}$$

$$c_{0r} \theta_{r+1}'' + c_{1r} \theta_{r+1}' + c_{2r} \theta_{r+1} + c_{3r} f_{r+1}''' + c_{4r} f_{r+1}'' + c_{5r} f_{r+1}' + c_{6r} f_{r+1} + \sigma_{0r} \frac{\partial \theta_{r+1}}{\partial \xi}$$

$$+ \sigma_{1r} \frac{\partial f_{r+1}''}{\partial \xi} + \sigma_{2r} \frac{\partial f_{r+1}}{\partial \xi} = 0, \tag{4.11}$$

and the boundary conditions (4.9) become

$$f_{r+1}' = A, \qquad Prf(\eta)_{r+1} + M\theta'(\eta)_{r+1} = 1, \qquad \theta_{r+1} = 0 \qquad \text{at} \qquad \eta = 0,$$

$$f_{r+1}' = 1, \qquad \theta_{r+1} = 0 \qquad \text{at} \qquad \eta \to \infty, \tag{4.12}$$

where the variable coefficients are given by

$$b_{0r} = -\lambda\left(\frac{m+1}{2}f_r + \frac{1-m}{2}\xi\frac{\partial f_r}{\partial\xi}\right),$$

$$b_{1r} = 1 + \lambda\left((3m-1)f_r' + (m-1)\eta f'' + \frac{1-m}{2}\xi\frac{\partial f_r'}{\partial\xi}\right),$$

$$b_{2r} = \frac{m+1}{2}f_r + \lambda\left((3m-1)f'' + (m-1)\eta f''' + \frac{1-m}{2}\xi\frac{\partial f_r''}{\partial\xi}\right) - \frac{1-m}{2}\xi\frac{\partial f_r}{\partial\xi},$$

$$b_{3r} = -2mf_r' - Ha^2\sin^2\psi - k_1 - 2F^*f_r' + \lambda(3m-1)f_r''' + \frac{1-m}{2}\xi\frac{\partial f_r'}{\partial\xi},$$

$$b_{4r} = \frac{m+1}{2}(f_r'' - \lambda f_r^{iv}),$$

$$\gamma_{0r} = \lambda\frac{1-m}{2}\xi f_r'',$$

$$\gamma_{1r} = \frac{1-m}{2}\xi(\lambda f_r''' + f_r'),$$

$$\gamma_{2r} = -\frac{1-m}{2}\xi(\lambda f_r^{iv} + f_r''),$$

$$c_{0r} = 1 + R_d,$$

$$c_{1r} = \frac{1-m}{2}\xi\frac{\partial f_r}{\partial\xi} - \frac{m-1}{2}\xi\frac{\partial f_r}{\partial\xi},$$

$$c_{3r} = Ec\lambda\left(-\frac{m+1}{2}f_r f_r'' + \frac{m-1}{2}\xi f_r''\frac{\partial f_r}{\partial\xi}\right),$$

$$c_{4r} = Ec\lambda\left[(3m-1)f_r'f_r'' - \frac{m+1}{2}f_r f_r''' + \frac{m-1}{2}\xi\left(f'''\frac{\partial f_r}{\partial\xi} - f'\frac{\partial f_r''}{\partial\xi}\right)\right],$$

$$c_{5r} = (m-1)\xi\frac{\partial\theta_r}{\partial\xi} + Ec\lambda\left(\frac{3m-1}{2}\xi f_r''^2 - \frac{m-1}{2}\xi f_r''\frac{\partial f_r''}{\partial\xi}\right), \qquad c_{2r} = \gamma_1,$$

$$c_{6r} = -Ec\lambda\frac{m+1}{2}f_r''f_r''',$$

$$\sigma_{0r} = (m-1)\xi f_r',$$

$$\sigma_{1r} = -Ec\lambda\frac{m-1}{2}\xi f_r'f_r'',$$

$$\sigma_{2r} = -(m-1)\xi\theta' + Ec\lambda\frac{m-1}{2}\xi f_r''f_r'''.$$

Applying spectral collocation of Chebyshev differentiation to (4.10) and (4.11), the equa-

tions can be simplified further by introducing coefficients as,

$$\Big[b_{0r} D^{iv} + b_{1r} D^3 + b_{2r} D^2 + b_{3r} D + b_{4r} + 2 \sum_{j=0}^{N_\xi} d_{ij} \big[\gamma_{0r} D^2 + \gamma_{1r} D$$

$$+ \gamma_{2r} I \big] \Big] f_{r+1} = R_{f,r}, \tag{4.13}$$

$$\Big[c_{3r} D^3 + c_{4r} D^2 + c_{5r} D + c_{6r} I + 2 \sum_{j=0}^{N_\xi} d_{ij} [\sigma_{1r} D^2 + \sigma_{2r} I] \Big] f_{r+1} + \Big[c_{0r} D^2 + c_{1r} D$$

$$+ c_{2r} + 2 \sum_{j=0}^{N_\xi} d_{ij} [\sigma_{0r} I] \Big] \theta_{r+1} = R_{\theta,r}. \tag{4.14}$$

Equations (4.13) and (4.14) can be expressed in their matrix–vector form as

$$
\begin{bmatrix}
\begin{bmatrix} \Pi_{11}^{0,0} & \Pi_{12}^{0,0} \\ \Pi_{21}^{0,0} & \Pi_{22}^{0,0} \end{bmatrix} & \begin{bmatrix} \Pi_{11}^{0,1} & \Pi_{12}^{0,1} \\ \Pi_{21}^{0,1} & \Pi_{22}^{0,1} \end{bmatrix} & \cdots & \begin{bmatrix} \Pi_{11}^{0,N_\xi} & \Pi_{12}^{0,N_\xi} \\ \Pi_{21}^{0,N_\xi} & \Pi_{22}^{0,N_\xi} \end{bmatrix} \\[2em]
\begin{bmatrix} \Pi_{11}^{1,0} & \Pi_{12}^{1,0} \\ \Pi_{12}^{1,0} & \Pi_{22}^{1,0} \end{bmatrix} & \begin{bmatrix} \Pi_{11}^{1,1} & \Pi_{12}^{1,1} \\ \Pi_{21}^{1,1} & \Pi_{22}^{1,1} \end{bmatrix} & \cdots & \begin{bmatrix} \Pi_{11}^{1,N_\xi} & \Pi_{12}^{1,N_\xi} \\ \Pi_{21}^{1,N_\xi} & \Pi_{22}^{1,N_\xi} \end{bmatrix} \\[2em]
\vdots & \vdots & \ddots \ddots & \vdots \\
\begin{bmatrix} \Pi_{11}^{N_\xi,0} & \Pi_{12}^{N_\xi,0} \\ \Pi_{21}^{N_\xi,0} & \Pi_{22}^{N_\xi,0} \end{bmatrix} & \begin{bmatrix} \Pi_{11}^{N_\xi,1} & \Pi_{12}^{N_\xi,1} \\ \Pi_{21}^{N_\xi,1} & \Pi_{22}^{N_\xi,1} \end{bmatrix} & \cdots & \begin{bmatrix} \Pi_{11}^{N_\xi,N_\xi} & \Pi_{12}^{N_\xi,N_\xi} \\ \Pi_{21}^{N_\xi,N_\xi} & \Pi_{22}^{N_\xi,N_\xi} \end{bmatrix}
\end{bmatrix}
\begin{bmatrix}
\begin{bmatrix} f_{r+1,0} \\ \theta_{r+1,0} \end{bmatrix} \\[1.5em]
\begin{bmatrix} f_{r+1,1} \\ \theta_{r+1,1} \end{bmatrix} \\[1.5em]
\vdots \\
\vdots \\
\begin{bmatrix} f_{r+1,N_\xi} \\ \theta_{r+1,N_\xi} \end{bmatrix}
\end{bmatrix}
=
\begin{bmatrix}
\begin{bmatrix} R_{f,r,0} \\ R_{\theta,r,0} \end{bmatrix} \\[1.5em]
\begin{bmatrix} R_{f,r,1} \\ R_{\theta,r,1} \end{bmatrix} \\[1.5em]
\vdots \\
\vdots \\
\begin{bmatrix} R_{f,r,N_\xi} \\ R_{\theta,r,N_\xi} \end{bmatrix}
\end{bmatrix}, \tag{4.15}
$$

where

$$\Pi_{11}^{i,i} = b_{0r}D^{iv} + b_{1r}D^3 + b_{2r}D^2 + b_{3r}D + b_{4r} + 2d_{ii}[\gamma_{0r}D^2 + \gamma_{1r}D + \gamma_{2r}I] \qquad (4.16.0)$$

$$\Pi_{11}^{i,j} = 2d_{ij}[\gamma_{0r}D^2 + \gamma_{1r}D + \gamma_{2r}I] \qquad (4.16.1)$$

$$\Pi_{12}^{i,i} = O = \text{zero matrix of size } (N_\eta + 1) \times (N_\eta + 1) \qquad (4.16.2)$$

$$\Pi_{12}^{i,j} = O = \text{zero matrix of size } (N_\eta + 1) \times (N_\eta + 1) \qquad (4.16.3)$$

$$\Pi_{21}^{i,i} = c_{3r}D^3 + c_{4r}D^2 + c_{5r}D + c_{6r}I + 2d_{ii}[\sigma_{1r}D^2 + \sigma_{2r}I] \qquad (4.16.4)$$

$$\Pi_{21}^{i,j} = 2d_{ij}[\sigma_{1r}D^2 + \sigma_{2r}I] \qquad (4.16.5)$$

$$\Pi_{22}^{i,i} = c_{0r}D^2 + c_{1r}D + c_{2r} + 2d_{ii}[\sigma_{0r}I] \qquad (4.16.6)$$

$$\Pi_{22}^{i,j} = 2d_{ij}[\sigma_{0r}I] \qquad (4.16.7)$$

After implementing the boundary conditions, Equation (4.15) can be solved for the unknown vectors f_{r+1} and θ_{r+1} at each ξ–level.

4.1 Results and Discussion

The present study uses the bivariate spectral quasilinearization method to generate a series of numerical results for the velocity and temperature. To validate the numerical code, the results have been calculated for $m = \lambda = Ha = \psi = 0$ and different values of η. From Table 4.1, where the results are compared with those of Hayat et al. [116], Kuo [117] and White [118], it is noted that there is good agreement.

Table 4.1: A comparison of $f(\eta)$ and $f'(\eta)$ with the numerical solutions by Hayat et al. [116], Kuo [117] and White [118] when $m = \lambda = Ha = \psi = 0$.

	$f(\eta)$				$f'(\eta)$			
η	Current	Hayat [116]	Kuo [117]	White [118]	Current	Hayat [116]	Kuo [117]	White [118]
0.0	0.000000	0.000000	0.000000	0.000000	0.000000	0.000000	0.000000	0.000000
0.1	0.002346	0.002346	0.002348	0.00235	0.046960	0.046956	0.046959	0.04696
0.3	0.021128	0.021127	0.021128	0.02113	0.140809	0.140807	0.140806	0.14081
0.5	0.058644	0.058641	0.058643	0.05864	0.234226	0.234227	0.234228	0.23423
0.7	0.114748	0.114749	0.114745	0.114747	0.326532	0.326534	0.326532	0.32653
0.9	0.189112	0.189113	0.189115	0.18911	0.416716	0.416716	0.416718	0.41672
1.1	0.281208	0.281205	0.281208	0.28121	0.503538	0.503536	0.50353	0.50354
1.3	0.390213	0.390213	0.390211	0.39021	0.585589	0.585587	0.585589	0.58559
1.5	0.515033	0.515032	0.515031	0.51503	0.661474	0.661472	0.661474	0.66147
2.2	1.054946	1.054943	1.054947	1.05495	0.863300	0.863302	0.863304	0.86330
3.0	1.795570	1.795565	1.795568	1.79557	0.969054	0.969053	0.969055	0.96905

(a)   (b)
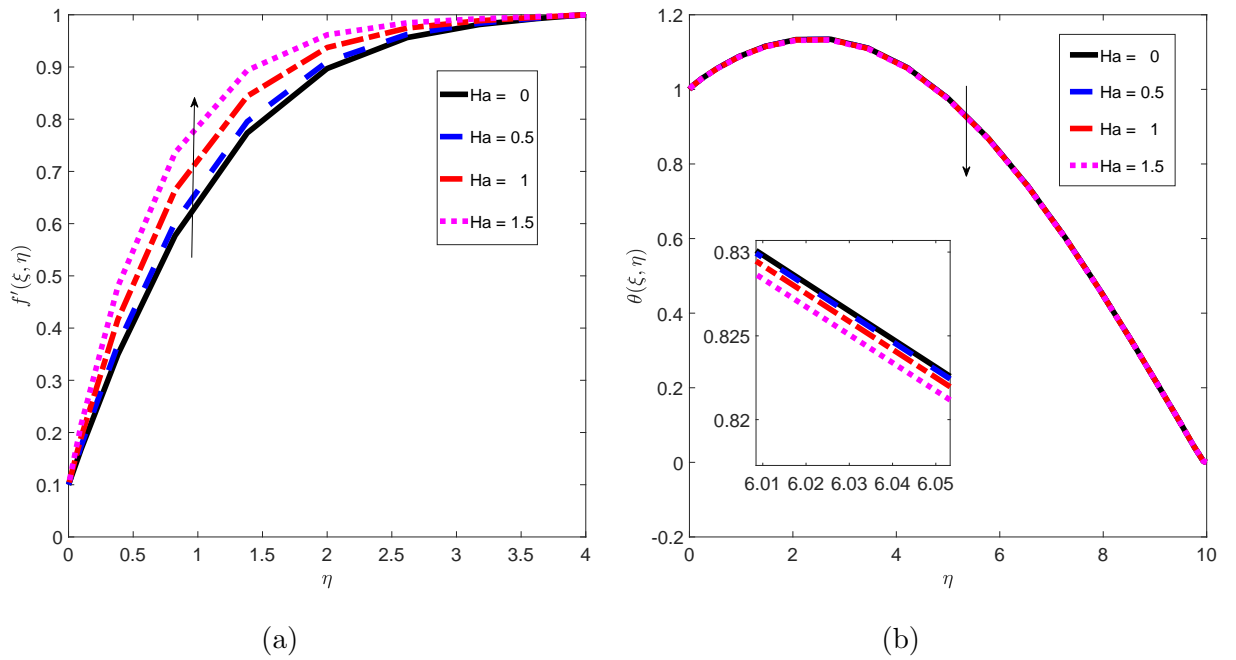
Figure 4.2: The variation of (a) velocity, and (b) temperature, profiles for different values of magnetic field parameter.

Figure 4.2 shows the impact of the magnetic field parameter on the velocity and the temperature profiles. The applied magnetic field increases the fluid velocity profile while reducing the temperature profiles. This means that the force which tends to oppose the

fluid flow reduces and increases the acceleration of the fluid flow. Hence, the rate of the fluid flow increases with the magnetic field parameter. The lower temperature suggests that the Lorentz force generates an electrically conducting fluid, reduces the thickness of the thermal boundary layer.

Table 4.2 shows the effect of the magnetic field parameter on the skin friction and heat transfer coefficient. It is observed that both skin friction and heat transfer increase with an increase in the magnetic field parameter. It is also observed that increasing the porous parameter will decrease the skin friction coefficient, which increasing the Nusselt number.

Table 4.2: The effect of porous parameter and magnetic field parameter.

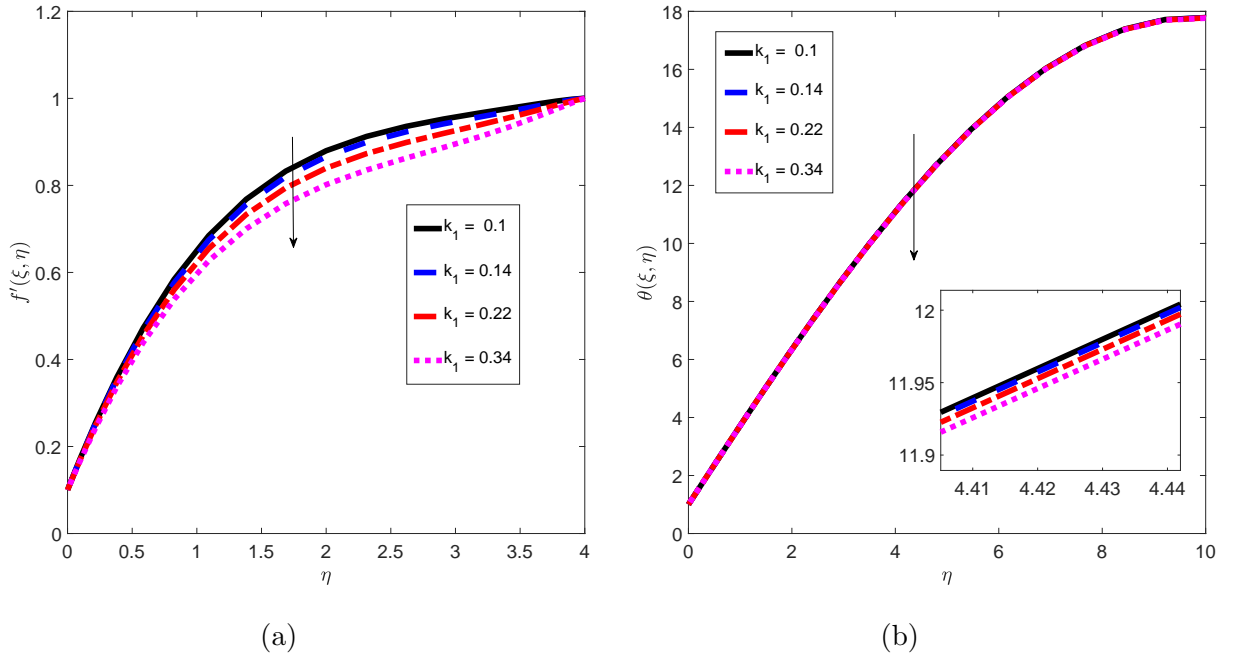| k_1	$-f''(0)$	$-\theta'(0)$	Ha	$-f''(0)$	$-\theta'(0)$
0.1	0.87123619	-0.05752645	0.2	0.79967347	0.12808539
0.41	0.86260513	-0.05751121	0.5	0.86291685	0.12819060
0.22	0.84595361	-0.05748386	0.6	0.89506838	0.12824843
0.34	0.82243508	-0.05744984	0.7	0.93228920	0.12831906

Figure 4.3: The variation of (a) velocity and (b) temperature, profiles for different values of the porous parameter.

The effect of a porous parameter, k_1, is shown in Figure 4.3. It is interesting to note that, with increasing the value of the porous parameter, both velocity and temperature profiles decrease in the boundary layer. This indicates that the porosity reduces the fluid velocity and the rate of heat transfer. As was observed in Table 4.2, increasing the porous parameter leads to a decrease in the skin friction coefficient whereas the reduced Nusselt number increases. This physically means that the resistance force exerted by the surface on the fluid flow reduces as the porous parameter increases.
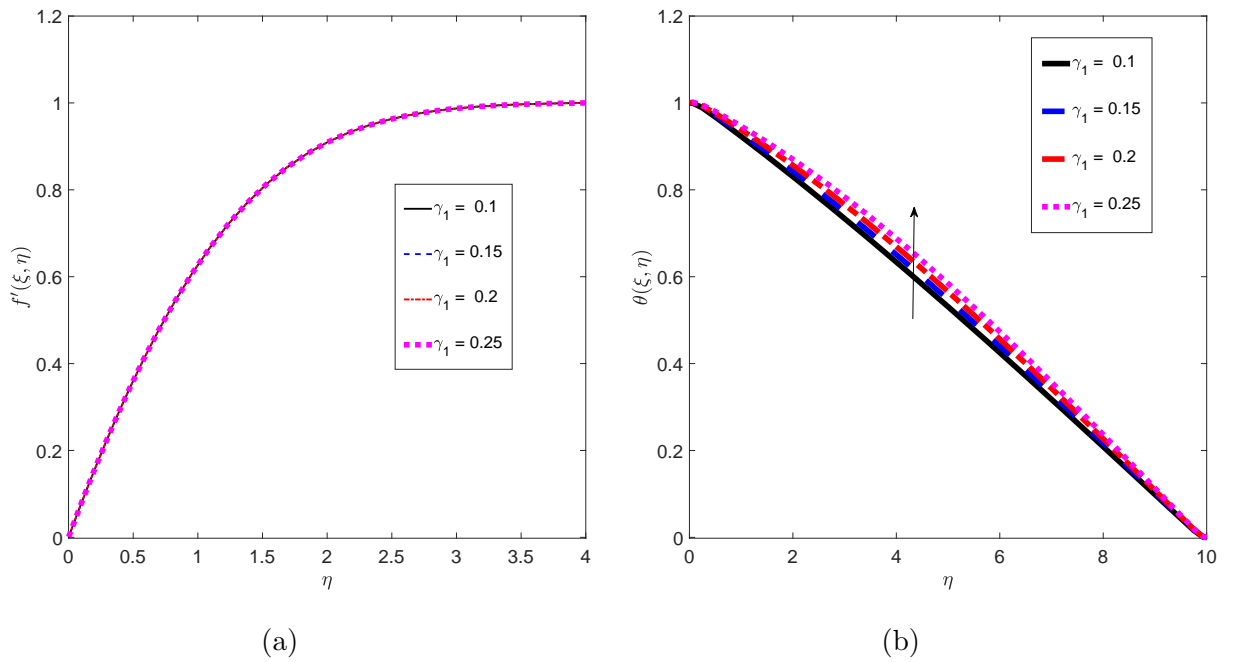

Figure 4.4: The variation of (a) velocity, $f'(\xi, \eta)$ and (b) temperature, $\theta(\xi, \eta)$ profiles for different values of heat generation/absorption parameter.

Figure 4.4 shows the effect of heat generation and the absorption parameter, γ_1, on the velocity and temperature profiles of the fluid. It is observed that temperature distribution increases with increase in the heat generation parameter while it decreases with increasing values of the heat absorption parameter. This is because the generation process produces more heat, which results in temperature rising. Figure 4.4 (a) demonstrates that increasing the heat generation and absorption parameter has no appreciable effect on the velocity profiles in the boundary layer. It is noted from Table 4.3 that with increasing heat generation and absorption parameter, the Nusselt number reduces, whereas this increase makes no difference to the values of the skin friction.

61

Table 4.3: The effect of wedge angle parameter, ψ and heat generation/absorption parameter, γ_1.

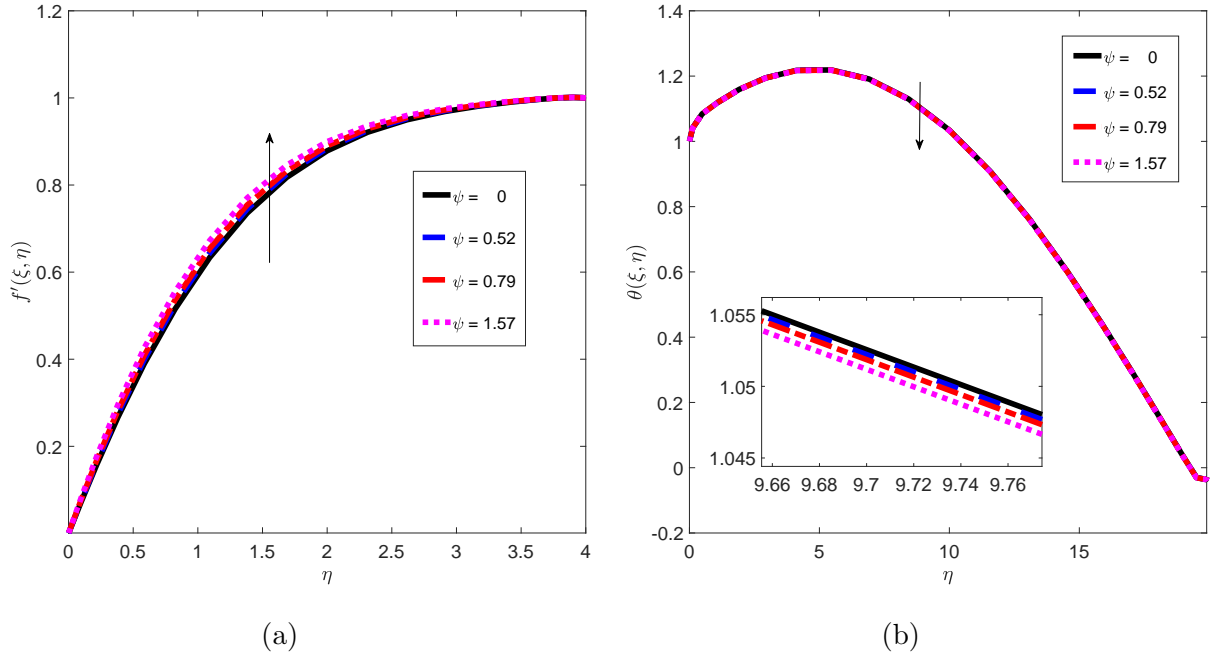| ψ	$-f''(0)$	$-\theta'(0)$	γ_1	$-f''(0)$	$-\theta'(0)$
0	0.83186973	-0.05768363	0.1	0.81653340	0.12870255
0.52	0.86145430	-0.05762752	0.15	0.81653340	0.05772039
0.79	0.89174909	-0.05756742	0.2	0.81653340	-0.02254204
1.57	0.94846158	-0.05744767	0.7	0.81653340	-0.11478144

Figure 4.5: The variation of (a) velocity, $f'(\xi, \eta)$ and (b) temperature, $\theta(\xi, \eta)$ profile for different values of wedge angle parameter.

Figure 4.5 shows the effect of the wedge angle parameter, ψ, on the velocity and temperature profiles in the second grade fluid. Figure 4.5 (a) shows that the fluid velocity increases with the wedge angle. Physically the wedge angle is related to the pressure gradient. The momentum boundary layer thickness increases with the wedge angle. Figure 4.5 (b) shows the effect of the inclination angle on the thermal boundary layer. It is observed that the fluid temperature decreases with an increasing wedge angle. The maximum temperature in the fluid occurs for the flow over a flat plate where $\psi = 0$. Table 4.3 also shows that an increase in the wedge angle parameter leads to an increase in the skin friction coefficient. Thus, the fluid heat transfer diminishes with increased wedge angle.

(a)　　　　　　　　　　　　　　　　　(b)
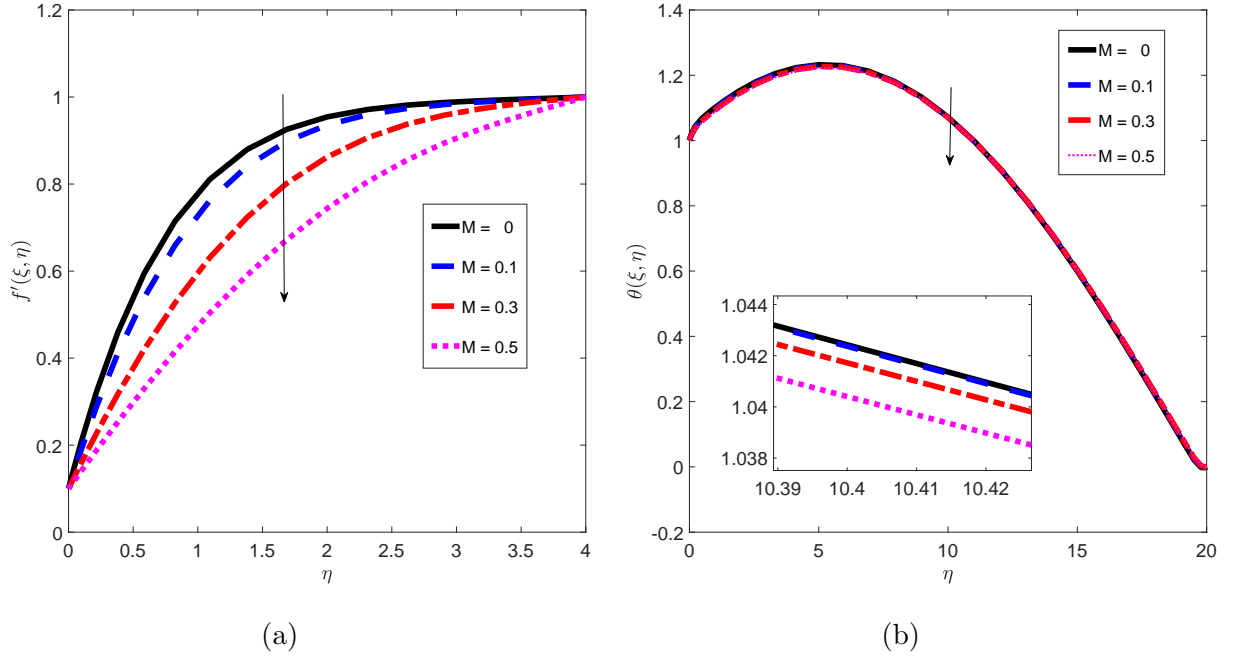
Figure 4.6: The variation of (a) velocity, $f'(\xi, \eta)$ and (b) temperature, $\theta(\xi, \eta)$ profiles for different values of melting parameter.

Figure 4.6 shows the variations of the melting parameter, M, on the fluid velocity and temperature profile. It is noted that both the velocity and temperature profiles decrease for the large values of the melting parameter. This means that heat transfer due to melting reduces the flow. Furthermore, increasing the melting parameter leads to increases in both momentum and thermal boundary layers.
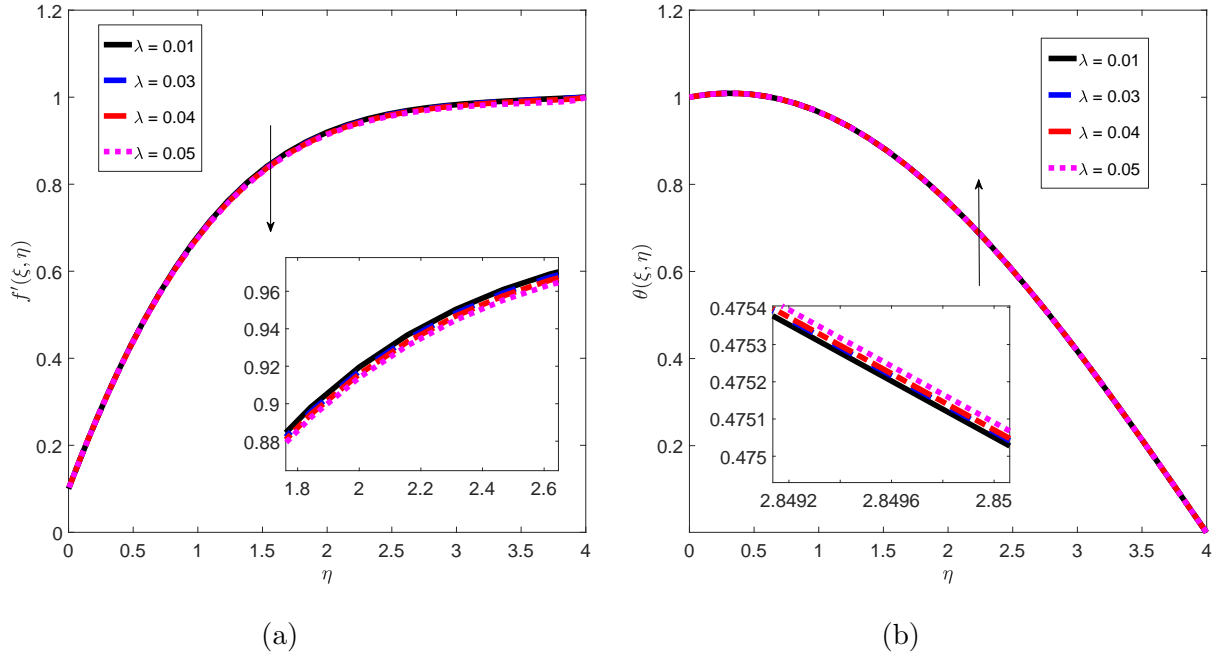
Figure 4.7: The variation of (a) velocity, and (b) temperature profiles for different values of second grade fluid parameter.

Figure 4.7 shows the effect of the second grade fluid parameter on the velocity and temperature profiles. It is observed that, with increases in the second grade parameter, the velocity profiles decrease, whereas the temperature profiles increase. This shows that the fluid flow is slow for high value of the second grade parameter. This is because the fluid exerts a resistance force on the wedge and there is a transfer of heat between the fluid and the plate. This is not surprising since the fluid is considered moving in a static plate.

4.2 Residual Error Analysis

Residual error analysis is used to show the convergence and accuracy of the solution method. The residual error norm for $f(\xi, \eta)$ and $\theta(\xi, \eta)$ obtained using BSQLM are shown in Figures 4.8 and 4.9, respectively. It is observed from Figure 4.8 that the BSQLM takes only 3 iterations to converge with an increase in the porous parameter. The residual error norm decreases with the number of iterations. This means that the approximate solutions obtained using the BSQLM method become more accurate as the iterative process continues. Moreover, the residual error norm decreases until convergence is achieved.
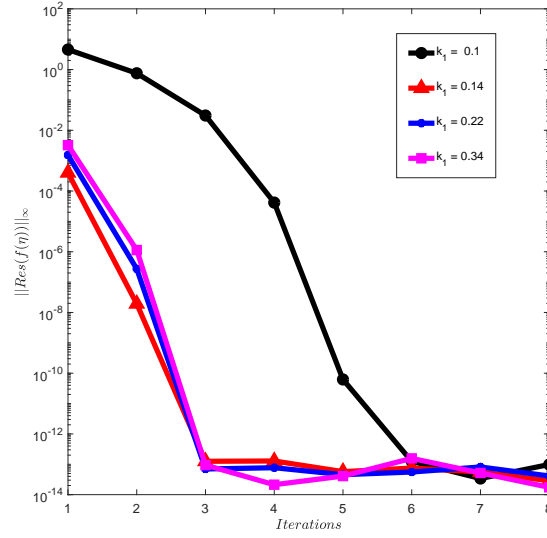
(a)

Figure 4.8: The residual error results for different values of the porous parameter.
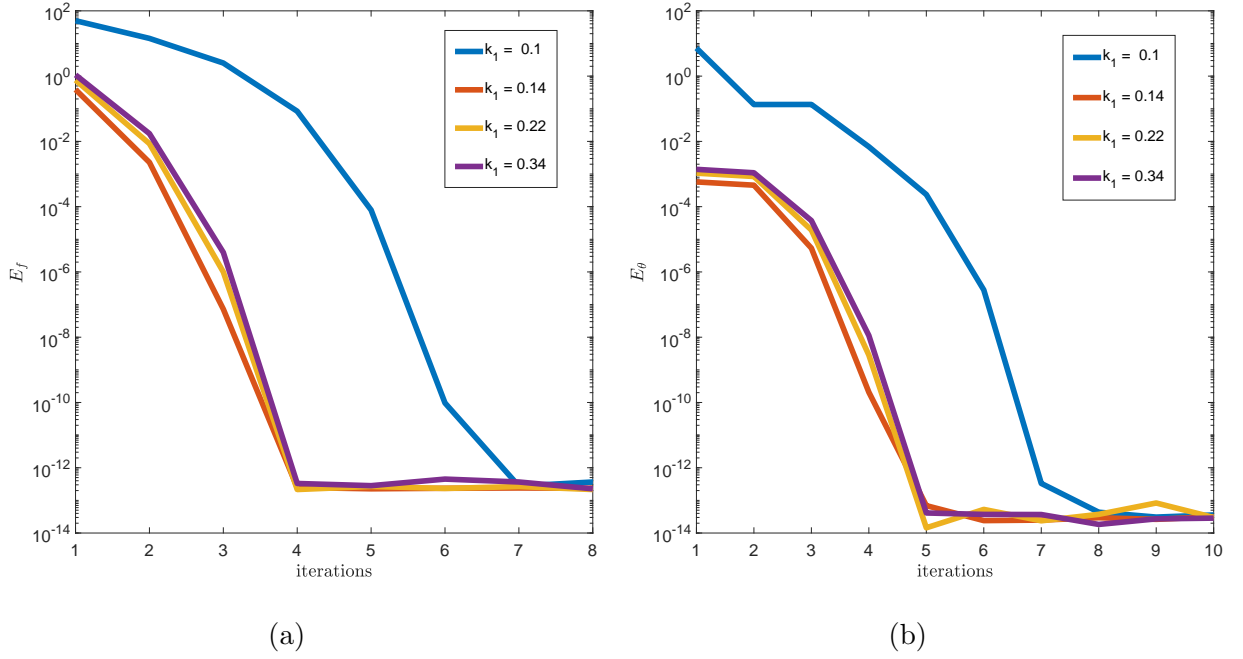
(a)   (b)

Figure 4.9: The error norm results against the number of iterations for different values of porous parameter.

In Figure 4.9 the influence of iterations on the convergence error norm E_f and E_θ of the bivariate spectral quasilinearization method is depicted. It is noted that the bivariate spectral quasilinearization method converges with 4 or 5 iterations at a maximum error

norm of 10^{-13} for the velocity profiles and and 10^{-14} for the temperature profiles. This indicates that BSQLM is an accurate method, and is appropriate for solving nonlinear partial differential equations. It is also noted that BSQLM gives parabolic graphs for the error norms, which indicate that the rate of convergence is second order. The iteration scheme requires 4 or 5 iterations to converge fully.

4.3   Summary

The characteristics of melting heat transfer in second grade nanofluid flowing over a porous wedge were analyzed. When results were compared to the findings in the literature they were found to be in good agreement. The results were presented through graphs and tables to illustrate the relationships between the fluid properties and the flow parameters. The findings in this chapter may be summarized as follows. Fluid flow is enhanced by increasing magnetic field and wedge parameters. The increase in the inclination angle leads to an increase in the fluid velocity and reduction in the temperature. Both the fluid velocity and temperature decrease with increasing porosity and melting parameters. The shear stress and heat transfer rate both increase by increasing an inclination angle for the wedge.The residual error analysis shows that the bivariate spectral quasilinearization method is an accurate method for solving the model equations for Falkner-Skan fluid flow.

Chapter 5

Second grade magnetohydrodynamic fluid flow over a convectively heated stretching sheet

In Chapter 4, we considered momentum and heat transport in a second grade fluid. In this chapter, we further increase the complexity of the boundary layer problem by including a solute transport equation. We model the fluid as flowing through a porous region, where it is impacted by a chemical reaction and viscous dissipation on a convectively heated stretching sheet. The BSQLM is used to numerically solve the flow equations. The numerical results of flow characteristics are discussed through graphs and tables. The impact of the magnetic field and thermal radiation on heat and mass transfer is analyzed. The convergence and accuracy of the method is determined using residual error analysis.

We study the steady two dimensional boundary layer flow of an incompressible and electrically conducting second grade fluid over a stretching sheet. A schematic representation of the physical model and coordinates system are shown in Figure 5.1.
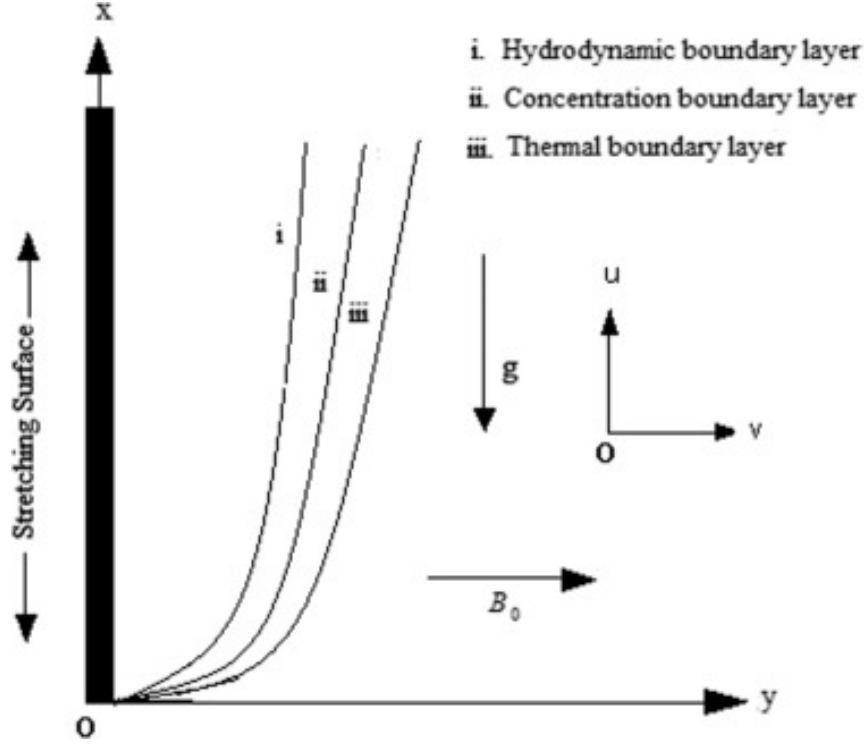
Figure 5.1: The problem set up and orientation of the coordinate system [30]

The x-axis is parallel to the sheet in the vertically upward direction and the y-axis is normal to it. The flow is along the x-axis, that is in the plane $y=0$, and the flow is restricted to $y>0$. There is viscous dissipation and joule heating. Since the fluid is second grade, the energy is stored in the fluid through frictional heating due to viscous dissipation and elastic deformation. There is thermal radiation in the flow. A uniform transverse magnetic field of strength B_0 is applied parallel to the y-axis. The induced magnetic field, magnetic Reynolds number and Hall effect are negligible. The flow is generated, due to the stretching of the sheet caused by simultaneous action of two equal and opposite forces along the x-axis. The sheet is stretched with the velocity $u_w = ax$ where a is a constant. Under these conditions, the boundary layer equations describing continuity, momentum, energy, and concentration are

$$u\frac{\partial u}{\partial x} + v\frac{\partial u}{\partial y} = 0,$$ (5.1)

$$u\frac{\partial u}{\partial x} + v\frac{\partial u}{\partial y} = \nu\frac{\partial^2 u}{\partial y^2} + \frac{\alpha_1}{\rho}\left[\frac{\partial}{\partial x}\left(u\frac{\partial^2 u}{\partial y^2}\right) - \frac{\partial u}{\partial y}\frac{\partial^2 u}{\partial x\partial y} + v\frac{\partial^3 u}{\partial y^3}\right] - \frac{\sigma B_0^2}{\rho}u - \frac{\nu}{k^*}u - Fu^2$$
$$+ g\beta_T(T - T_\infty) + g\beta^*(C - C_\infty),$$ (5.2)

$$u\frac{\partial T}{\partial x} + v\frac{\partial T}{\partial y} = \frac{k}{\rho C_p}\frac{\partial^2 T}{\partial^2 y^2} + \frac{\mu}{\rho C_p}\left(\frac{\partial u}{\partial y}\right)^2 - \frac{\partial q_r}{\partial y} + \alpha_1\frac{\partial u}{\partial y}\left[\frac{\partial}{\partial y}\left(u\right)\frac{\partial u}{\partial x} + v\frac{\partial u}{\partial y}\right)\right]$$
$$+ \sigma B_0^2 u^2,$$ (5.3)

$$u\frac{\partial C}{\partial x} + v\frac{\partial C}{\partial y} = D_B\frac{\partial^2 C}{\partial y^2} + \frac{D_T}{T_\infty}\frac{\partial^2 T}{\partial y^2} - k_r(C - C_\infty).$$ (5.4)

The corresponding boundary conditions for the present model are

$$u = u_w, \qquad v = v_0, \qquad T = T_w, \qquad C = C_w \qquad \text{at} \qquad y = 0,$$

$$u \to 0, \qquad \frac{\partial u}{\partial x} \to 0, \qquad T \to T_\infty, \quad C \to C_\infty \qquad \text{as} \qquad y \to \infty.$$ (5.5)

In terms of radiant heat transfer, the fluid here is considered to be optically thick (see Section 1.5). Accordingly, the diffusion approximation model that is used for radiative transfer includes an approximate form of the radiative heat flux gradient, qr, in the y-direction, which is called the Rosseland or diffusion approximation. It has the following form:

$$q_r = -\frac{4\sigma*}{3k*}\frac{\partial^2 T^4}{\partial y}.$$ (5.6)

Assuming that the differences in temperature within the flow are such that T^4 can be expressed as a linear combination of the temperature, expanding T^4 in a Taylor series about T_∞ and neglecting higher order terms, we get

$$T^4 = 4T_\infty^4 T - 3T_\infty^4. \tag{5.7}$$

Thus we have,

$$\frac{\partial q_r}{\partial y} = -\frac{16T_\infty^3 \sigma^*}{3k^*} \frac{\partial^2 T}{\partial y^2}. \tag{5.8}$$

Here u and v are the velocity components in the x and y directions, respectively, g is the acceleration due to gravity, β_T is the coefficient of thermal expansion, β^* is the concentration expansion coefficient, T is the fluid temperature, T_∞ is the ambient temperature, C is the solute concentration, C_∞ is ambient concentration, σ^* is the Stefan-Boltzman constant, k is the thermal conductivity of the fluid, c_p is the specific heat at constant pressure, q_r is the radiation heat flux, D_m is the molecular diffusivity, v_0 is the suction/injection velocity, T_m is the mean fluid temperature and C_w is the concentration at the wall, k_r is the rate of chemical reaction, where $k_r > 0$ represents a destructive reaction, $k_r < 0$ represents a generative reaction and $k_r = 0$ indicates no reaction. The similarity transformations below are introduced:

$$u = U_0 x^m f'(\xi, \eta), \qquad v = -\frac{1}{2}(\nu U_0)^{\frac{1}{2}} x^{\frac{m-1}{2}} \{(m+1)f + (1-m)(\xi \frac{\partial f}{\partial \xi} - \eta f'),$$

$$T - T_\infty = (T_w - T_\infty)\theta(\xi, \eta), \qquad \xi = \left(\frac{\nu}{U_0}\right)^{\frac{1}{2}} x^{\frac{1-m}{2}}, \qquad \eta = \left(\frac{U_0}{\nu}\right)^{\frac{1}{2}} x^{\frac{m-1}{2}} y.$$

Equation (5.1) is automatically satisfied. Then, the model equations (5.2) - (5.4) reduce to the non-dimensionalized form shown below:

70

$$U_0^2 x^{2m-1}\left\{\frac{1-m}{2}\xi f'\frac{\partial f'}{\partial \xi} + mf'^2 - \frac{m+1}{2}ff'' - \frac{1-m}{2}\xi f''\frac{\partial f}{\partial \xi}\right\} = U_0^2 x^{2m-1}f'''$$

$$+ \frac{\alpha_1 U_0^3 x^{3m-2}}{\rho\nu}\left\{\frac{1-m}{2}\xi\left(f'''\frac{\partial f'}{\partial \xi} + f^{iv}\frac{\partial f}{\partial \xi}\right) + (3m-1)f'f''' + \frac{1-m}{2}\xi f'\frac{\partial f'''}{\partial \xi}\right.$$

$$\left. + \frac{m+1}{2}f'f^{iv} + \frac{3m-1}{2}f''^2\right\} - \frac{\nu U_0 x^m}{k}f' - FU_0^2 x^{2m}f'^2 - \frac{\sigma B_0^2 U_0 x^m}{\rho}f' \qquad (5.9)$$

$$\rho C_p U_0 x^{m-1}(T_w - T_\infty)\left\{\frac{1-m}{2}\xi f'\frac{\partial \theta}{\partial \xi} - \frac{m+1}{2} - \frac{1-m}{2}\xi\frac{\partial f}{\partial \xi}\theta'\right\} = \frac{k_r}{\nu}(T_w - T_\infty)U_0 x^{m-1}\theta''$$

$$+ \frac{4\sigma^*}{3k_1}\frac{4T_\infty^3 U_0}{\nu}x^{m-1}(T_w - T_\infty)\theta'' + \frac{\mu}{\nu}U_0^3 x^{3m-1}f''^2 + \frac{\alpha_1 U_0^4}{\nu}x^{4m-2}\left\{\frac{3m-1}{2}f'f''^2 - \frac{m+1}{2}ff''f'''\right.$$

$$\left. + \frac{1-m}{2}\xi\left(f'f''\frac{\partial f''}{\partial \xi} - f''f'''\frac{\partial f}{\partial \xi}\right)\right\} + Q(T_w - T_\infty)\theta \qquad (5.10)$$

$$U_0 x^{m-1}(C_w - C_\infty)\left\{\xi f'\frac{\partial \phi}{\partial \xi} - \xi\frac{\partial f}{\partial \xi} - \frac{m+1}{2}f\phi'\right\} = \frac{D_B}{\nu}U_0 x^{m-1}(C_w - C_\infty)\phi''$$

$$+ \frac{D_T}{T_\infty\nu}\frac{(T_w - T_\infty)}{(C_w - C_\infty)} \qquad (5.11)$$

and then the above equation (5.9 - 5.11) reduces to

$$f''' + \frac{m+1}{2}ff'' - mf'^2 - Ha^2 f' - k_1 f' - F^* f'^2 + Gr_t\theta + Gr_c\phi + \lambda\left[(3m-1)f'f''' - \right.$$

$$\frac{m+1}{2}ff^{iv} - \frac{3m-1}{2}f''^2 + \frac{m-1}{2}\xi\left(f^{iv}\frac{\partial f}{\partial \xi} - f'''\frac{\partial f'}{\partial \xi} + f''\frac{\partial f''}{\partial \xi} - f'\frac{\partial f'''}{\partial \xi}\right)\right] -$$

$$\left. \frac{m-1}{2}\xi\left(f''\frac{\partial f}{\partial \xi} - f'\frac{\partial f'}{\partial \xi}\right) = 0, \qquad (5.12)\right.$$

$$(1 + R_d)\theta'' + Pr\left(\frac{m+1}{2}\right)f\theta' + PrEc\left[f''^2 + Ha^2 f'^2 + \lambda f''\left(\frac{3m-1}{2}f'f'' - \frac{m+1}{2}ff'''\right.\right.$$

$$\left.\left. + \frac{m-1}{2}\xi\left(f'''\frac{\partial f}{\partial \xi} - f'\frac{\partial f''}{\partial \xi}\right)\right)\right] - Pr\frac{m-1}{2}\xi\left(\theta'\frac{\partial f}{\partial \xi} - f'\frac{\partial \theta}{\partial \xi}\right) = 0, \qquad (5.13)$$

$$\frac{1}{Sc}\phi'' + \frac{m+1}{2}f\phi' - Kr\phi + Sr\theta'' + \frac{1-m}{2}\xi\left(\frac{\partial f}{\partial\xi}\phi' - f'\frac{\partial\phi}{\partial\xi}\right) = 0. \qquad (5.14)$$

The boundary conditions (5.5) then turns into

$$f = 0, \qquad f' = 1, \qquad \theta = 1, \qquad \phi = 1 \qquad \text{at} \qquad \eta = 0,$$

$$f' \to 1, \qquad f'' \to 0, \qquad \theta \to 0, \qquad \phi \to 0 \qquad \text{as} \qquad \eta \to \infty, \qquad (5.15)$$

such that

$$Ha^2 = \frac{\sigma B_0^2}{\rho U_0 x^{m-1}}, \qquad \lambda = \frac{\alpha_1 U_0 x^{m-1}}{\rho\nu}, \qquad Ec = \frac{U_0^2 x^2 m}{C_p(T-w-T_\infty)}, \qquad k_1 = \frac{\nu}{kU_0 x^{m-1}}, \qquad F* = Fx,$$

$$Gr_t = \frac{g\beta_t(T_w-T_\infty)}{U_0^2 x^{2m-1}}, \qquad Gr_c = \frac{g\beta_c(C_w-C_\infty)}{U_0^2 x^{2m-1}}, \qquad R_d = \frac{16T_\infty^3 \sigma*}{3kk*}, \qquad Pr = \frac{\nu\rho C_p}{k}, \qquad Sc = \frac{\nu}{D_B},$$

$$Sr = \frac{D_T(T_w-T_\infty)}{\nu T_\infty(C_w-C_\infty)}, \qquad Kr = \frac{k_r}{U_0 x^{m-1}}.$$

In the quasilinearization method the subscripts r and $r+1$ denote the previous and current iterations, respectively. Accordingly, the previous solutions are denoted by f_r, θ_r and ϕ_r, while those for the current iteration level are denoted by f_{r+1}, θ_{r+1} and ϕ_{r+1}. We make the assumption that the difference between the current and previous solutions is small. The spectral quasilinearization scheme corresponding to the equations (5.12 - (5.14) gives

$$d_{0r}f_{r+1}^{iv} + d_{1r}f_{r+1}''' + d_{2r}f_{r+1}'' + d_{3r}f_{r+1}' + d_{4r}f_{r+1} + d_{5r}\theta_{r+1} + d_{6r}\phi_{r+1} + \beta_{0r}\frac{\partial f_{r+1}'''}{\partial\xi} + \beta_{1r}\frac{\partial f_{r+1}''}{\partial\xi}$$

$$+ \beta_{2r}\frac{\partial f_{r+1}'}{\partial\xi} + \beta_{3r}\frac{\partial f}{\partial\xi} = R_{f,r}, \qquad (5.16)$$

$$g_{0r}\theta_{r+1}'' + g_{1r}\theta_{r+1}' + g_{2r}\theta_{r+1} + g_{3r}f_{r+1}''' + g_{4r}f_{r+1}'' + g_{5r}f_{r+1}' + g_{6r}f_{r+1} + \epsilon_{0r}\frac{\partial\theta_{r+1}}{\partial\xi} + \epsilon_{1r}\frac{\partial f_{r+1}''}{\partial\xi}$$

$$+ \epsilon_{2r}\frac{\partial f_{r+1}}{\partial\xi} = R_{\theta,r}, \qquad (5.17)$$

$$h_{0r}\phi_{r+1}'' + h_{1r}\phi_{r+1}' + h_{2r}\phi_{r+1} + h_{3r}\theta_{r+1}'' + h_{4r}f_{r+1}' + h_{5r}f_{r+1} + \kappa_{0r}\frac{\partial\phi_{r+1}}{\partial\xi}$$

$$+ \kappa_{1r}\frac{\partial f_{r+1}}{\partial\xi} = R_{\theta,r}, \qquad (5.18)$$

where,

$$d_{0r} = \lambda\left(\frac{m-1}{2}\xi\frac{\partial f_r}{\partial \xi} - \frac{m+1}{2}f_r\right),$$

$$d_{1r} = 1 + \lambda\left((3m-1)f_r' - \frac{m-1}{2}\xi\frac{\partial f_r'}{\partial \xi}\right),$$

$$d_{2r} = \frac{m+1}{2}fr - \lambda(3m-1)f'' + \frac{m-1}{2}\xi\left(\lambda\frac{\partial f_r''}{\partial \xi} - \frac{\partial f_r}{\partial \xi}\right),$$

$$d_{3r} = -2mf_r' - Ha^2 - k_1 - 2F^*fr' + \lambda(3m-1)f_r''' + \frac{m-1}{2}\xi\left(\frac{\partial f_r'}{\partial \xi} - \lambda\frac{\partial f_r'''}{\partial \xi}\right),$$

$$d_{4r} = \frac{m+1}{2}(f_r'' - \lambda f_r^{iv}),$$

$$d_{5r} = Gr_t,$$

$$d_{6r} = Gr_c,$$

$$\beta_{0r} = -\lambda\frac{m-1}{2}\xi f_r',$$

$$\beta_{1r} = \lambda\frac{m-1}{2}\xi f_r'',$$

$$\beta_{2r} = \frac{m-1}{2}\xi(f_r' - \lambda f_r'''),$$

$$\beta_{3r} = \frac{m-1}{2}\xi(\lambda f_r^{iv} - f_r''),$$

$$g_{0r} = 1 + R_d,$$

$$g_{1r} = -Pr\frac{m-1}{2}\xi\frac{\partial f_r}{\partial \xi} + Pr\left(\frac{m+1}{2}f_r\right),$$

$$g_{2r} = 0,$$

$$g_{3r} = PrEc\lambda\left(\frac{m-1}{2}\xi f_r''\frac{\partial f_r}{\partial \xi} - \frac{m+1}{2}f_r f_r''\right),$$

$$g_{4r} = 2PrEcf'' + PrEc\lambda\left[(3m-1)f_r'f_r'' - \frac{m+1}{2}f_r f_r''' + \frac{m-1}{2}\xi\left(f_r'''\frac{\partial f_r}{\partial \xi} - f_r'\frac{\partial f_r''}{\partial \xi}\right)\right],$$

$$g_{5r} = PrEc\left(2Ha^2f_r'f'' + \lambda\frac{3m-1}{2}f_r''^2\right) + \frac{m-1}{2}\xi\left(\frac{\partial Pr\theta_r}{\partial \xi} - PrEc\lambda\frac{\partial f_r''}{\partial \xi}\right),$$

$$g_{6r} = Pr\frac{m+1}{2}(\theta_r - Ec\lambda f_r''f_r'''),$$

$$\epsilon_{0r} = Pr\frac{m-1}{2}\xi f_r',$$

$$\epsilon_{1r} = -PrEc\lambda\frac{m-1}{2}\xi f_r'f_r'',$$

$$\epsilon_{2r} = \frac{m-1}{2}\xi(PrEc\lambda f_r''f_r''' - Pr\theta_r'),$$

$$h_{0r} = \frac{1}{Sc},$$

$$h_{1r} = \frac{m+1}{2}f_r + \frac{1-m}{2}\xi\frac{\partial f_r}{\partial\xi},$$

$$h_{2r} = -Kr,$$

$$h_{3r} = Sr,$$

$$h_{4r} = -\frac{1-m}{2}\xi\frac{\partial\phi_r}{\partial\xi},$$

$$h_{5r} = \frac{m+1}{2}\phi_r',$$

$$\kappa_{0r} = -\frac{1-m}{2}\xi f_r',$$

$$\kappa_{1r} = \frac{1-m}{2}\xi\phi'.$$

Applying spectral collocation of Chebyshev differentiation into equations (5.16) - (5.18), we get

$$\left[d_{0r}D^{iv} + d_{1r}D^3 + d_{2r}D^2 + d_{3r}D + d_{4r}I + 2\sum_{j=0}^{N_\xi}d_{ij}[\beta_{0r}D^3 + \beta_{1r}D^2 + \beta_{2r}D^1 + \beta_{3r}I]\right]f_{r+1}$$

$$+ [d_{5r}]\theta_{r+1} + [d_{6r}]\phi_{r+1} = R_{f,r}, \tag{5.19}$$

$$\left[g_{0r}D^2 + g_{1r}D + g_{2r}I + 2\sum_{j=0}^{N_\xi}d_{ij}[\epsilon_{0r}I]\right]\theta_{r+1} + \left[g_{4r}D^2 + g_{5r}D^1 + g_{6r}I + 2\sum_{j=0}^{N_\xi}d_{ij}[\epsilon_{1r}D^2\right.$$

$$\left.+ \epsilon_{2r}I]\right]f_{r+1} = R_{\theta,r}, \tag{5.20}$$

$$\left[h_{0r}D^3 + h_{1r}D + h_{2r}I + 2\sum_{j=0}^{N_\xi} d_{ij}[\kappa_{0r}I]\right]\phi_{r+1} + [h_{3r}D^2]\theta_{r+1} + \left[h_{4r}D1 + h_{5r}I\right.$$

$$\left. + 2\sum_{j=0}^{N_\xi} d_{ij}[\kappa_{1r}I]\right]f_{r+1} = R_{\phi,r}. \tag{5.21}$$

We are required to solve the following system linear Equations (5.19) to (5.21), given by

$$\begin{bmatrix}
\begin{bmatrix} \Pi_{11}^{0,0} & \Pi_{12}^{0,0} & \Pi_{13}^{0,0} \\ \Pi_{21}^{0,0} & \Pi_{22}^{0,0} & \Pi_{23}^{0,0} \\ \Pi_{31}^{0,0} & \Pi_{32}^{0,0} & \Pi_{33}^{0,0} \end{bmatrix} & \begin{bmatrix} \Pi_{11}^{0,1} & \Pi_{12}^{0,1} & \Pi_{13}^{0,1} \\ \Pi_{21}^{0,1} & \Pi_{22}^{0,1} & \Pi_{23}^{0,1} \\ \Pi_{31}^{0,1} & \Pi_{32}^{0,1} & \Pi_{33}^{0,1} \end{bmatrix} & \cdots & \begin{bmatrix} \Pi_{11}^{0,N_\xi} & \Pi_{12}^{0,N_\xi} & \Pi_{13}^{0,N_\xi} \\ \Pi_{21}^{0,N_\xi} & \Pi_{22}^{0,N_\xi} & \Pi_{23}^{0,N_\xi} \\ \Pi_{31}^{0,N_\xi} & \Pi_{32}^{0,N_\xi} & \Pi_{33}^{0,N_\xi} \end{bmatrix} \\
\begin{bmatrix} \Pi_{11}^{1,0} & \Pi_{12}^{1,0} & \Pi_{13}^{1,0} \\ \Pi_{12}^{1,0} & \Pi_{22}^{1,0} & \Pi_{23}^{1,0} \\ \Pi_{31}^{1,0} & \Pi_{32}^{1,0} & \Pi_{33}^{1,0} \end{bmatrix} & \begin{bmatrix} \Pi_{11}^{1,1} & \Pi_{12}^{1,1} & \Pi_{13}^{1,1} \\ \Pi_{21}^{1,1} & \Pi_{22}^{1,1} & \Pi_{23}^{1,1} \\ \Pi_{31}^{1,1} & \Pi_{32}^{1,1} & \Pi_{33}^{1,1} \end{bmatrix} & \cdots & \begin{bmatrix} \Pi_{11}^{1,N_\xi} & \Pi_{12}^{1,N_\xi} & \Pi_{13}^{1,N_\xi} \\ \Pi_{21}^{1,N_\xi} & \Pi_{22}^{1,N_\xi} & \Pi_{23}^{1,N_\xi} \\ \Pi_{31}^{1,N_\xi} & \Pi_{32}^{1,N_\xi} & \Pi_{33}^{1,N_\xi} \end{bmatrix} \\
\vdots & \vdots & \ddots & \vdots \\
\begin{bmatrix} \Pi_{11}^{N_\xi,0} & \Pi_{12}^{N_\xi,0} & \Pi_{13}^{N_\xi,0} \\ \Pi_{21}^{N_\xi,0} & \Pi_{22}^{N_\xi,0} & \Pi_{23}^{N_\xi,0} \\ \Pi_{31}^{N_\xi,0} & \Pi_{32}^{N_\xi,0} & \Pi_{33}^{N_\xi,0} \end{bmatrix} & \begin{bmatrix} \Pi_{11}^{N_\xi,1} & \Pi_{12}^{N_\xi,1} & \Pi_{13}^{N_\xi,1} \\ \Pi_{21}^{N_\xi,1} & \Pi_{22}^{N_\xi,1} & \Pi_{23}^{N_\xi,1} \\ \Pi_{31}^{N_\xi,1} & \Pi_{32}^{N_\xi,1} & \Pi_{33}^{N_\xi,1} \end{bmatrix} & \cdots & \begin{bmatrix} \Pi_{11}^{N_\xi,N_\xi} & \Pi_{12}^{N_\xi,N_\xi} & \Pi_{13}^{N_\xi,N_\xi} \\ \Pi_{21}^{N_\xi,N_\xi} & \Pi_{22}^{N_\xi,N_\xi} & \Pi_{23}^{N_\xi,N_\xi} \\ \Pi_{31}^{N_\xi,N_\xi} & \Pi_{32}^{N_\xi,N_\xi} & \Pi_{33}^{N_\xi,N_\xi} \end{bmatrix}
\end{bmatrix}
\begin{bmatrix} \begin{bmatrix} f_{r+1,0} \\ \theta_{r+1,0} \\ \phi_{r+1,0} \end{bmatrix} \\ \begin{bmatrix} f_{r+1,1} \\ \theta_{r+1,1} \\ \phi_{r+1,1} \end{bmatrix} \\ \vdots \\ \begin{bmatrix} f_{r+1,N_\xi} \\ \theta_{r+1,N_\xi} \\ \phi_{r+1,N_\xi} \end{bmatrix} \end{bmatrix}
=
\begin{bmatrix} \begin{bmatrix} R_{f,r,0} \\ R_{\theta,r,0} \\ R_{\phi,r,0} \end{bmatrix} \\ \begin{bmatrix} R_{f,r,1} \\ R_{\theta,r,1} \\ R_{\phi,r,1} \end{bmatrix} \\ \vdots \\ \begin{bmatrix} R_{f,r,N_\xi} \\ R_{\theta,r,N_\xi} \\ R_{\phi,r,N_\xi} \end{bmatrix} \end{bmatrix},$$

$$\tag{5.22}$$

where

$$\Pi_{11}^{i,i} = d_{0r}D^{iv} + d_{1r}D^3 + d_{2r}D^2 + d_{3r}D + d_{4r}I + 2d_{ii}[\beta_{0r}D^3 + \beta_{1r}D^2 + \beta_{2r}D^1 + \beta_{3r}I]$$

$$(5.23.0)$$

$$\Pi_{11}^{i,j} = 2d_{ij}[\beta_{0r}D^3 + \beta_{1r}D^2 + \beta_{2r}D^1 + \beta_{3r}I] \tag{5.23.1}$$

$$\Pi_{12}^{i,i} = d_{5r}I \tag{5.23.2}$$

$$\Pi_{12}^{i,j} = O = \text{zero matrix of size } (N_\eta + 1) \times (N_\eta + 1) \tag{5.23.3}$$

$$\Pi_{13}^{i,i} = d_{6r} \tag{5.23.4}$$

$$\Pi_{13}^{i,j} = O = \text{zero matrix of size } (N_\eta + 1) \times (N_\eta + 1) \tag{5.23.5}$$

$$\Pi_{21}^{i,i} = g_{4r}D^2 + g_{5r}D^1 + g_{6r}I + 2d_{ii}[\epsilon_{1r}D^2 + \epsilon_{2r}I] \tag{5.23.6}$$

$$\Pi_{21}^{i,j} = 2d_{ij}[\epsilon_{1r}D^2 + \epsilon_{2r}I] \tag{5.23.7}$$

$$\Pi_{22}^{i,i} = g_{0r}D^2 + g_{1r}D + g_{2r}I + 2d_{ii}[\epsilon_{0r}I] \tag{5.23.8}$$

$$\Pi_{22}^{i,j} = 2d_{ij}\epsilon_{0r}I \tag{5.23.9}$$

$$\Pi_{23}^{i,i} = O = \text{zero matrix of size } (N_\eta + 1) \times (N_\eta + 1) \tag{5.23.10}$$

$$\Pi_{23}^{i,j} = O = \text{zero matrix of size } (N_\eta + 1) \times (N_\eta + 1) \tag{5.23.11}$$

$$\Pi_{31}^{i,i} = h_{4r}D1 + h_{5r}I + 2d_{ii}[\kappa_{1r}I] \tag{5.23.12}$$

$$\Pi_{31}^{i,j} = 2d_{ij}[\kappa_{1r}I] \tag{5.23.13}$$

$$\Pi_{32}^{i,i} = h_{3r}D^2 \tag{5.23.14}$$

$$\Pi_{32}^{i,j} = O = \text{zero matrix of size } (N_\eta + 1) \times (N_\eta + 1) \tag{5.23.15}$$

$$\Pi_{33}^{i,i} = h_{0r}D^3 + h_{1r}D + h_{2r}I + 2d_{ii}[\kappa_{0r}]I \tag{5.23.16}$$

$$\Pi_{33}^{i,j} = 2d_{ij}[\kappa_{0r}]I. \tag{5.23.17}$$

After the implementing boundary conditions, the solutions for the above equations can be obtained for unknown vectors f_{r+1}, θ_{r+1} and ϕ_{r+1} at each ξ–level.

5.1 Numerical results and discussion

Numerical results are obtained using the bivariate spectral quasilinearization method to gain insight into the effects of the parameters describing the flow characteristics of a second grade fluid over a convectively heated stretching sheet. The numerical results are illustrated graphically in Figures 5.2 to 5.5 and given in Tables 5.1 to 5.4. There are many parameters in the mathematical model. We considered the effects of radiation, the second grade parameter, and the Soret number. In the simulation the default values of the other parameters are, unless otherwise specified, $\lambda = 0.02$, $m = 1$, $k_1 = 0.1$, $F^* = 0.21$, $Gr_t = 0.02$, $Gr_c = 0.05$, $Rd = 0.21$, $Ha = 0.05$, $Pr = 0.075$ $Ec = 0.03$, $Sc = 0.01$, $Sr = 0.02$, $Kr = 0.3$ unless otherwise specified.
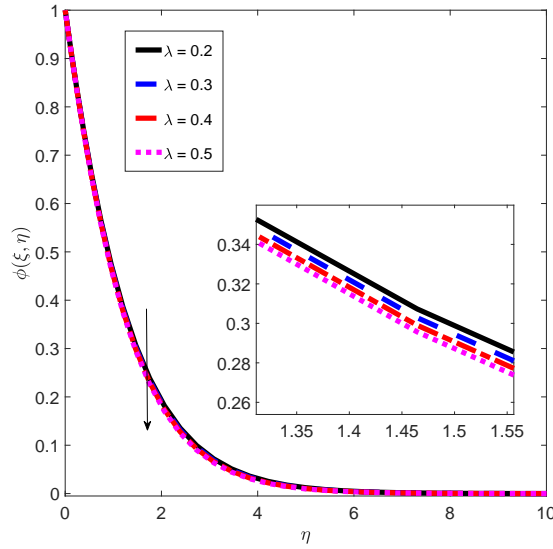
Figure 5.2 shows the variation of the fluid velocity, temperature and concentration distribution across the boundary layer for various values of the second grade fluid parameter. It is seen from Figure 5.2. (a) that the velocity of the fluid across the boundary layer increases with increasing values of the second grade parameter. The velocity also decreases asymptotically to zero at the edge of the hydrodynamic boundary layer. From Figures 5.2 (b) and (c), it is observed that the temperature and concentration profiles decrease with an increase in the second grade parameter. Hence the thickness of the thermal boundary layer reduces.
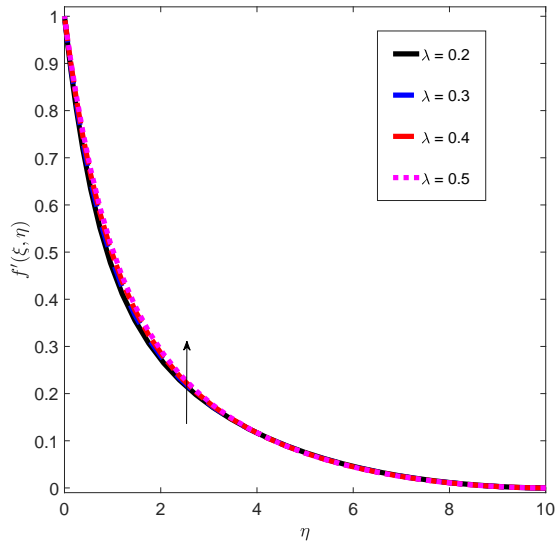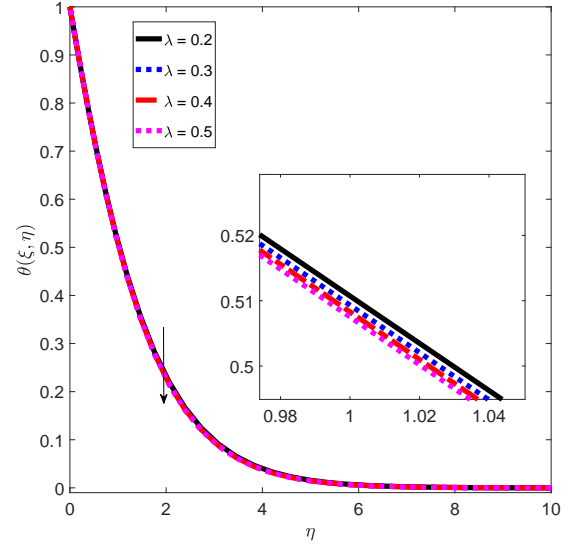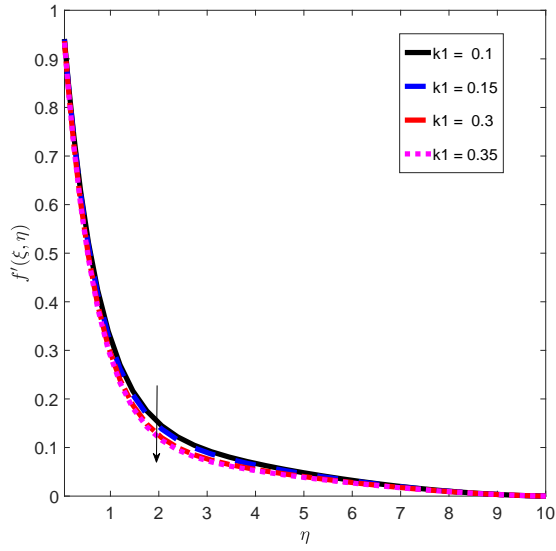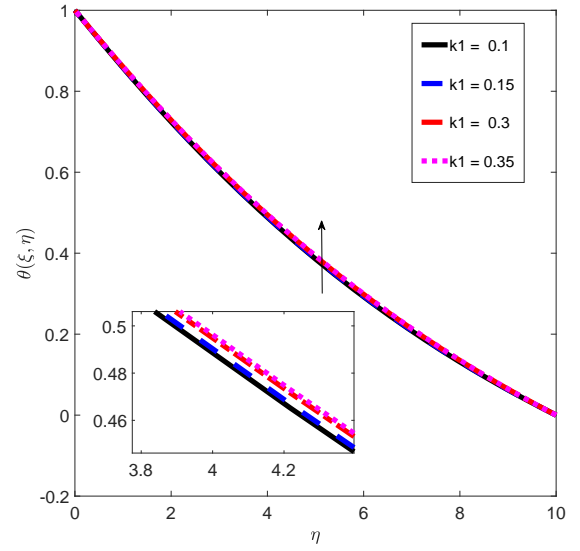
Figure 5.2: The variation of (a) the fluid velocity, (b) temperature, and (c) concentration profiles for different values of the second grade fluid parameter.

Figure 5.3 shows the effect of the porous medium parameter on the fluid velocity, temperature and concentration profiles. The effect of the porous medium parameter is to increase the resistance to the fluid motion. This causes the fluid velocity to reduce, as in Figure 5.3. (a). From Figure 5.3 (b) and (c), it is observed that increasing the porous medium parameter leads to an increase in temperature and concentration profiles of the fluid in
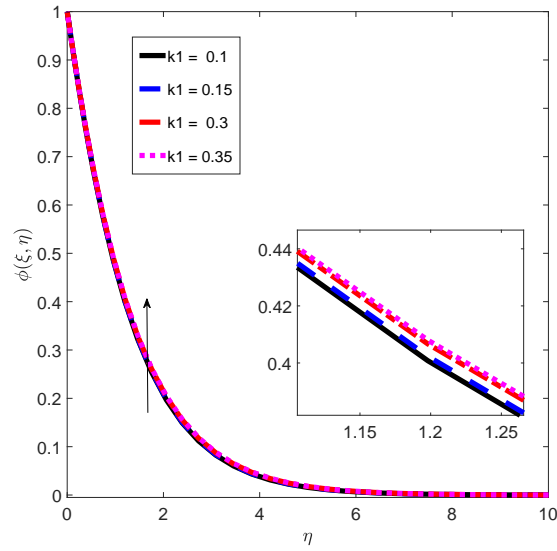
the boundary layer. This indicates that due to an increase in the thermal and solutal boundary thickness, the rate of heat and mass transfer also increases.

(a)

(b)

(c)

Figure 5.3: The variation of (a) the fluid velocity, (b) temperature, and (c) concentration profiles for different values of the porous parameter.

Figure 5.4: The variation of (a) the fluid velocity, (b) temperature, and (c) concentration profiles for different values of the chemical reaction parameter.

Figure 5.4 displays the behaviour of the fluid velocity, temperature, and concentration distribution for various values of the modified chemical reaction parameter, Kr. Figures 5.4 (a) and (c) show that an increase in the modified chemical reaction parameter leads to an increase of the fluid velocity and concentration in the boundary region, while from Figure 5.4 (b) it is observed that the temperature distribution increases uniformly with

increasing modified chemical reactions.

Kr	-$f''(0)$	-$\theta'(0)$	-$\phi'(0)$
0	2.66722324	0.17529406	0.10620809
0.5	2.67068378	0.17505819	0.12220341
1	2.67388378	0.19351450	0.13724764
1.5	2.67685367	0.17464091	0.15145713
2	2.67961920	0.17445544	0.16492910

Table 5.1: The effect of chemical reaction parameter on the skin friction coefficient, Nusselt number, and Sherwood number.

The influence of the chemical reaction parameter on the skin friction coefficient, the Nusselt number, and the Sherwood number are shown in Table 5.1. It is observed from this table that the skin friction coefficient and the Sherwood number increase with the chemical reaction parameter. The Nusselt number decreases as the chemical reaction parameter increases. It is interesting to note that for both $0 < Kr < 1$ and $Kr > 1$, similar results were obtained.

Figure 5.5 represents the velocity, the temperature, and the concentration profiles for various values of the magnetic field parameter. From Figure 5.5 (a), it is observed that the velocity of the fluid flow decreases with the magnetic field parameter. This is due to the transverse magnetic field that opposes the transport phenomenon since the presence of a magnetic field produces a drag-like force, called the Lorentz force, which acts in the opposite direction to the fluid motion. The increase in the magnetic field parameter increases the fluid temperature and concentration. This means that the momentum boundary layer thickness decreases while the reverse trend is observed for thermal and concentration boundary layer thickness. The increase of the solutal concentration in the boundary layer is due to an increase in the solutal boundary layer thickness.
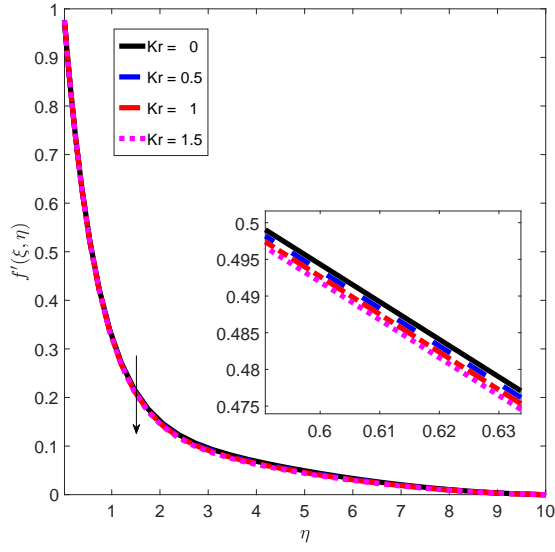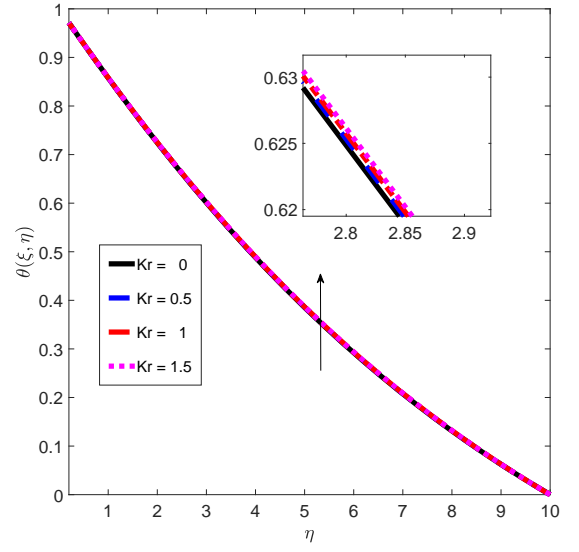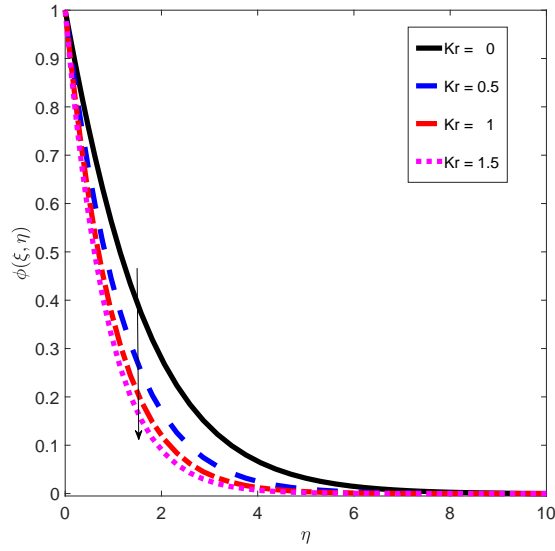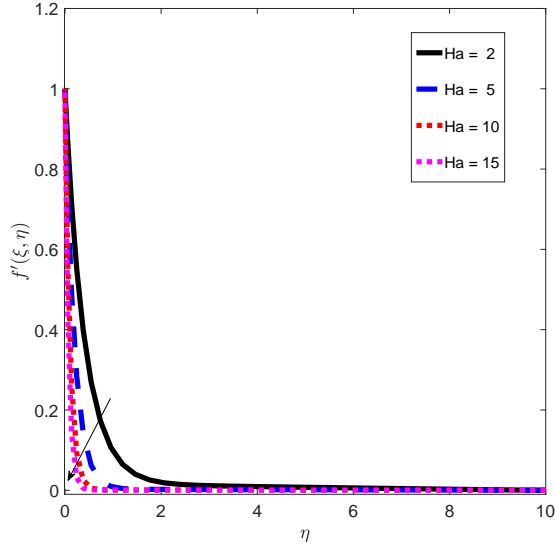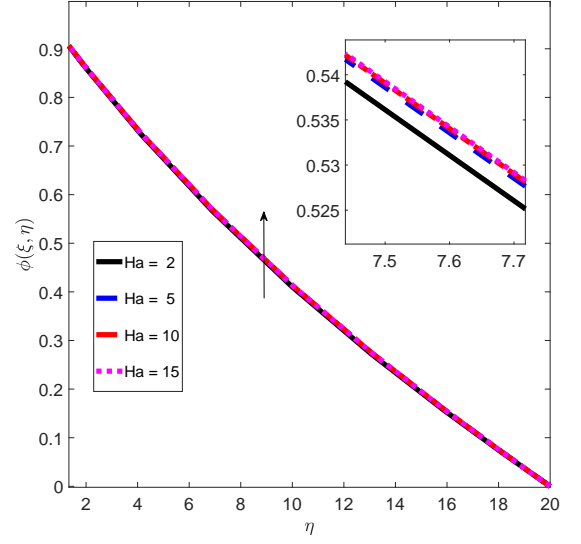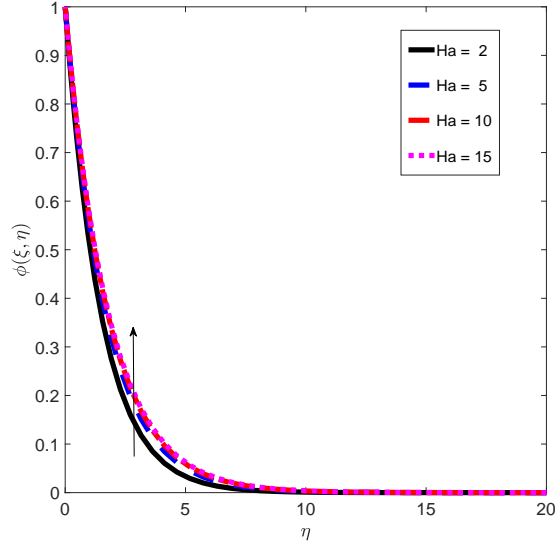
Figure 5.5: The variation of (a) the fluid velocity, (b) temperature, and (c) concentration profiles for different values of the magnetic field parameter.

Ha	$-f''(0)$	$-\theta'(0)$	$-\phi'(0)$
2	5.20507486	0.15328656	0.11376221
5	10.96414856	0.13719372	0.11267517
10	20.64273204	0.12129146	0.11221609
15	30.00798591	0.10743574	0.11205294

Table 5.2: Shows the effect of magnetic field parameter.

In Table 5.2, it is shown that the skin friction coefficient increase with the magnetic field parameter. Physically, a positive value for the skin friction implies that the fluid exerts a drag force on the sheet and a negative value implies the opposite meaning. The rate of a mass transfer decreases with the increase of the magnetic field parameter, whereas the heat transfer rate is not affected by this variation.

R_d	$-f''(0)$	$-\theta'(0)$	$-\phi'(0)$
0	2.67039799	0.15509296	0.11593358
0.2	2.66937520	0.17418849	0.11592695
0.4	2.66863869	0.19351450	0.11592221
0.8	2.66765113	0.23258055	0.11591589

Table 5.3: The effect of the the thermal radiation parameter.

It is clear from Table 5.3 that the magnitude of the skin friction coefficient decreases with an increase in the thermal radiation parameter. Increasing the thermal radiation parameter results in rising of the heat rate transfer of the fluid. However, there is no significant difference in the values of the mass rate transfer with increasing thermal radiation parameter.

	$-\theta'(0)$		
Sr	Present results	Das [119]	Olajuwon[120]
0.2	1.59872	1.58882	1.59570
0.5	1.170501	1.72067	1.17050
0.7	0.373686	0.37381	0.37350
2.0	2.675600	2.59830	2.67560

Table 5.4: The comparison of $-\theta'(0)$ for various values of the soret number, Sr.

The accuracy of our numerical solutions can be verified by comparison with those of Olajuwon[120] and Das [119], as presented for particular cases in Table 5.4. To check the validity of the numerical code, the values of the Nusselt number have been calculated for $Ec = Kr = 0$ and different values of Soret number. The comparison shows an excellent agreement among the results. Thus the use of the present BSQLM numerical technique is justified.

5.2   Residual error analysis

Residual error analysis is considered here to verify the convergence and accuracy of the method. The residual error is calculated by obtaining an approximate solution and inserting it back into the original system of equations. To determine the level of accuracy of the BSQLM approximate solution at a particular time level, in order to compare it with the exact solution, we use the maximum error or infinity error norm which is defined as

$$E_N = \text{Max}_i\{|u(y_i, t) - u^*(y_i, t)|\}, 0 \le i \le N, \tag{5.24}$$

where $u^*(y_i, t)$ is the approximate solution and $u(y_i, t)$ is the exact solution at the time level, t, as reported by Motsa et al. [111]. The convergence of the method will be elucidated if the infinity error norms approach zero with increasing the collocation point. Increasing in collocation points leads to a decrease in the error norms.

Figure 5.6 displays the residual error norms of the solutions for the system of equations (5.12 - 5.14) obtained using the BSQLM. It is observed from the graphs that as the number of iterations increases, the norm of the residual error decreases. The maximum convergence of the error norm for this method is given by the porous parameter. The BSQLM converges at the smaller residual error norm of 10^{-11} for velocity and temperature distributions, and 10^{-13} for concentration profiles after 3 and 4 iterations, respectivly. This means that the approximate solutions obtained using the BSQLM method gets more accurate as the iterative process continues. The residual error norm decreases to a point where convergence is achieved and that convergence point shows the level of accuracy of

the method. It is also observed that the BSQLM takes 4 or 5 iterations to converge as the values of the varying parameters increases.

(a)

(b)

(c)
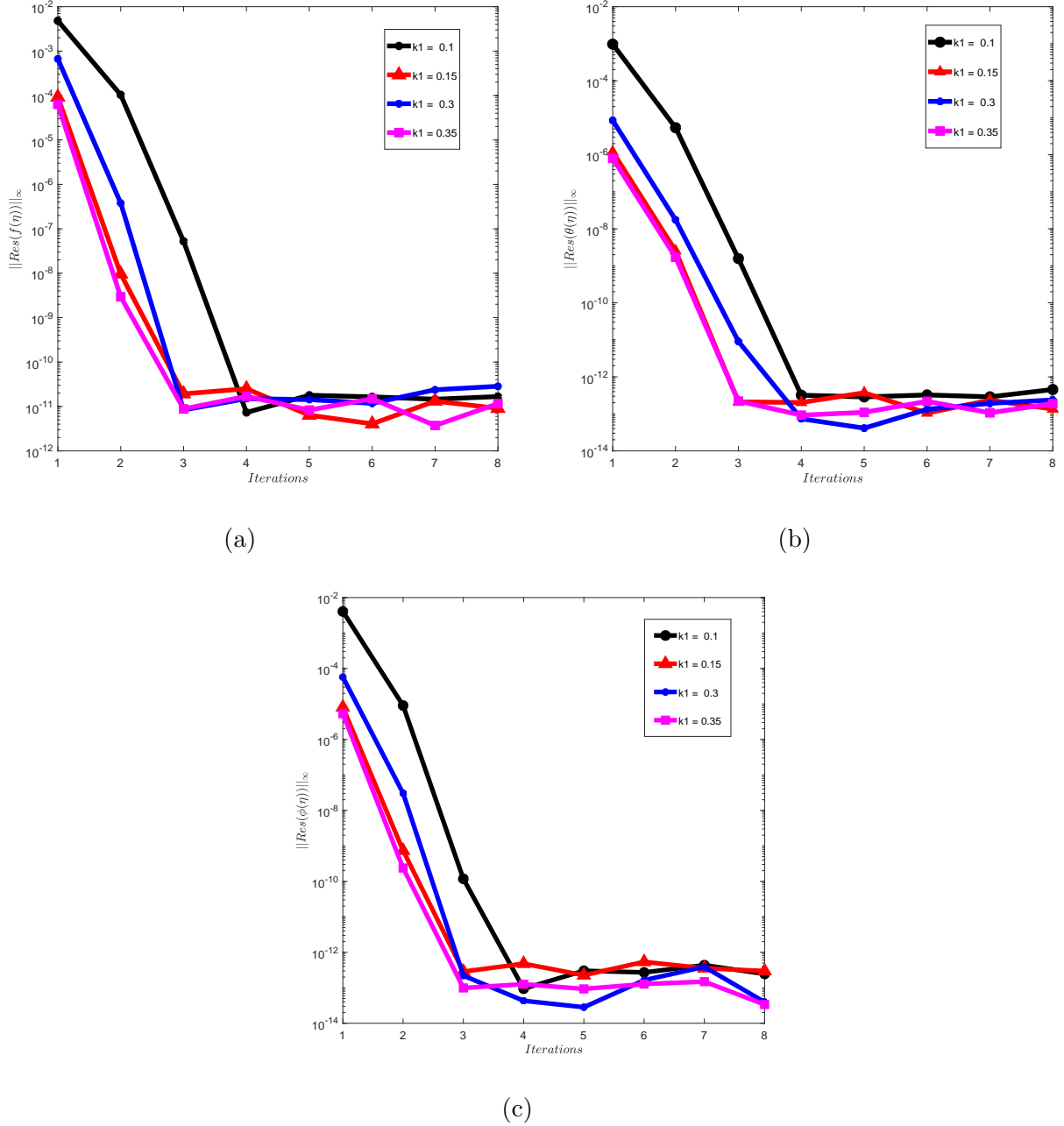
Figure 5.6: The residual error results for different values of porous parameter.

Figure 5.7 shows clearly the influence of increasing iterations on the convergence error norm of the bivariate spectral quasilinearization method. It is noted that with increasing parameter values the method converges after few iterations. The maximum convergence

error norm of this method is given by the porous parameter. However, the BSQLM converges at the error norm of 10^{-9} for velocity, 10^{-11} for the temperature, and 10^{-12} for concentration distributions after 4 iterations. Furthermore, the BSQLM gives parabolic graphs for error norms, which indicates that the residual error norm for SQLM is of the second order. The results from Figure 5.7 shows that the BSQLM is an accurate solution method for solving these nonlinear second grade problems.
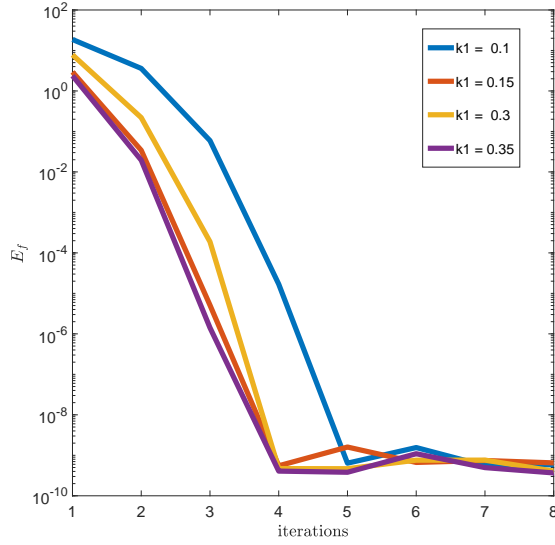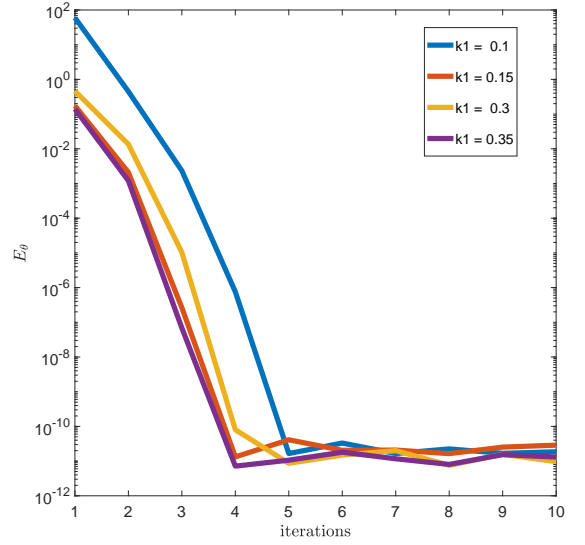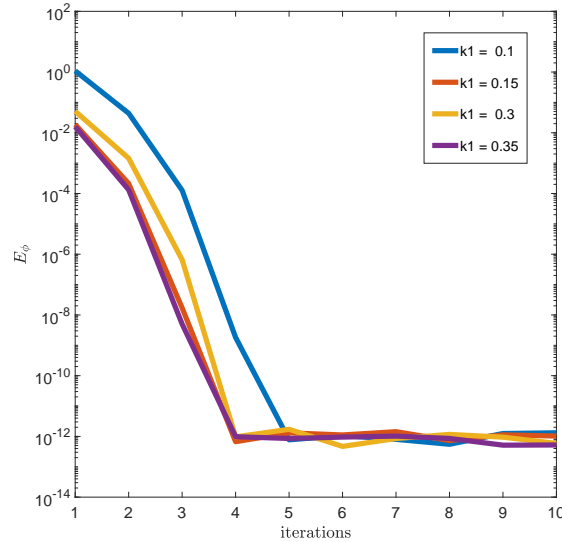
Figure 5.7: The error norm error results against the number of iterations for different values of porous parameter.

5.3 Summary

The work in this chapter investigated the second grade magnetohydrodynamic fluid flow over a convectively heated stretching sheet. The partial differential equations that describe the flow were solved numerically using the bivariate spectral quasilinearization method. The influence of different parameters on the fluid properties was analyzed. Results show that the fluid velocity in the boundary layer region increases with an increase in values of the second grade fluid parameter and decreases with increasing values of the porous parameter, chemical reaction parameter and the magnetic field parameter. The temperature profiles decrease with the second grade fluid parameter while that are enhanced by an increase in the porous parameter, chemical reaction parameter and the magnetic field parameter. Moreover, the fluid concentration increases with an increase in the porous, and magnetic field parameters, but, decreases under the influence of the second grade parameter and the chemical reaction parameter. Consequently, the rate of heat transfer rises with large values of the thermal radiation parameter but the effect is reversed for the skin friction. The residual error analysis shows BSQLM to be an accurate method for solving the nonlinear boundary layer second grade fluid problem.

Chapter 6

Conclusion

In this study, the bivariate spectral quasilinearization method (BSQLM) was used to obtain the numerical solutions of partial differential equations describing different second grade fluid flows. For each of these, a suitable transformation was used to non-dimensionalize the system of equations. The results obtained were presented through graphs and tables to illustrate the dependence of the parameters. The impact of parameters characterizing the flow was then analyzed. The residual error analysis was also used to determine the convergence and accuracy of the method.

In Chapter 2, the problem of an incompressible MHD flow of a second grade fluid in a porous channel was investigated using the method to obtain the numerical solutions. The results showed that BSQLM is an appropriate method for solving the second grade fluid third order partial differential equations.

In Chapter 3, the same method was then applied to a system of nonlinear partial differential equations. The objective was to solve a system of non-similar boundary layer equations that model an electrically conducting incompressible second grade fluid moving past a stretching surface. The effect of the second grade fluid parameter and magnetic field on the velocity and temperature profiles was investigated. An increase in the second grade fluid parameter resulted in an increase in the fluid velocity and a decreases in the temperature profiles, whereas increasing the magnetic field parameter showed the opposite

effect. Among other results, we showed that the shear stress decreases with an increase in the suction parameter and the second grade fluid parameter, whereas the heat transfer rate increases for these changes. The convergence of the method was determined by the residual error analysis. It was found that the bivariate spectral quasilinearization method is convergent, and so it is an appropriate method for solving nonlinear partial differential equations.

In Chapter 4, the characteristics of melting heat transfer in second grade nanofluid flowing over a porous wedge were analyzed. The bivariate spectral quasilinearization method was used to solve the non-dimensionalized systems of equations. The present results were found to be in good agreement with those in the literature. When investigating the effects of the parameters on the flow characteristics, we found that fluid flow was enhanced by increasing the magnetic field and wedge parameters. The increase of inclination angle increased the fluid velocity and decreased the temperature. Second grade parameters had an opposite effect in the velocity and temperature profiles. The residual error analysis showed that the bivariate spectral quasilinearization method is an appropriate method for solving the second grade nanofluid flow.

In Chapter 5, the effect of a chemical reaction and viscous dissipation on MHD second grade fluid flow past a convectively heated stretching sheet was studied, with the same quasilinearization method being used to numerically solve the system of equations. The impact of the magnetic field and thermal radiation on heat and mass transfer were also analyzed and indicated that heat transfer increases with the thermal radiation whereas, the mass transfer decreases. The magnetic field parameter resulted in both heat and mass transfer to decrease. To check the validity of the numerical code, the values of the heat rate transfer were calculated for different values of the Soret number, and comparison among the results showed excellent agreement. As before, the convergence and accuracy of the method were determined using the residual error analysis. It was found that the bivariate spectral quasilinearization method is convergent and accurate method for solving nonlinear second grade problem.

Overall, it was observed that the bivariate spectral quasilinearization method is a very efficient and accurate method to obtain approximate solutions for a variety of nonlinear second grade fluid problems, ranging from ODEs to PDEs. Further research may indicate whether the behaviour of this method remains the same under other conditions; for instance considering second grade fluid past a moving wedge or finding numerical solutions for second grade fluid flow in cylindrical polar coordinates.

References

[1] PD Ariel. A numerical algorithm for computing the stagnation point flow of a second grade fluid with/without suction. *Journal of Computational and Applied Mathematics*, 59(1):9–24, 1995.

[2] AM Siddiqui, M KamranAlam, S Islam, MT Rahim, and M Elahi. A class of exact solutions of second grade fluid. *International Journal of Physical Sciences*, 6(24): 5601–5608, 2011.

[3] NSP RAO. *Theoretical study of boundary Layer flow problems in Newtonian/non-Newtonian fluids*. Chennai, Unpublished PhD thesis, DR.M.G.R Educational and Research Institute University, Chennai, 2010.

[4] A Sojoudi and SC Saha. Shear thinning and shear thickening non-Newtonian confined fluid flow over rotating cylinder. *American Journal of Fluid Dynamics*, 2(6): 117–121, 2012.

[5] BC Sakiadis. Boundary-layer behavior on continuous solid surfaces: II. Boundary layer equations on a continuous flat surface. *AIChE Journal*, 7(2):221–225, 1961.

[6] BC Sakiadis. Boundary layer behaviour on continuous solid surfaces. I. Boundary layer equations for two-dimensional and axisymmetric flow. *AIChE Journal*, 2:26–28, 1960.

[7] LJ Crane. Flow past a stretching plate. *Zeitschrift für angewandte Mathematik und Physik*, 21(4):645–647, 1970.

[8] KR Rajagopal, TY Na, and AS Gupta. Flow of a viscoelastic fluid over a stretching sheet. *Rheologica Acta*, 23(2):213–215, 1984.

[9] A Chakrabarti and AS Gupta. Hydromagnetic flow and heat transfer over a stretching sheet. *Quarterly of Applied Mathematics*, 37(1):73–78, 1979.

[10] YS Wu. *Theoretical studies of non-Newtonian and Newtonian fluid flow through porous media*. Unpublished PhD thesis, University of California, Berkeley, 1990.

[11] MM Simpson and WS Janna. Newtonian and non-Newtonian fluids: Velocity profiles, viscosity data, and laminar flow friction factor equations for flow in a circular duct. In *ASME 2008 International Mechanical Engineering Congress and Exposition*, pages 173–180, 2008.

[12] AJ Chamkha, AM Aly, and MA Mansour. Similarity solution for unsteady heat and mass transfer from a stretching surface embedded in a porous medium with suction/injection and chemical reaction effects. *Chemical Engineering Communications*, 197(6):846–858, 2010.

[13] K Bhattacharyya, MS Uddin, and GC Layek. Application of scaling group of transformations to steady boundary layer flow of Newtonian fluid over a stretching sheet in presence of chemically reactive species. *Journal of Bangladesh Academy of Sciences*, 35(1):43–50, 2011.

[14] BJ Gireesha, B Mahanthesh, IS Shivakumara, and KM Eshwarappa. Melting heat transfer in boundary layer stagnation-point flow of nanofluid toward a stretching sheet with induced magnetic field. *Engineering Science and Technology, an International Journal*, 19(1):313–321, 2016.

[15] F Mabood, WA Khan, and AI Md Ismail. MHD flow over exponential radiating stretching sheet using homotopy analysis method. *Journal of King Saud University-Engineering Sciences*, 29(1):68–74, 2017.

[16] P Capobianchi, FT Pinho, M Lappa, and MSN Oliveira. Thermocapillary motion of a Newtonian drop in a dilute viscoelastic fluid. *Journal of Non-Newtonian Fluid Mechanics*, 270(1):8–22, 2019.

[17] M Wei, L Sun, P Qi, C Chang, and C Zhu. Continuous phenomenological modeling for the viscosity of shear thickening fluids. *Nanomaterials and Nanotechnology*, 8., https://doi.org/10.1177/1847980418786551.

[18] S Cao, Q He, H Pang, K Chen, W Jiang, and X Gong. Stress relaxation in the transition from shear thinning to shear jamming in shear thickening fluid. *Smart Materials and Structures*, 27(8):085013, 2018.

[19] IM Mahbubul (editor). *Preparation, characterization, properties, and application of nanofluid.* ISBN 9780128132456, https://doi.org/10.1016/B978-0-12-813245-6.00012-5. William Andrew Publishing, 2018.

[20] I Ahmad. On unsteady boundary layer flow of a second grade fluid over a stretching sheet. *Advanced Theory in Applied Mechanics*, 6(2):95–105, 2013.

[21] RS Rivlin and JL Ericksen. Stress-deformation relations for isotropic materials. In GI Barenblatt, and DD Joseph (Eds.). In *Collected Papers of RS Rivlin*, pages 911–1013. Springer-Verlag, New York, 1997.

[22] MR Mohyuddin and EE Ashraf. Inverse solutions for a second-grade fluid for porous medium channel and Hall current effects. In *Proceedings of the Indian Academy of Sciences-Mathematical Sciences*, volume 114, pages 79–96. Springer, 2004.

[23] T Hayat, N Ahmed, M Sajid, and S Asghar. On the MHD flow of a second grade fluid in a porous channel. *Computers and Mathematics with Applications*, 54(3): 407–414, 2007.

[24] SK Parida, S Panda, and M Acharya. Magnetohydrodynamic (MHD) flow of a second grade fluid in a channel with porous wall. *Meccanica*, 46(5):1093–1102, 2011.

[25] S Nadeem, A Rehman, C Lee, and J Lee. Boundary layer flow of second grade fluid in a cylinder with heat transfer. *Mathematical Problems in Engineering*, Article ID 640289:13 pages, 2012.

[26] T Akbar, R Nawaz, M Kamran, and A Rasheed. Magnetohydrodynamic (MHD)

flow analysis of second grade fluids in a porous medium with prescribed vorticity. *AIP Advances*, 5(11):117133, 2015.

[27] RA Shah, S Rehman, M Idrees, M Ullah, and T Abbas. Similarity analysis of MHD flow field and heat transfer of a second grade convection flow over an unsteady stretching sheet. *Boundary Value Problems*, 2017(1):162, 2017.

[28] C Fetecau, A Nazar, I Khan, and NA Shah. First exact solution for a second grade fluid subject to an oscillating shear stress induced by a sphere. *Journal of Nonlinear Science*, 19(2):186–195, 2018.

[29] M ur Rahman, M Khan, and M Manzur. Boundary layer flow and heat transfer of a modified second grade nanofluid with new mass flux condition. *Results in Physics*, 10:594–600, 2018.

[30] K Das, RP Sharma, and A Sarkar. Heat and mass transfer of a second grade magnetohydrodynamic fluid over a convectively heated stretching sheet. *Journal of Computational Design and Engineering*, 3(4):330–336, 2016.

[31] S Aman, Z Ismail, MZ Salleh, and I Khan. Flow analysis of second grade fluid with wall suction/injection and convective boundary condition. *Journal of Advanced Research in Fluid Machanics and Thermal Sciences*, 58(1):135–143, 2016.

[32] LR Prasad and GV Reddy. Heat transfer on MHD flow of second grade fluid through a porous medium in rotating channel with Hall effects. *Journal of Computer and Mathematical Sciences*, 10(7):1435–1449, 2019.

[33] S Abbasbandy, T Hayat, R Ellahi, and S Asghar. Numerical results of a flow in a third grade fluid between two porous walls. *Zeitschrift für Naturforschung A*, 64 (1-2):59–64, 2009.

[34] RL Fosdick and KR Rajagopal. Thermodynamics and stability of fluids of third grade. *Proceedings of the Royal Society of London. A. Mathematical and Physical Sciences*, 369(1738):351–377, 1980.

[35] ME Erdoğan. Plane surface suddenly set in motion in a non-Newtonian fluid. *Acta Mechanica*, 108(1-4):179–187, 1995.

[36] T Hayat, AH Kara, and E Momoniat. Exact flow of a third-grade fluid on a porous wall. *International Journal of Non-Linear Mechanics*, 38(10):1533–1537, 2003.

[37] T Hayat and AH Kara. Couette flow of a third-grade fluid with variable magnetic field. *Mathematical and Computer Modelling*, 43(1-2):132–137, 2006.

[38] T Hayat, F Shahzad, and M Ayub. Analytical solution for the steady flow of the third grade fluid in a porous half space. *Applied Mathematical Modelling*, 31(11): 2424–2432, 2007.

[39] T Hayat, R Naz, and M Sajid. Heat transfer for flow of a third-grade fluid between two porous plates. *Zeitschrift für Naturforschung A*, 65(10):837–843, 2010.

[40] M Keimanesh, MM Rashidi, AJ Chamkha, and R Jafari. Study of a third grade non-Newtonian fluid flow between two parallel plates using the multi-step differential transform method. *Computers and Mathematics with Applications*, 62(8):2871–2891, 2011.

[41] H Zaman, A Sohail, , and Ubaidullah. Stokes first problem for an unsteady MHD third-grade fluid in a non-porous half space with Hall currents. *Open Journal of Applied Sciences*, Article ID:43476(3):11 pages, 2014.

[42] M Zeb, S Islam, AM Siddiqui, and T Haroon. Analysis of third-grade fluid in helical screw rheometer. *Journal of Applied Mathematics*, Article ID:43476:11 pages, 2013.

[43] I Ullah, I Khan, and S Shafie. Hydromagnetic Falkner-Skan flow of Casson fluid past a moving wedge with heat transfer. *Alexandria Engineering Journal*, 55(3): 2139–2148, 2016.

[44] VM Falkner and SW Skan. Some approximate solutions of the boundary-layer for flow past a stretching boundary. *SIAM Journal on Applied Mathematics*, 49:1350–1358, 1931.

[45] N Riley and PD Weidman. Multiple solutions of the Falkner–Skan equation for flow past a stretching boundary. *SIAM Journal on Applied Mathematics*, 49(5): 1350–1358, 1989.

[46] M Guedda and Z Hammouch. On similarity and pseudo-similarity solutions of Falkner–Skan boundary layers. *Fluid Dynamics Research*, 38(4):211–223, 2006.

[47] A Ishak, R Nazar, and I Pop. Falkner-Skan equation for flow past a moving wedge with suction or injection. *Journal of Applied Mathematics and Computing*, 25(1-2): 67–83, 2007.

[48] MA Seddeek, AA Afify, and AM Al-Hanaya. Similarity solutions for a steady magnetohydrodynamic Falkner-Skan flow and heat transfer over a wedge considering the effects of variable viscosity and thermal conductivity. *Application and Applied Mathematics*, 4(2):301–313, 2009.

[49] RA Khan. Iterative scheme for solution to the Falkner-Skan boundary layer wedge flow problem. *General Mathematics Notes*, 1(2):1–10, 2010.

[50] MJ Martin and ID Boyd. Falkner-Skan flow over a wedge with slip boundary conditions. *Journal of Thermophysics and Heat Transfer*, 24(2):263–270, 2010.

[51] C Duque-Daza, D Lockerby, and C Galeano. Numerical solution of the Falkner-Skan equation using third-order and high-order-compact finite difference schemes. *Journal of the Brazilian Society of Mechanical Sciences and Engineering*, 33(4):381–392, 2011.

[52] FA Hendi and M Hussain. Analytic solution for MHD Falkner-Skan flow over a porous surface. *Journal of Applied Mathematics*, Article ID 123185:9 pages, 2012.

[53] MM Keshtkar. The Falkner-Skan flow over a wedge with variable parameters. *Journal of Applied Science and Agriculture*, 9(2):453–463, 2014.

[54] V Marinca, RD Ene, and B Marinca. Analytic approximate solution for Falkner-Skan equation. *The Scientific World Journal*, Article ID 617453:22 pages, 2014.

[55] CSK Raju and N Sandeep. Nonlinear radiative magnetohydrodynamic Falkner-Skan flow of Casson fluid over a wedge. *Alexandria Engineering Journal*, 55(3):2045–2054, 2016.

[56] AG Madaki, M Abdulhameed, M Ali, and R Roslan. Solution of the Falkner–Skan wedge flow by a revised optimal homotopy asymptotic method. *SpringerPlus*, 5(1): 513, 2016.

[57] L Bougoffa and RT Alqahtani. Further solution of the Falkner-Skan equation. *Romanian Journal of Physics*, 63:102, 2018.

[58] Chapter 1 - introduction to basic. In D.H. Bacon, editor, *Basic Heat Transfer*, pages 1 – 11. Butterworth-Heinemann, 1989. ISBN 978-0-408-01275-1. doi: https://doi.org/10.1016/B978-0-408-01275-1.50006-4.

[59] John H Lienhard. *A heat transfer textbook*. Dover Publications, Englewood Cliffs, 2019.

[60] A Faghri, Y Zhang, and JR Howell. *Advanced heat and mass transfer*. Global Digital Press, Columbia, 2010.

[61] Scott K and Hughes R. *Industrial membrane separation technology*. Springer Science & Business Media, Dordrecht, 2012.

[62] WHH Banks. Similarity solutions of the boundary-layer equations for a stretching wall. *Journal de Mecanique Theorique et Appliquee*, 2:375–392, 1983.

[63] WHH Banks and MB Zaturska. Eigensolutions in boundary-layer flow adjacent to a stretching wall. *IMA Journal of Applied Mathematics*, 36(3):263–273, 1986.

[64] G Pontrelli. Flow of a fluid of second grade over a stretching sheet. *International Journal of Non-linear Mechanics*, 30(3):287–293, 1995.

[65] BN Rao. Flow of a fluid of second grade over a stretching sheet. *International Journal of Non-Linear Mechanics*, 31(4):547–550, 1996.

[66] S Liao. On the analytic solution of magnetohydrodynamic flows of non-Newtonian fluids over a stretching sheet. *Journal of Fluid Mechanics*, 488:189–212, 2003.

[67] S Liao. A new branch of solutions of boundary-layer flows over an impermeable stretched plate. *International Journal of Heat and Mass Transfer*, 48(12):2529–2539, 2005.

[68] M Miklavčič and C Wang. Viscous flow due to a shrinking sheet. *Quarterly of Applied Mathematics*, 64(2):283–290, 2006.

[69] T Fang. Boundary layer flow over a shrinking sheet with power-law velocity. *International Journal of Heat and Mass Transfer*, 51(25-26):5838–5843, 2008.

[70] R Cortell. Flow and heat transfer of an electrically conducting fluid of second grade over a stretching sheet subject to suction and to a transverse magnetic field. *International Journal of Heat and Mass Transfer*, 49(11-12):1851–1856, 2006.

[71] MS Abel and N Mahesha. Heat transfer in MHD viscoelastic fluid flow over a stretching sheet with variable thermal conductivity, non-uniform heat source and radiation. *Applied Mathematical Modelling*, 32(10):1965–1983, 2008.

[72] S Nadeem, A Hussain, MY Malik, and T Hayat. Series solutions for the stagnation flow of a second-grade fluid over a shrinking sheet. *Applied Mathematics and Mechanics*, 30(10):1255, 2009.

[73] M Sajid and T Hayat. The application of homotopy analysis method for MHD viscous flow due to a shrinking sheet. *Chaos, Solitons and Fractals*, 39(3):1317–1323, 2009.

[74] T Fang, S Yao, J Zhang, and A Aziz. Viscous flow over a shrinking sheet with a second order slip flow model. *Communications in Nonlinear Science and Numerical Simulation*, 15(7):1831–1842, 2010.

[75] FT Akyildiz, DA Siginer, K Vajravelu, JR Cannon, and RA Van Gorder. Similarity solutions of the boundary layer equations for a nonlinearly stretching sheet. *Mathematical Methods in the Applied Sciences*, 33(5):601–606, 2010.

[76] RA Van Gorder, E Sweet, and K Vajravelu. Nano boundary layers over stretching surfaces. *Communications in Nonlinear Science and Numerical Simulation*, 15(6): 1494–1500, 2010.

[77] A Ahmad and S Asghar. Flow of a second grade fluid over a sheet stretching with arbitrary velocities subject to a transverse magnetic field. *Applied Mathematics Letters*, 24(11):1905–1909, 2011.

[78] K Bhattacharyya and K Vajravelu. Stagnation-point flow and heat transfer over an exponentially shrinking sheet. *Communications in Nonlinear Science and Numerical Simulation*, 17(7):2728–2734, 2012.

[79] L Zheng, J Niu, X Zhang, and L Ma. Dual solutions for flow and radiative heat transfer of a micropolar fluid over stretching/shrinking sheet. *International Journal of Heat and Mass Transfer*, 55(25-26):7577–7586, 2012.

[80] PM Patil. Effects of surface mass transfer on steady mixed convection flow from vertical stretching sheet with variable wall temperature and concentration. *International Journal of Numerical Methods for Heat and Fluid Flow*, 22(3):287–305, 2012.

[81] M Misra, N Ahmad, and ZU Siddiqui. Unsteady boundary layer flow past a stretching plate and heat transfer with variable thermal conductivity. *World Journal of Mechanics*, 2(1):35, 2012.

[82] PK Mahanta. Numerical study on heat transfer of non-Newtonian fluid flow over stretching surface with variable viscosity in uniform magnetic field. *International Journal of Scientific and Research Publications*, 2(12):1–9, 2012.

[83] S Asghar, A Ahmad, and A Alsaedi. Flow of a viscous fluid over an impermeable shrinking sheet. *Applied Mathematics Letters*, 26(12):1165–1168, 2013.

[84] M Khan and A Shahzad. On boundary layer flow of a Sisko fluid over a stretching sheet. *Quaestiones Mathematicae*, 36(1):137–151, 2013.

[85] S Chaudhary and P Kumar. MHD slip flow past a shrinking sheet. *Applied Mathematics*, 4(03):574, 2013.

[86] A Munir, A Shahzad, and M Khan. Heat transfer for MHD second grade fluid flow over a porous nonlinear radially stretching sheet. *Walailak Journal of Science and Technology*, 12(9):763–773, 2015.

[87] M Khan and M ur Rahman. Flow and heat transfer to modified second grade fluid over a non-linear stretching sheet. *AIP Advances*, 5(8):087157, 2015.

[88] NAA Bakar, N Bachok, N.Md Arifin, and I Pop. Stability analysis on the flow and heat transfer of nanofluid past a stretching/shrinking cylinder with suction effect. *Results in Physics*, 9:1335–1344, 2018.

[89] MS Kumar, N Sandeep, BR Kumar, and PA Dinesh. A comparative analysis of magnetohydrodynamic non-Newtonian fluids flow over an exponential stretched sheet. *Alexandria Engineering Journal*, 57(3):2093–2100, 2018.

[90] S Liao. Notes on the homotopy analysis method: some definitions and theorems. *Communications in Nonlinear Science and Numerical Simulation*, 14(4):983–997, 2009.

[91] S Liao. *Homotopy analysis method in nonlinear differential equations*. Springer Heidelberg, 2012.

[92] M Turkyilmazoglu. A note on the homotopy analysis method. *Applied Mathematics Letters*, 23(10):1226–1230, 2010.

[93] D Lu and J Liu. Application of the homotopy analysis method for solving the variable coefficient KdV-burgers equation. *Abstract and Applied Analysis*, Special Issue (2013), Article ID 309420:4 pages, 2014.

[94] G Akram and M Sadaf. Application of homotopy analysis method to the solution of ninth order boundary value problems in AFTI-F16 fighters. *Journal of the Association of Arab Universities for Basic and Applied Sciences*, 24:149–155, 2017.

[95] P Zhou. *Finite Difference Method*. Springer, Berlin, 1993.

[96] M Kurulay and M Bayram. Approximate analytical solution for the fractional modified KdV by differential transform method. *Communications in Nonlinear Science and Numerical Simulation*, 15(7):1777–1782, 2010.

[97] J Noye (Editor). Finite difference techniques for partial differential equations. *North-Holland Mathematics Studies*, 83:95–354, 1984.

[98] SM Garba, AB Gumel, and JM-S Lubuma. Dynamically-consistent non-standard finite difference method for an epidemic model. *Mathematical and Computer Modelling*, 53(1-2):131–150, 2011.

[99] RE Mickens. Exact solutions to a finite-difference model of a nonlinear reaction-advection equation: Implications for numerical analysis. *Numerical Methods for Partial Differential Equations*, 5(4):313–325, 1989.

[100] T Cebeci and P Bradshaw. *Physical and computational aspects of convective heat transfer*. Springer Science & Business Media, Verlag, 2012.

[101] FS Al-Shibani, AI Md Ismail, and FA Abdullah. The implicit Keller box method for the one dimensional time fractional diffusion equation. *Journal of Applied Mathematics and Bioinformatics*, 2(3):69, 2012.

[102] T Ritschel. Numerical methods for solution of differential equations. *Technical University of Denmark*, Kongens Lyngby, 2013.

[103] E Fehlberg. Low-order classical Runge-Kutta formulas with stepsize control and their application to some heat transfer problems. *National Aeronautics and Space Administration*, Washington, 1969.

[104] D Gottlieb and SA Orszag. *Numerical analysis of spectral methods: theory and applications*. Society for Industrial and Applied Mathematics, Philadelphia, 1983.

[105] C Canuto, MY Hussaini, A Quarteroni, and TA Zang. *Spectral methods: Fundamentals in single domains*. Springer Science & Business Media, Berlin, 2007.

[106] J Shen, T Tang, and LL Wang. *Spectral methods: algorithms, analysis and applications*, volume 41. Springer Science & Business Media, Heidelburg, 2011.

[107] VM Magagula. *Bivariate pseudospectral collocation algorithms for nonlinear partial differential equations.* Unpublished PhD thesis, University of KwaZulu-Natal, Durban, 2016.

[108] SS Motsa. A new spectral relaxation method for similarity variable nonlinear boundary layer flow systems. *Chemical Engineering Communications*, 201(2):241–256, 2014.

[109] SS Motsa. A new spectral local linearization method for nonlinear boundary layer flow problems. *Journal of Applied Mathematics*, Article ID 423628:15 pages, 2013.

[110] SS Motsa, PG Dlamini, and M Khumalo. Spectral relaxation method and spectral quasilinearization method for solving unsteady boundary layer flow problems. *Advances in Mathematical Physics*, Article ID 341964:12 pages, 2014.

[111] SS Motsa, VM Magagula, and P Sibanda. A bivariate Chebyshev spectral collocation quasilinearization method for nonlinear evolution parabolic equations. *The Scientific World Journal*, Article ID 581987:13 pages, 2014.

[112] SS Motsa and IL Animasaun. Bivariate spectral quasi-linearisation exploration of heat transfer in the boundary layer flow of micropolar fluid with strongly concentrated particles over a surface at absolute zero due to impulsive. *International Journal of Computing Science and Mathematics*, 9(5):455–473, 2018.

[113] K Vajravelu and T Roper. Flow and heat transfer in a second grade fluid over a stretching sheet. *International Journal of Non-Linear Mechanics*, 34(6):1031–1036, 1999.

[114] K Vajravelu and D Rollins. Hydromagnetic flow of a second grade fluid over a stretching sheet. *Applied Mathematics and Computation*, 148(3):783–791, 2004.

[115] A Postelnicu and I Pop. Falkner–Skan boundary layer flow of a power-law fluid past a stretching wedge. *Applied Mathematics and Computation*, 217(9):4359–4368, 2011.

[116] T Hayat, A Shafiq, M Imtiaz, and A Alsaedi. Impact of melting phenomenon in the

Falkner-Skan wedge flow of second grade nanofluid: A revised model. *Journal of Molecular Liquids*, 215:664–670, 2016.

[117] BL Kuo. Heat transfer analysis for the Falkner-Skan wedge flow by the differential transformation method. *International Journal of Heat and Mass Transfer*, 48(23-24): 5036–5046, 2005.

[118] FM White. Viscous fluid flow, 2nd edition, McGraw-Hill. *New York*, 1991.

[119] K Das. Influence of chemical reaction and viscous dissipation on MHD mixed convection flow. *Journal of Mechanical Science and Technology*, 28(5):1881–1885, 2014.

[120] BI Olajuwon. Convection heat and mass transfer in a hydromagnetic flow of a second grade fluid in the presence of thermal radiation and thermal diffusion. *International Communications in Heat and Mass Transfer*, 38(3):377–382, 2011.